

Annual Technical Volume of **Aerospace Engineering Division Board**

**Theme:
Agricultural Applications of
Unmanned Aerial Vehicles**



The Institution of Engineers (India)

Aerospace Engineering Division Board (2015-2016)

About the Division Board

The Institution of Engineers (India) has established Aeronautical Engineering Division in the year 1978, which was further renamed as Aerospace Engineering Division. This Division consists of quite a large number of corporate members from Government, Public and Private sectors.

Various types of technical activities organized by the Aerospace Engineering Division include All India Seminars, All India Workshops, Lectures, Panel Discussions etc., which are held at various State/Local Centres of the Institution. Apart from these, National Convention of Aerospace Engineers, an Apex activity of this Division is also organized each year on a particular theme approved by the Council of the Institution. In the National Convention, several technical sessions are arranged on the basis of different sub-themes along with a Memorial Lecture in the memory of "Dr Vikram Sarabhai", the eminent Scientist and former Chairman of Atomic Energy Commission, Govt of India, which is delivered by the experts in this field.

In order to promote the research and developmental work taking place in the field of aerospace engineering, the Institution also publishes Aerospace Engineering Division Journal twice in a year, where mainly the researches and its findings are focused. Due to multi-level activities related to this engineering discipline, this division covers different sub-areas such as:

Application of Laser Techniques for Diagnostic and Repairs of Aerospace Structures

- Nano-material Technology and its application in different fields
- Smart materials and their applications to Aerospace, Mechanical and Civil Structures
- Organ and Tissue Replacements by Mechanical Structures
- Lab on a Chip (Biochemical Area)
- Compliant Structures at Nano and Multiple Scales
- Development of Materials with Biomechanical Properties for Therapeutic Purposes
- Biosynthesis of Chemicals
- Bioinformatics
- Nano-Technology and its application in different fields of Aerospace & Aviation
- Smart Materials and their application to Aerospace, Mechanical and Civil Structures
- Application of Smart Materials on Human Systems
- Micro and Nano Air Vehicles and their Sensors
- Reusable Launch Vehicle
- Air Traffic Control (ATC)

Micro-thruster and Fuel Cells for Propulsion

- Management of Infrastructure in Aviation
- Development of Micro and Nano Satellites
- Magneto Hydro Dynamic for active flow control of hypersonic vehicles
- Separation dynamics of multi body systems
- Aerodynamic characteristics for rarefied flows
- Morphing wings design
- Flying wing aircrafts for low radar cross sections
- Aero acoustics
- Sea Plane/Hydro-Plane

In order to promote the research and developmental work in the field of Aerospace Engineering, the Institution also publishes Journal of The Institution of Engineers (India): Series C in collaboration with M/S Springer which is an internationally peer reviewed journal. The journal is published four times in a year and serves the national and international engineering community through dissemination of scientific knowledge on practical engineering and design methodologies pertaining to Mechanical, Aerospace, Production and Marine engineering.

Annual Technical Volume
2015-16

**Agricultural Applications of
Unmanned Aerial Vehicles**



The Institution of Engineers (India)
Aerospace Engineering Division Board



H C S Berry, FIE
PRESIDENT

The Institution of Engineers (India)

AN ISO 9001 : 2008 CERTIFIED ORGANISATION

(ESTABLISHED 1920, INCORPORATED BY ROYAL CHARTER 1935)

HEADQUARTERS : 8 GOKHALE ROAD, KOLKATA - 700 020, INDIA

Ph : (91) (33) 2223 1979 • E-mail : president@ieindia.org • Web Site : <http://www.ieindia.org>

*"96 Years of Relentless Journey towards
Engineering Advancement for Nation-building"*



It is a matter of immense pleasure that Aerospace Engineering Division Board of the Institution has successfully published the first Annual Technical Volume on the theme 'Agricultural Applications of Unmanned Aerial Vehicles'.

Moreover, it's a matter of proud that our learned Corporate Members attached to the Aerospace Engineering Division have contributed papers for this publication related to the application of unmanned aerial vehicle in agricultural fertilization, application and control of mobile robots in agriculture, agricultural remote sensing of unmanned aerial vehicles, application of Drones in precision agriculture etc.

On this occasion, I would like to take the opportunity to congratulate the Members of Aerospace Engineering Division for their sincere efforts and whole hearted support in bringing out this Annual Technical Volume.

I sincerely believe that the practicing professionals in the relevant fields will be immensely benefited from this compilation and be a part of competent workforce for future technological development of the country.

H C S Berry



The Institution of Engineers (India)

AN ISO 9001: 2008 CERTIFIED ORGANISATION
(ESTABLISHED 1920, INCORPORATED BY ROYAL CHARTER 1935)
8 GOKHALE ROAD, KOLKATA - 700 020

*“96 years of Relentless Journey towards
Engineering Advancement for Nation-building”*

Prof (Dr) N R Bandyopadhyay, FIE, FAScT

Chairman

Committee for Advancement of Technology and Engineering (CATE)



It's a matter of immense pleasure that as per the decision taken during 126th Meeting of CATE/682nd Meeting of the Council, held at Panchmarhi, Madhya Pradesh on June 21, 2014, the Aerospace Engineering Division Board of the Institution has been successful in bringing out the first edition of Annual Technical Volume on the theme 'Agricultural Applications of Unmanned Aerial Vehicles'.

At this outset, I congratulate the Chairman and the Members of the Aerospace Engineering Division Board for their sincere effort in bringing out the volume.

The Volume is an excellent collection of the best papers presented during the All India Seminars and National Conventions organised by various Centres of the Institution under the aegis of Aerospace Engineering Division Board. The valuable contributions of the Corporate Members attached to Aerospace Engineering Division of the Institution are also duly acknowledged.

I sincerely believe that this compiled volume will be of immense help to the practising and professional engineers working in diverse field of Aerospace Engineering.

N R Bandyopadhyay
Editor in Chief

Message from Consulting Editor



The UAV is an acronym for Unmanned Aerial Vehicle, which is an aircraft with no pilot on board. UAVs can be remote controlled aircraft (e.g. flown by a pilot at a ground control station) or can fly autonomously based on pre-programmed flight plans or more complex dynamic automation systems. UAVs are currently used for a number of missions, including reconnaissance and attack roles.

The UAVs have a key role in various civilian applications also.

The application of UAV in area of agriculture is one of the major societal application of UAV. While remote sensing satellites provide information about crop, agriculture and other related fields in a global sense, the use of UAV helps in detailing agriculture studies in micro level in area specific way.

ASDB felt that it will be appropriate to bring out the Annual Technical Volume from an area useful to common man. Let me thank the Members of the Division Board and Technical Department of IEI for the relentless efforts in bringing out this volume.

With warm regards,

Yours sincerely,

A handwritten signature in black ink, appearing to read 'S R Vijayamohanakumar', written over a stylized graphic element that resembles a pen nib or a signature flourish.

S R Vijayamohanakumar
Chairman
Aerospace Engineering Division Board
The Institution of Engineers(India)

Annual Technical Volume of
Aerospace Engineering Division Board

President

Mr H C S Berry, FIE

Chief Editor

Prof (Dr) N R Bandyopadhyay, FIE, FAScT
Chairman, CATE

Secretary and Director General - I/C

Dr Anil Kumar, FIE

Consulting Editor

Mr S R Vijayamohanakumar, FIE
Chairman, ASDB

Members of the Editorial Board (Session 2015-2016)

Prof. R M Vasagam, FIE ; Dr S C Sharma, FIE

Publishers

Dr Anil Kumar, Secretary and Director General- I/C
for The Institution of Engineers (India)

Publication Office

The Institution of Engineers (India)
8 Gokhale Road, Kolkata 700020
Ph : 2223-8311 /14-16 / 33-34
Fax : (033) 2223-8345
website : www.ieindia.org
e-mail : technical@ieindia.org

Editorial Team

Technical Department, IEI

Mr S Chaudhury

Mr N Sengupta	Mr K Sen	Dr S Ghosh
Mr T Chakraborty	Ms A Dutta	Ms S Biswas Sett
Mr Partha Mukhopadhyay	Mr T K Roy	Mr S Bagchi
Ms H Roy	Ms N Sikdar	Mr P Mukhopadhyay

The Institution of Engineers (India), 8 Gokhale Road, Kolkata 700020 as a body accepts no responsibility for the statements made by individuals in the paper and contents of papers published herein

The Institution of Engineers (India) subscribes to the Fair Copying Declaration of the Royal Society. Reprints of any portion of the publication may be made provided that reference thereto be quoted.

As per Bye-Law 119, copyright of each paper published in Institution Journals or Proceedings in full or in abstract at its Centres shall lie with the Institution.

Contents

Agricultural Applications of Unmanned Aerial Vehicles <i>Partha Sinha</i>	13
Agriculture Fertilization using Unmanned Aerial Vehicle <i>Johnson Tellis, John Nikhil Poyyayial, Shrajan Bhandary, Jagath Biddappa</i>	21
Autonomous Mobile Robot in Agriculture <i>C. Vignesh, P Anush, B. Jagadeeswaran, N. Ranjith Raj, P. Srinivasan</i>	26
Concept of VAL (Varying Axial Load) Application for Structural Qualification of an Interstage Structure of a 3T Class Launch Vehicle : Evolution and Validation <i>S S Resmi, Selvakumari D Rachel</i>	29
Design and Fabrication of Slipstream Deflection Mechanism for a Remotely Controlled Airship <i>Kapse Subhash Prachi, Dhanashree Ahire, Gauri Borhade, Milind Murugkar, Rajkumar S Pant</i>	39
Design and Fabrication of a Portable Semi-Rigid Airship <i>Loharkar Shubham Anil, Alap Kshirsagar, Rajkumar S. Pant</i>	45
Design Feasibility Study of an Agriculture Remote Sensing UAV <i>R S Anand, M Dineshkumar</i>	54
Drones for Precision Agriculture <i>K V Srinivasan</i>	59
Kalman Filter based INS-GPS Integration for Navigation Over Short Distances and at Low Speeds <i>C V Navyashree, Sachit S Rao, V Parameswaran</i>	63
Real Time Obstacle Avoidance and Navigation of a Quad-Rotor MAV using Optical Flow Algorithms <i>Prashanth K Ramaswamy, B Nagaraja, Govind R. Kadambi, S. R. Shankapal</i>	70
Swarming Nano Airborne Drones (SNAD) Artificial Intelligence in Drones for Defence Indoor Surveillance on hijacked Buildings <i>B. Madhan Kumar</i>	76
Tethered Aerostat Systems for Agricultural Applications in India <i>Rajkumar S. Pant</i>	82



Agricultural Applications of Unmanned Aerial Vehicles

Partha Sinha

*Visiting Asst. Professor to GRD-IMT (Dehra Dun) & Head of Dept.
CAD/CAM at DSS Group of Institutions, Dehra Dun, Uttrakhand, 248001*

✉ partha138@rediffmail.com

Abstract

Agriculture today is highly sophisticated, based on Big Data analysis and farmers around the globe are data hungry. Unfortunately they are not provided with all that they need to sustain this industry, though agriculture being one of the foremost employment generating sectors. Agro industry today extends to Animal Husbandry, Crops, Dairy, Fertilizers & Pesticides, Fisheries, Floriculture, Horticulture, Irrigation, Organic Farming, Plant protection, Seeds, Sericulture, Soil & Water Conservation, Storage, Marketing & Pricing activities and so on. The vastness of agriculture practices brings issues like crop health, crop growth, canopy thickness, weather issues, irrigation, soil conditions, nitrogen deficiency, cattle health, grazing issues, soil productivity variances, security and anomalies, disaster management, crop insurance policies to name a few. Precision farming is thus the call of the day and farmers worldwide have resorted to farming techniques involving Remote Sensing, Geographic Information System, Global Position System and Unmanned Aerial Vehicles. This paper looks into the depths of UAV applications in agriculture in different countries and tries to present the on-going efforts to digitalize farming through UAV led farming methodology and also brings out the various on-going programmes under the present Indian government. The paper tries to present the technical aspects of UAV based farming technology as embraced by Governments and Private farmers along with the present Regulatory Restrictions imposed on the private usage of UAVs in countries like USA and India and it brings out the pros and limitations of applications in different areas as well.

Keywords: *UAV; Precision Agriculture; UAV Sensors; Crop Health Index; Agricultural Insurance*

Introduction

Agriculture industry in the year 2016 is more complicated than ever. Agricultural management is becoming more and more difficult for all countries. It is difficult for farmers to analyze and to react to problems like disease outbreak among cattle and crop alike. Equally difficult are the ways to monitor the critical aspects of agriculture like plant health measurement, livestock detection, water source detection, surveillance and security. Monitoring of crops and managing farmlands today is done by satellites, manned planes and by walking the field or on horsebacks. However this is not a rewarding exercise, being time consuming and exhausting.

Further, the large and growing sizes of farmlands in developed and developing countries today call for precision farming. For example if the farmlands of USA, EU countries and of Australia are considered, 41% of U.S. total land area is farmland. In 1900, the average farm size was 147 acres, presently it is 441 acres [1]. The average farm size in the EU-27 rose from 11.9 hectares (29.40554 acres) to 14.5 hectares (35.83028 acres) between 2005 and 2010 [2].

In Australia, farmlands size to 50 hectares (123.553 acres), and a similar proportion (between 50 and 500 hectares (1235.53 acres) [3]. Agricultural UAVs have revolutionised the very concept of farming by creating methodical and precision than ever, ready backup data and verified strategy.



Agriculture

Agriculture is the world's largest provider of jobs. It provides employment to more than 1.3 billion people worldwide [4]. About 40 percent of the global workforce is actively engaged in agriculture and allied industries and is world's largest provider of jobs[5]. In more than 50 countries agriculture engages 50% of the population; this value shifts to 75% in poorer countries [6].

Precision Agriculture

Precision Agriculture is all about Agriculture Big Data Analytics, collecting real time data on crop maturity, air quality, weather, water sources, soil behaviour versus seed adaptation, fertilizer versus pesticide, optimization of planting, harvesting and distribution of crops and more. These data help to set predictive and preventive analytics and to make smart decisions. Components of precision agriculture include Geographic

Information System (GIS), Remote Sensing (RS), Global Position System (GPS), SS Toolbox, yield monitor and adept use of UAV based information system.

Precision Farming with UAV

The onset of precision farming with UAVs is a boon to farmers worldwide. Agricultural UAVs are expected to capture 80 per cent of the commercial UAV market and has the potential to generate more than 100,000 jobs in the US alone [7].

Definition of UAV

An UAV (unmanned air vehicle) comprises a number of sub-systems including the aircraft, its payloads, the control station(s), aircraft launch and recovery sub-systems, support sub-systems, communication sub-systems, transport sub-systems, etc. Different types of UAV with their applications [8] are shown in **Table 1**.

Table 1 : Categories of Systems Based upon Air Vehicle Types [8]

SI No	UAV Type	Application
1	HALE – High altitude long endurance	Extremely long-range reconnaissance and surveillance, fly over 15000 m
2	MALE– Medium altitude long endurance	Long-range reconnaissance and surveillance, fly between 5000–15000 m
3	TUAV – Medium Range or Tactical UAV	Range between 100 and 300 km operated by land and naval forces
4	Close-Range UAV	Diverse military/civilian purposes
5	MUAV or Mini UAV– Relate to UAV of below a certain mass (yet to be defined) probably below 20 kg	Can be hand-launched, operating at ranges up to about 30 km
6	Micro UAV or MAV	A wing-span not greater than 150 mm, principally used for operations in urban environments, particularly within buildings
7	NAV – Nano Air Vehicles	Used in swarms for purposes like radar confusion or conceivably, if camera, propulsion and control sub-systems can be made small enough, for ultra-short range surveillance
8	RPH	Remotely piloted helicopter or vertical take-off UAV

Types of Agricultural UAVs

Agricultural UAVs are either fixed wing type or rotary wing types capable of STOL/VTOL. Most fly up to 400 ft.

General application of UAV in agriculture includes.

Plant Research

1. Hybrid phenology / trait assessment for breeding.
2. Canopy profiling.
3. Crop counting.



4. Temperature / pressure profiling.
5. Spore, dust, pollen collection.
6. Water quality assessments and survey.
7. Methane and CO₂ sensing.
8. Wirelessly collect data from ground sensors.

Crop Production

1. Precision Agriculture prescription data.
2. Crop status (growing stage, yield estimates, and so on).
3. Tiling/drainage evaluation and survey.
4. Time-saving pre-assessment for field tasks.
5. Drainage estimates and topography.
6. Planting evaluation and replanting requirements.
7. Pathogen introduction and tracking & Weed levels.

Crop Protection

1. Prevent birds that cause disease to crops.
2. Prevent birds from eating high value crops.
3. Identify wildlife that may consume crops.
4. Detect and track plant disease.

Advantages of UAV

1. Fly autonomously and on Demand.
2. Fly under Cloud Cover and deliver satellite images without cloud hazards.
3. Hand launch.
4. Fully automated flight & landing.
5. Monitor flight / live update of flight plan possible.
6. Capable of developing three-dimensional maps of the fields and the nearby terrain allowing the user to get a better idea of the layout.
7. Low-cost and on-demand sensing capabilities with minimal human involvement.

8. Not dependent on weather disrupted solutions (GIS & satellite).
9. Increases sampling performance by 30-35%.

Some of the Popular Applications of UAV in Agriculture

1. Aerial Application- Used for Crop Spraying or dusting; suitable for all kinds of complex terrain, crops and plantations of varying heights.
2. Pesticide Spraying- An UAV can identify whether a plantation requires spraying or not. Insect pest control in rice paddies, soybeans and wheat crops is extensively used all over world.
3. Disease Detection, Parasite Monitoring and Mitigation- Through built-in algorithms and multi band cameras in less time getting high-resolution aerial images by flying at a lower altitude, resulting in much clearer data and images.
4. Moisture Monitoring- Visual spectrum (RGB), near-infrared (NIR), and infrared/thermal remotely sensed data and some vegetation indices (VIs) are used for the soil moisture monitoring.
5. Crop Growth Monitoring- UAV-based RGB imaging delivers valuable data for productive crop monitoring.
6. Livestock detection and Tracking- Counting and monitoring of livestock spreaded over large areas by aerial imaging and video recordings.
7. Disease Outbreak Tracking- The extensively developed image processing framework is used for the detection and mapping of invasive woody weeds from remotely sensed red-green-blue aerial images.
8. Remote Aerial Monitoring- UAV helicopters are extensively used to perform aerial photography.
9. Weed Infestation Monitoring- The UAV has the capability of using a multi-band



multi-spectral camera with the objective of generating a weed map.

10. Create precise maps of nitrogen deficiencies- The agriculture drone units are guided by algorithms designed to pinpoint field locations that need nitrogen measurements.

Table 2 : A typical field statistics data that can be generated by an UAV

15.4 ha	Field Area
4.484 ha	Crop Area
29.12%	Crop Coverage

UAV Navigation-Control System

UAVs have sensor systems which provide an estimate of the vehicle's full state vector. The state vector consists of three position coordinates; three components of the velocity vector and three to nine parameters describing the vehicle's attitude.

In addition to state sensing and estimation, UAVs need control and guidance systems that allow them to manoeuvre in a way consistent with their mission.

The complete state of the UAV comprises its position, velocity, attitude, airspeed, angle of attack, side slip angle, and rotation (pitch, roll, and yaw) rates. Position, velocity, and attitude are also known as the navigation state.

The sensors used to measure these quantities are called navigation sensors. There are inertial measurement unit (IMU) and global positioning system (GPS) receiver.

Working Principle of UAV

The UAV is flown on site and when retrieve the farmers can extract the data and directly visualize it. Whether farmers need to change seeds, use more or less fertilizers or use different chemical altogether, that can increase the yields and decrease the expenses - Agricultural UAVs provide cost effective, reliable aerial imagery with better and more accurate big data. Survey data can be immediately examined and verified for quality in the field with tools like automated ground control point system, or data compression. The data can then be uploaded for automated 2D or 3D orthomosaic processing as well as analysis in the cloud. Field statistics data that can be generated by UAV is shown in **Table 2**.

UAVs Equipment and Uses

This typical equipment includes cameras for taking pictures and videos, infrared cameras, and sensors that will allow the UAVs to collect data and then analyse it. A Typical Agricultural UAV has the hardware configuration[9] as shown in **Table 3**.

TYPICAL UAV SENSORS

Visual Sensors

Equipped with High resolution, low distortion camera capable of producing images or video, which is applied for:

1. Aerial mapping and imaging
2. Plant counting
3. Surveillance

Table 3 : Typical UAV Hardware

On-board Sensors :	Humidity	Temperature	Pressure	Incident Light
Processors :	720 MHz dual-core Linux CPU			
Interfaces :	Wifi	Ethernet	Serial	USB
	Digital	Analogue	IIC	
Weight :	5.3lbs			
Wingspan :	4.9ft			
Payload :	Capacity -2.2lbs Swappable			



4. Photogrammetry and 3D reconstruction
5. Emergency response
6. Surveying and land use applications

Multispectral Sensors: These sensors are applied for

1. Plant health measurement
2. Plant counting
3. Vegetation index calculation
4. Water quality assessment

Thermal Infrared Sensors: These sensors are applied for

1. Surveillance and security
2. Heat signature detection
3. Livestock detection
4. Water temperature detection and water source identification
5. Emergency response

Light Detection and Ranging (LIDAR) Sensor

Most airborne LIDAR systems have a LIDAR sensor, a GPS receiver, an inertial measurement unit (IMU), an onboard computer and data storage devices. A typical Agricultural UAV has a short range, 270° scanning LASER range finder. It penetrates through vegetation and can perform plant height measurements by collecting range information from the plant canopy and the ground below.

Hyperspectral Sensor

Hyperspectral imaging (HSI) provides a detailed reflectance spectrum for every pixel in an image.

Hyperspectral sensors are used widely in:

1. Vegetation index calculation
2. Plant health measurement
3. Full spectral sensing
4. Water quality assessment
5. Spectral research and development
6. Mineral and surface composition surveys

Besides sensors, a typical agriculture UAV has one or more of the following application features.

GEOSPATIAL APPLICATIONS

Data are transformed into actionable information in order to generate real-time decisions.

Plant Height

An UAV can readily provide 3D data to analyse crop height and density from different angles.

Plant Counting

UAVS have Plant Counting algorithm that works by asking users to help identify parts of their field (ground, plants, rows, etc.). Based on the user's inputs, the algorithm identifies plant rows, determining the gaps within each row and thus generating the plant count.

Canopy Cover

An UAV can quickly assess crop coverage in later growth stages reported as a coverage percentage.

Automated Anomalies Detection

UAV generated 3D data is able to see anomalies in the field commonly associated with weeds.

Season Monitoring

Multiple flights of the UAVs throughout the growing season and at key decision points reveal changes, trends, patterns, and anomalies.

Crop Health Indices

Many UAVs carry agricultural vegetation indices to identify crop stress, track rogue plants and detect early infestations.

Some of the vegetation indices use only the Red, Green and Blue spectral bands.

Green-Red Ratio Vegetation Index (GRVI) and Normalised Green-Red Difference Index (NGRDI): These two are used for reflectance in the Red and Green parts of the spectrum.

Leaf Area Index: It characterises plant canopies.

Normalized Difference Vegetation Index (NDVI): It is the Ratio of the reflectance in the near infra-

Red and red portions of the electromagnetic spectrums.

$$NDVI = \frac{G-R}{G+R}$$

Visible Vegetation Index (VVI): It provides a measure of the amount of vegetation or greenness of an image using only the information from visible spectrum. It can be expressed as [10]

$$VVI = \left[\frac{1 - |(R - R_0)/(R + R_0)|}{1 + |(R - R_0)/(R + R_0)|} \right] \left[\frac{1 - |(G - G_0)/(G + G_0)|}{1 + |(G - G_0)/(G + G_0)|} \right] \left[\frac{1 - |(B - B_0)/(B + B_0)|}{1 + |(B - B_0)/(B + B_0)|} \right]^{1/w}$$

where, R, G, and B are the red, green, and blue components of the image, respectively; R_0, G_0, B_0 is vector of the reference green colour and w is a weight exponent that adjusts the sensitivity of the scale.

True colour images allow determining crop variation maps of an entire field.

Enhanced Normalized Difference Vegetation Index

This is a close equivalent to NDVI used through low flying UAVs and is correlated with leaf area values and plant vigour generating a Georeferenced Index Image.

Use of UAV in Agricultural Practices in Countries other than India.

UAVs are fast evolving into a robust tool for precision agriculture. In near future Agriculture industry will be the biggest user of this technology.

Most of the European nations, Canada, Australia and Japan and to a limited extent, USA have put UAVs to practical applications in agriculture.

Figure 1 shows low response from Asia and a non-presently conspicuous USA where FAA regulations levy a first time offence of \$10,000 to \$1,00,000 for flying a UAV for commercial purposes[11].

UAV in India

Agriculture, with its allied sectors, is the largest livelihood provider in India and a major contributor to Nation's Gross Domestic Product (GDP). India covers 2.4% [12] of the world's geographical area, yet it feeds 16.9% [12] of the world's population and 15% of the world's livestock.

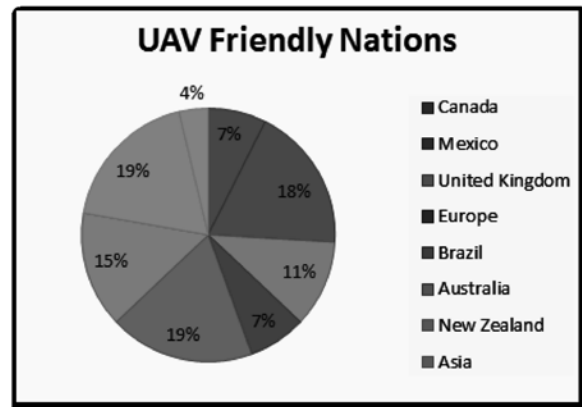


Figure 1 : Percentage Share of Major Countries having UAV-Friendly Skies-Friendly Ratings

GDP from Agriculture in India increased to 5131.90 IND Billion in the fourth quarter of 2015 from 2986.92 IND Billion in the third quarter of 2015. [13] More than 55% of Indian population is dependent on agro industry for livelihood. Indian Agriculture is confronted with several issues of agricultural productivity, remunerative prices for farmers; land policy, agrarian distress, crop damage due to natural calamity and so on. There is a further issue of low average productivity at the national level and high variation in it regionally.

For Example Punjab and Haryana have excellent agricultural productivity, while some parts of Rajasthan, Madhya Pradesh, Maharashtra, Chhattisgarh, Odisha, and Karnataka suffer from quite low yields. In India UAV application in agriculture is still in infancy, though UAVs can go a long way in aiding activities like:

1. Sowing seeds
2. Spraying pesticides
3. Crop insurance
4. Crop mapping
5. Gauge crop damage from natural calamities.

The "Pradhan Mantri Fasal Bima Yojana"[14] plans to use satellite imaging and remote sensing technology for quick estimation of losses and to help farmers and insurance companies in early settlement of claims.

Agriculture Insurance Company of India along with Skymet [15], has conducted tests in parts of Gujarat and Rajasthan to see how UAVs can be used to survey groundnut crops and help map crop diseases along with helping insurance companies settle claims.

On 05-October-2015 Minister of State for Agriculture & Farmers' Welfare, Dr. Sanjeev Kumar Balyan launched "KISAN" Project [C(K) rop Insurance using Space technology And Geoinformatics] of Department of Agriculture, Cooperation and FW, Ministry of Agriculture and FW.

The project proposed use of Space Technology and Geoinformatics (GIS, GPS and Smartphone) technology along with high resolution data from UAV/Drone based imaging for improvement in yield estimation and better planning of Crop Cutting Experiments (CCEs), needed for crop. Some of the UAV companies present in India are Precision Hawk, SkyMet, Amigo Optima, Quidich and Techbaaz [16].

Limitations

- *Flight autonomy-bound by Battery Capacity*

It can be defined as the amount of time a UAV can fly without landing due to lack of power. Flight autonomy takes into account the different aspects like the type of engine, the aerodynamics, the weight; wind conditions importantly the type of battery. One of the most common batteries for commercial UAVs is a Lithium Polymer battery, which provides around 2Ah of service to the UAV. It delivers one hour of autonomy with an engine that needs 2A to work, getting autonomy for 25 minutes considering regular conditions, with 5mph wind, having no load capacity [17].

- *Regulation in Countries like USA and India and Regulatory Condition for Commercial use of UAV in USA*

As per FAA Section 333 [18] under special rules for Certain Unmanned Aircraft Systems, the Secretary of Transportation determines if certain

unmanned aircraft systems may operate safely in the national airspace system; which types of aircrafts do not create a hazard to the users of the National Aerospace System, to the public or to the national security.

As per SEC. 334. PUBLIC UNMANNED AIRCRAFT SYSTEMS [19], the Secretary of Transportation can allow a government public safety agency to operate an unmanned aircraft weighing 4.4 pounds or less, if operated with the following guidelines:

- 1 UAV must fly below 400ft above the ground.
- 2 UAV must be operated only during the daytime.
- 3 UAV must be seen and maintained inside the visual line of the operator
- 4 UAV must be further than 5 miles from the closest airport, heliport, seaplane base, space port, or other location with aviation activities.
- 5 UAV must be flown within Class G airspace.

- *Regulatory Condition for Commercial use of UAV in India*

The Office of The DGCA through a Public Notice has declared that it is in the process of formulating the regulations for certification & operation for use of UAS in the Indian Civil Airspace. Till such regulations are issued, no non-government agency, organization, or an individual will launch a Unmanned Aerial System (UAS) in Indian Civil Airspace for any purpose whatsoever[20].

- *Technical Decisions*

There is still no international or even country – wise protocol of UAV development for agricultural applications. Hence no standard design has been patented or standardised for a given type of application.

Conclusion

New generation of engineers, developers and ministries worldwide have joined hands to incorporate environment friendly, accurate, data backed UAVs in agro and allied industries.



Under joint conduct by Mahalanobis National Crop Forecast Centre, Indian Space Research Organisation, India Meteorological Department, State Agriculture Departments and Remote Sensing Centres, Climate Change, Agriculture and Food Security (CCAFS), India too has joined the elite club of nations by carrying pilot studies of rice crop in Kurukshetra (Haryana), Shimoga (Karnataka), Seoni (Madhya Pradesh) and of cotton in Yavatmal (Maharashtra) during the Kharif season of 2015.

In Rabi 2015, similar studies were carried out in wheat yields of Karnal and Hissar (Haryana), Ahmednagar (Maharashtra) and Vidisha and Hoshangabad (Madhya Pradesh). Sorghum [Gulbarga (Karnataka)], Sholapur (Maharashtra) Raichur (Karnataka) will soon participate in similar studies in rice cultivation. UAV applications in agriculture and allied industries have a long way to go and people should welcome that. Precision farming with UAV will certainly take a giant leap in near future and on a global scale. In years to come no sky will be unfriendly for UAVs.

References

1. <http://www.agday.org/media/factsheet.php>, "Promote Ag Day", Agriculture Fact Sheet.
2. http://ec.europa.eu/eurostat/statistics-explained/index.php/Agriculture_statistics_-_the_evolution_of_farm_holdings, "EuroStat -Statistics explained".
3. <http://www.abs.gov.au/AUSSTATS/abs@.nsf/Lookup/4102.0Main+Features10Dec+2012>, "Australian Bureau of Statistics", "Farming - Big Business And Small", Para 4th.
4. <http://www.fao.org/rural-employment/agricultural-sub-sectors/crop-farming/en/>, Food and Agriculture Organization of the United Nations.
5. http://www.momagri.org/UK/agriculture-s-key-figures/With-close-to-40-%25-of-the-global-workforce-agriculture-is-the-world-s-largest-provider-of-jobs-_1066.html, "A new vision for agriculture".
6. http://www.momagri.org/UK/agriculture-s-key-figures/With-close-to-40-%25-of-the-global-workforce-agriculture-is-the-world-s-largest-provider-of-jobs-_1066.html, "A New Vision for Agriculture".
7. "Indian Express", "Drone Crop Surveys to Ease Farmers' Lives" by Mathew Joy Maniyamkott, Bangalore, Published: 24th August 2015.
8. "Unmanned Aircraft Systems, UAVs Design, Development and Deployment" by Reg Austin, page 37-38.
9. <http://www.precisionhawk.com>, "Hardware"
10. "The use of Unmanned Aerial Systems (UAS) in Agriculture" by Ioanna Simelli, Apostolos Tsagaris, para5.1 "Indices used in UAVs in Agriculture Research".
11. "The World of UAVs in Agriculture" By Robert Blair – Kendrick, IDAHO, U.S.A. page18 of 42," Fly The Friendly Skies".
12. http://censusindia.gov.in/Census_And_You/area_and_population.aspx
13. "India GDP from Agriculture", 2011-2016.
14. "Pradhan Mantri Fasal Bima Yojana (PMFBY)", "Acreage Discrepancy" pages14-15
15. The Economic Times, "Drones to help Rajasthan, Gujarat Farmers Detect Crop Diseases" by Madhvi Sally, ET Bureau Feb 19, 2015.
16. The Hindu, "Drones to help gauge crop damage", Oct. 6, 2015 Page 13, Para 3.
17. "MS&E 238:Leading Trends in Information Technology", page8, para2, by José Ruggiero, Pedro Vázquez, Enrique de Muguerza
18. https://www.faa.gov/uas/legislative_programs/section_333/, Federal Aviation Administration, Section 333 of the FAA Modernization and Reform Act of 2012 (FMRA), SEC. 333. Special Rules for Certain Unmanned Aircraft Systems, (b) Assessment of Unmanned Aircraft Systems.
19. https://www.faa.gov/uas/legislative_programs/section_333/, Federal Aviation Administration, Section 333 of the FAA Modernization and Reform Act of 2012 (FMRA). SEC. 334. Public Unmanned Aircraft Systems.
20. http://dgca.nic.in/public_notice/PN_UAS.pdf



Agriculture Fertilization using Unmanned Aerial Vehicle

**Johnson Tellis, John Nikhil Poyyayial,
Shrajan Bhandary, Jagath Biddappa**

*Sahyadri College of Engineering & Management,
Mangalore 575007*

✉ johnpayyayial@gmail.com

Abstract

This paper explores the use of commercial components to design and build an Unmanned Aerial Vehicle (UAV) capable of performing numerous missions in commercial and industrial scenarios. In agricultural sector, farmers usually face problems such as non-uniform sprinkling of fertilizers either to the crown of the tree or at the center of the crop fields, monotonous work of monitoring acres of land with lack of human resources and irregular meteorological conditions. The project aims to design an X8-Octocopter with self-sustained flight via wireless communication. The scheduler program manages the following tasks: controller input, data from the Inertial Measurement Units (IMU), GPS and compass, and motors controlled by Pulse Width Modulation (PWM) ports of the processor. Hence this paper provides reliable solution of UAV's with heavier payloads to carry fertilizers with considerable flight time.

Keywords: *Unmanned Aerial Vehicle; Aerially fertilize; X8-Octocopter; IMU; GPS*

Notations

$u(t)$: Controller output
K_p	: Proportional gain, a tuning parameter
K_i	: Integral gain, a tuning parameter
K_d	: Derivative gain, a tuning parameter
e	: Error
t	: Time or instantaneous time (the present)
τ	: Variable of integration; takes values from time 0 to the present t.

Introduction

Multirotor copters are emerging as a popular platform for unmanned aerial vehicle (UAV) research, due to the simplicity of their construction and maintenance, their ability to hover, and their vertical take-off and landing (VTOL) capability [1].

A multirotor copter is an under actuated force controlled vehicle with 6 degrees of freedom. Force actuation implies two motions: translational and rotational motion, which can be approximated as a double integrator system from command to altitude angle or horizontal position. The key to control such systems is to provide artificial damping through feedback of rotational and translational velocity [2]. By using the angular rates measured by the on-board gyroscopes and accelerometers, the rotational velocity of each of the rotors is manipulated for a stable flight. These are performed at a high baud rate by the on-board embedded flight controller.

The interest of the research community in the multirotor design can be linked to two main advantages over other comparable vertical take-off and landing (VTOL) UAVs. One, multirotors do not require complex mechanical control



linkages for rotor actuation, relying instead on fixed pitch rotors and using variation in motor speed for vehicle control. This simplifies both the design and maintenance of the vehicle. Second, the use of multiple rotors ensures that individual rotors are smaller in diameter than the equivalent main rotor on a helicopter.

Octocopter is a multirotor copter that is lifted and propelled by eight rotors. Unlike most of the copters, octocopters use four sets of identical fixed pitched propellers; four clockwise (CW) and four counter-clockwise (CCW). Propellers are classified by length and pitch. Generally, increased propeller pitch and length will draw more current. Also the pitch can be defined as the travel distance of one single prop rotation. In a nutshell, higher pitch means slower rotation, but will increase the vehicle speed which in turn uses more power. Generally a propeller with low pitch numbers can generate more torque. The motors don't need to work as hard so it pulls less current with this type of propeller. A higher pitch propeller moves greater amount of air, which could create turbulence and cause the aircraft to wobble when hovering. When it comes to the length, propeller efficiency is closely related to the contact area of a prop with air, so a small increase in prop length will increase the propeller efficiency. For larger copters that carry huge payloads, large propellers and low-KV motors tend to work better. These have more rotational momentum and will easily maintain the aircraft's stability [3].

Proposed Framework

Construction

Keeping in mind, maximum stability and the build weight to be as minimal as possible, aluminium alloys were used for arms and base plate. Compared to other materials, aluminium is lighter than carbon fiber with similar properties of rigidity and strength. To obtain the required calculated thrust, EMAX 380KV brushless motors with 15*4 inch carbon fiber propellers were used to obtain expected performance to carry the payload. For reliable stability and flight controls, 3DR's Pixhawk flight controller was utilized as

the brain of the Octocopter [4]. Other sensors such as IMU, GPS and compass were also embedded on the copter. The controller was configured using Mission Planner software. In order to power all the equipment's in the copter, 24V, 4000mAH LIPO batteries were used. In addition to catch a bird's eye view, a three axis gimbal with aerial camera GOPRO was embedded with ground station having a TFT screen with BOSCOM's 5.8GHz 500mW video transmitter for live feed from the copter to the screen.

Fertilizer System

It consists of a tank with a pump placed under the octocopter for pumping fertilizers through steel pipelines in each arm. Each arm consists of a sprinkler attached to the end of pipe. The sprinkler system is triggered using a switch. The switch takes signals from the hand-held remote control and is switched ON or OFF depending on the user application. This allows the user to switch it whenever required, to avoid pollution and economize operations.

PID System

The proportional–integral–derivative controller (PID controller) plays an important role in the keeping the UAV stable and safe in mid-air. A block diagram of PID controller is shown in **Figure 1**. The PID controller continuously calculates an error value which is the difference between a desired set-point and a measured process variable. The controller attempts to minimize the error over time by adjustment of a control variable, in this case the rotational velocity of the motors[5]. The wireless transceivers use Serial Peripheral Interface (SPI) to send control signals from the hand-held controller to the Octocopter. The IMU use I2C to send acceleration, stabilization and direction vectors. The controller then uses the data provided by the IMU and compares it with the values from the hand-held controller. The PID controller then calculates the required speed at which motors should rotate and hence stabilizes the orientation of the vehicle.

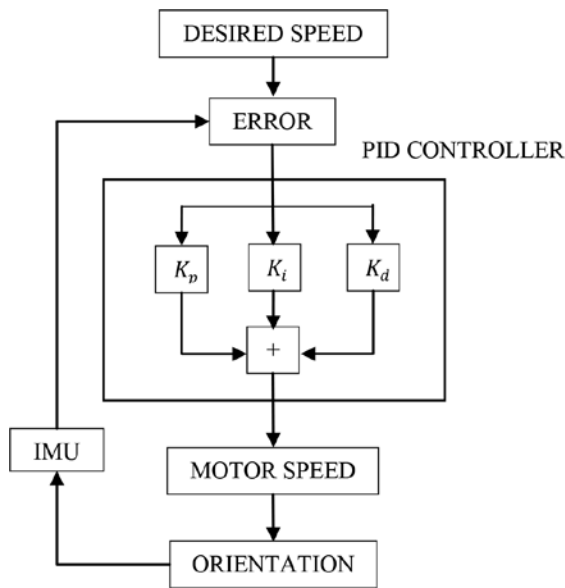


Figure 1: Block diagram of the PID system.

The control variable is given as:

$$u(t) = K_p e(t) + K_i \int_0^t e(\tau) d\tau + K_d \frac{de(t)}{dt} \quad (1)$$

The values of the proportional, integral and differential parameters must be tuned appropriately to navigate properly in different flight modes as well as harsh weather conditions [6].

Experiments & Results

Calculations

Thrust = 2*[Weight of the drone + Weight of carried object] + [Total from above * 0.20]

Inputs: Weight of the drone=2.3Kg

Weight of the carried object = 2.7Kg +0.8Kg (some more extra we have added)

i.e., Thrust = 2*[2.3+2.7+0.8]+(2*[2.3+2.7+0.8]) *0.20}

=11.6+ [11.6*0.20]

=13.92Kg

Thrust per motor = Total thrust / Number of Motors

= 13.92 / 8

= 1.74 Kg

Max current=Battery capacity*Discharge rate/ (1000*number of motors)

For a given 8 motors, propeller size 15*4 inch, 22.2V, 4000mAh 35C two LIPO batteries.

Max current=4000mAh*40/ (1000*8)=20A.

Total current=160A.

Power=VI

Power=22.2*20

=444 W (for 1 motor)

Power = 444*8

=3552 W (for 8 motors)

Flight Time

A constant current draw of 25A from a 4000mAh will get you, 4000mAh/ (1000*25) =0.16 hours.

i.e., 0.16*60= 9.6 minutes with one battery.

Hence with two batteries it gives the flight time of 19.2 minutes. Experimental values of x and t axis of accelerometer with respect to time are shown in **Figure 2 to Figure 4**. Further, experimental values of x, y and z axis of gyroscope with respect to time is shown in **Figure 5 to Figure 7**.

Flight Modes

Stabilize : Stabilize mode allows the user to fly the vehicle manually, but automatically-levels the roll and pitch axis. Pilot's roll and pitch input control the lean angle of the copter. When the pilot releases the roll and pitch sticks the vehicle

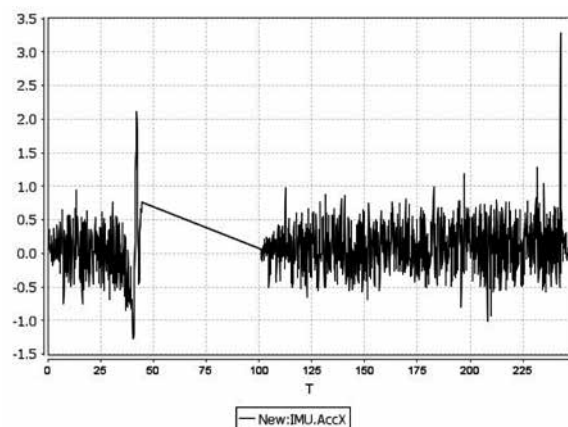


Figure 2 : Experimental value of x-axis of accelerometer with respect to time

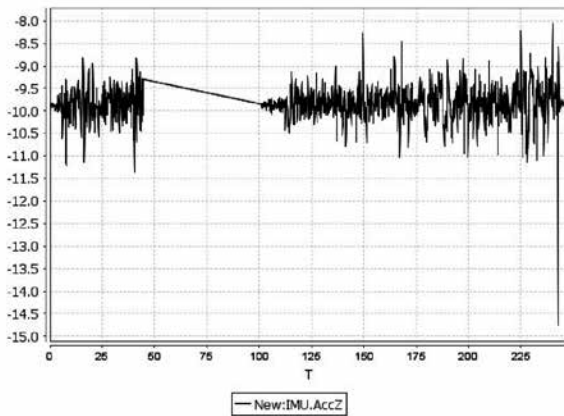


Figure 3 : Experimental value of y-axis of accelerometer with respect to time

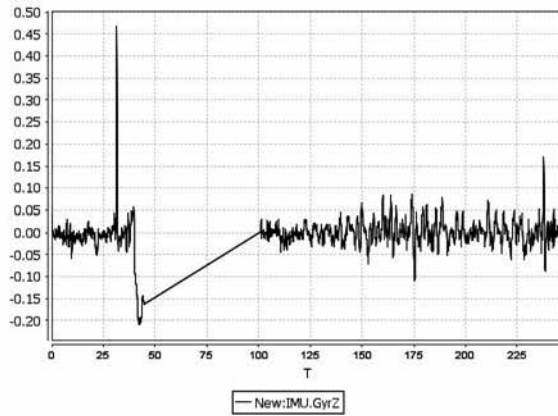


Figure 6 : Experimental value of y-axis of gyroscope with respect to time

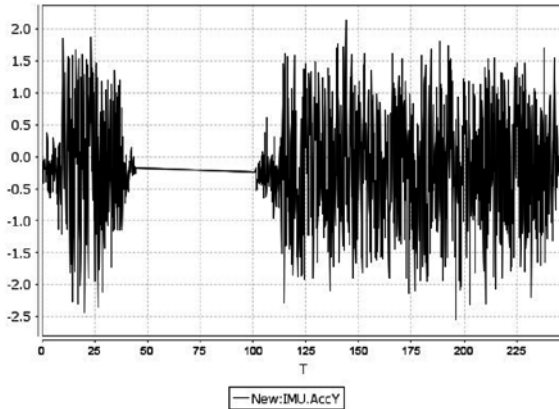


Figure 4 : Experimental value of z-axis of accelerometer with respect to time

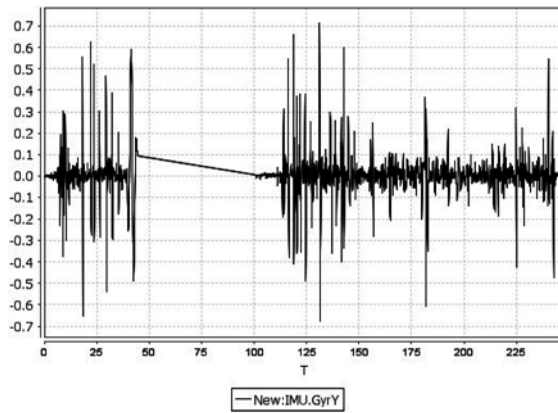


Figure 7 : Experimental value of z-axis of gyroscope with respect to time

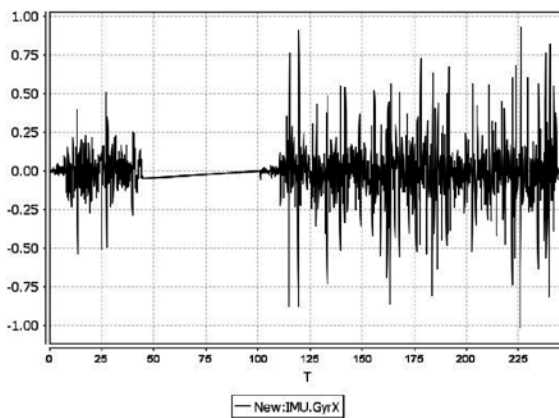


Figure 5 : Experimental value of x-axis of gyroscope with respect to time

automatically levels itself. The pilot needs to regularly input roll and pitch commands to keep the vehicle in place as it is pushed around by the wind. Pilot's yaw input controls the rate of change of the heading. When the pilot releases the yaw stick the vehicle will maintain at its current heading. Pilot's throttle input controls the average motor speed, meaning that constant adjustment of the throttle is required to maintain altitude. If the pilot pulls the throttle completely down the motors will go to their minimum rate and if the vehicle is flying it will lose attitude control and tumble.

Altitude Hold: In altitude hold mode, the copter maintains a consistent altitude while allowing roll, pitch, and yaw to be controlled normally. When altitude hold mode is selected, the throttle is automatically controlled to maintain the current altitude. Roll, Pitch and yaw operate the same as

in Stabilize mode meaning that the pilot directly controls the roll and pitch lean angles and the heading.

Loiter: Loiter Mode automatically attempts to maintain the current location, heading and altitude. The pilot may fly the copter in Loiter mode as if it were in manual. Releasing the sticks will continue to hold position. Horizontal location can be adjusted with the Roll and Pitch control sticks with the default maximum horizontal speed being 5m/s. When the pilot releases the sticks the copter will slow down to a stop.

RTL (Return-to-Launch): In return to launch (RTL) mode, the copter navigates from its current position to hover above the home position. The copter will first rise to Return-to-Launch-Altitude (RTL_ALT) before returning home or maintain the current altitude if the current altitude is higher than RTL_ALT.

Auto: In Auto mode the copter will follow a pre-programmed mission course stored in the autopilot which is made up of navigation commands (i.e. way points) and do commands (i.e. commands that do not affect the location of the copter including triggering a camera shutter). During the mission the pilot's inputs such as roll, pitch and throttle are ignored but the yaw can be overridden with the yaw stick. This allows the pilot to aim the nose of the copter as the copter flies the mission. The X8 octocopter with hand held controller is shown in **Figure 8**.

Conclusion

The propulsion system enabled the octocopter to successfully carry up to 5kg of fertilizer. The



Figure 8 : The X8-Octocopter with the hand-held controller

combination of speed and power allowed the copter to cover 3acres in an hour which is 20 times faster than normal method of spraying. The flight controller integrated with the copter instantly and precisely responds to the pilot's input and can successfully switch between all the flight modes. The wave points were given to the octocopter using the software for autonomous sprinkling with the aid of the GPS.

Acknowledgement

Authors are thankful to Dr. Manjappa Sarathy, Director of Research and Consultancy at Sahyadri College of Engineering and Management for his valuable guidance and suggestions. Authors are also grateful to Dr. U. M. Bhushi, Principal, Sahyadri College of Engineering and Prof. Steven L Fernandes, Electronics and Communication Department, Sahyadri College of Engineering and Management for their encouragement and support.

References

1. P. Pounds, R. Mahony, and P. Corke, "Modelling and control of octorotor robot. In: Australasian Conference on Robotics and Automation (ACRA)", 2006.
2. H. Huang, G. Hoffmann, S. Waslander, and C. Tomlin, "Aerodynamics and Control of Autonomous Octorotor Helicopters in Aggressive Maneuvering. In: Proceedings of the IEEE International Conference on Robotics and Automation (ICRA), p. 3277-3282, 2009.
3. Paul Edward, Ian Pounds, "Design, Construction and Control of a Large Quadrotor Micro Air Vehicle. In: A thesis of Philosophy of the Australian National University, 2007.
4. Lorenz Meier, Petri Tanskanen, Lionel Heng, Gim Hee Lee, Friedrich Fraundorfer, Marc Pollefeys (). PIXHAWK: A Micro Aerial Vehicle Design for Autonomous Flight using Onboard Computer Vision. In: Proceedings of European Community's Seventh Framework Programme (FP7), 2007-2013.
5. https://en.wikipedia.org/wiki/PID_controller.
6. B. Kada, Y. Ghazzawi. "Robust PID Controller Design for an UAV Flight Control System. In: Proceedings of the World Congress on Engineering and Computer Science 2011 Vol II WCECS 2011, 2011.



Autonomous Mobile Robot in Agriculture

**C. Vignesh, P. Anush, B. Jagadeeswaran,
N. Ranjith Raj, P. Srinivasan,**

*Department of Mechatronics, Kumaraguru College of Technology,
Coimbatore, 641049*

✉ vigneshmay95@gmail.com

Abstract

Nowadays scarcity of labours in agricultural sector is higher and will become worse in coming years. Main objective of the present study is to introduce autonomous mobile robots “Agri-bot” in agricultural field to automate farming processes and thereby to reduce labour issue and automation of cultivation. For various activities in agriculture sectors such as irrigation, fertilizer pouring, spraying pesticides for crops etc., we are using an automated guided vehicle “Agri-bot” type mobile robot for cultivation. This robot is assisted by Internet of Technology (IoT), image processing and centralized decision making for delivery of water, fertilizer, and spraying pesticides. With this technology the agri-bot will monitor the live status of crops and update to web for centralized monitoring, records all the data about cultivation process for future use.

The agri-bot will measure moisture content level, soil fertility level, humidity level and NPK-1test level for analysis. If required parameter levels are not meet the central control will actuates the mobile robot to pour the necessary fertilizers like potassium, nitrogen and phosphate etc., to the field. Remedial actions for certain problems in farming like fungal attack, insect attack are identified by the robot by sampling method and remedial actions are taken by the robot as per human instructions. The centralized data set could help in planning the future cultivation requirement form the past experience.

Keywords: *Image processing; Moisture content; Fertilizer; Agriculture automation; IOT*

Introduction

Agriculture is humankind’s oldest and still its most important economic activity, providing the food, feed, fibre, and fuel necessary for our survival. With the global population expected to reach nine billion by 2050 [1], agricultural production must double if it is to meet the increasing demands for food and bioenergy. In the current generation most of the countries do not have sufficient skilled man power specifically in agricultural sector and it affects the growth of developing countries. So it’s a time to automate the sector to overcome this problem. In India there are 70% people dependent on agriculture [1]. So we need to study agriculture. Given limited land, water and labour resources,

it is estimated that the efficiency of agricultural productivity must increase by 25% to meet that goal, while limiting the growing pressure that agriculture puts on the environment. Robotics and automation can play a significant role in society meeting 2050 agricultural production needs.

For six decades robots have played a fundamental role in increasing the efficiency and reducing the cost of industrial production and products. In the past twenty years, a similar trend has started to take place in agriculture, with GPS- and vision-based self-guided tractors and harvesters already being available commercially. More recently, farmers have started to experiment with autonomous systems that automate or augment operations

such as pruning, thinning, and harvesting, as well as mowing, spraying, and weed removal.

During the nineteenth and twentieth centuries, AKA the eighteen and nineteen hundreds, was a very busy time for agricultural development. During this time period, some of our modern agricultural machines, such as the lawnmower and the tractor, were invented and put to use worldwide [2]. In that period the tractor was not only used mainly for agriculture purpose, but also transport support.

Further, the lawnmower is used to cut the grass surface in an even height. After some time the first agriculture robot was invented. These robots are used for harvesting plants with human support. Most of them used to reduce the labours. For this generation we need to develop the performance of the agri-bots to improve the agriculture base. A robot called WP5 is used in agriculture field to pick the pepper from the plant [3]. It has two cameras in the gripper to help the robot to detect the fruits. We are also designing a similar type of robot to measure the moisture, temperature, pH level of the soil and provide the necessary water. And also the robot could be used to harvest the fruit and packing the fruit and also it could find about the quality of the fruit. By all these properties the robot is automatically done its working daily.

Working Principle of the Robot

Agri-bot is fixed with tri wheel concept base. To control the direction of the robot we can trigger the either motors. To go left the left side motor is kept at off mode and right side motor is given the pulse width modulation (PWM) signal to driver for running the motor, this will give the robot the turning action required in left side vice versa for right hand side turning direction. Base of agri-bot is fixed with an actuator which has a 3 degree for the arm.

The arm is fixed with the rubber gripper, used to pick the fruit from the plant; attachment of image sensor for identification of the fruits over the gripper for more accurate sensing of the object. Lighting for the image sensor is fixed on gripper's

i.e. the movable arm. When the image sensor sense the fruit then the agri-bot moves close to the plant, align itself to the position of the fruit and the arm do the correction in order to hold the fruit. Then an actuator with a sharp knife will release the cord by cutting it. Cultivated fruit are placed in storage container present the agri-bot. Thus finishing this cycle, the agri-bot moves towards to next plant, repeat the same procedure.

Before moving to next plant, the health condition of plant is monitored for requirement of the supplementary minerals, amount of water required are sensed; for this on board sensor are used to measure the pH level, moisture level, and temperature level of the plants soil and fruits colour using

various sensors are present in agri-bot. With these data the centralized control unit can dispatch the water with required menials through controller centralized pluming system.

Design

The robot arm and arm base are shown in **Figure 1** to **Figure 3**.

Future Scope

The agri-bot was designed for cultivation of a single crop namely tomato's, the reason choose this crop due the lesser time duration for the cultivation of the tomato. This concept could be enhanced for various other air borne crops too. Future work, the plantation to cultivation the

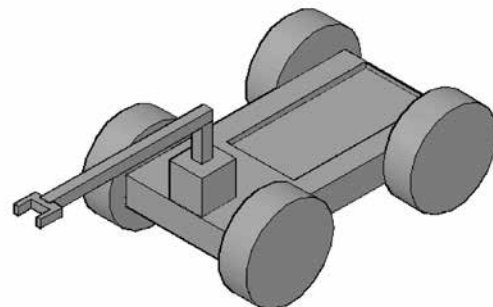


Figure 1 : Robot arm with base

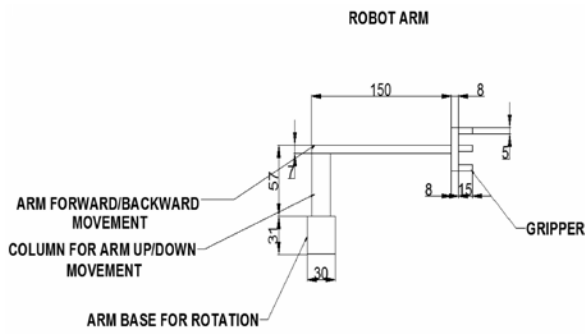


Figure 2 : Drawing of Robot arm

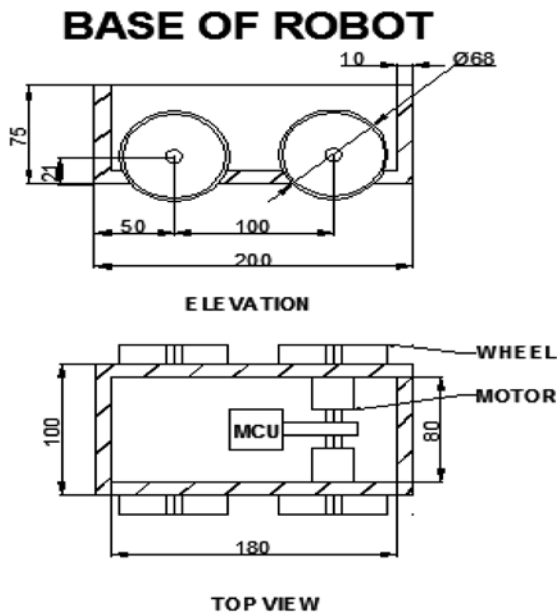


Figure 3 : Drawing of Robot base

entire life cycle of the crops will be taken care by the agri-bot with addition a AGV concept for better handling capabilities and multi functional arm to handle the various stages of the cultivation.

Conclusion

Agri-bot was developed and testing the various functionalities of it. The finding of the work is that by having agri-bot the indoor farming could be revolutionized with the 4th industrial revolution. In recent years, problems faced by farmer, have especially to find human labour becoming time consuming and resource wastage. This situation plays a major role because a single farmer, who can't produce a huge volume of cultivation. Agri-bot will assist the farmer to cultivate a large production. Our project "Agri-bot" will be farmer's friend to solve labour problems, timely supply of minerals watering the plants and cultivating it.

References

1. IEEE, "Robotics and Automation Society- Agriculture Robotics and Automation".
2. G D K Dattatraya, M V Mhatarde, M Shrihari, S G Joshi, "Robotic agriculture machine – International Journal of Innovative Research in Science", Engineering and Technology.
3. www.cropsrobots.eu – WP5 fruit picking robot.



Concept of VAL (Varying Axial Load) Application for Structural Qualification of an Interstage Structure of a 3T Class Launch Vehicle : Evolution and Validation

S S Resmi, Selvakumari D Rachel

Structural Design and Engineering Group, STR Entity

Vikram Sarabhai Space Centre, Thiruvananthapuram, 695022

✉ resmi_deepu@vssc.gov.in

Abstract

Interstage structures of launch vehicles are subjected to a set of loads including circumferentially varying axial load, bending moment (BM) and shear forces. These loads are usually specified in terms of loads/ moments on both ends of the structure. Generally, a concept called equivalent axial load is worked out and made use of during the design and later for qualifying the structure on ground before flight. For an interstage structure that was recently designed the loading was found to be unsymmetrical over circumference and could not be easily reduced to an equivalent axial loading. Hence the procedure for design and qualification methodology was deviating from the usually followed routine ways and is novel for the present design. So estimation of interface loads (as design inputs) had to be necessarily carried out from a large model representing the vehicle structure along with adjoining structures with known loads applied at appropriate locations. This exercise was carried out for flight condition as well as for structural qualification level condition with the test adaptors above and below the interstage. Strains and displacements were predicted using empirical calculations and FEM (commercial code-NASTRAN) employing these interface loads. Strain gauges, LVDT, DIC (Digital Image Correlation) and Photo-elasticity were used to measure the response of the prototype under qualification level loads. Comparison between prediction and measured data is presented along with the details of degree of refinement of the FE model. This paper highlights the process of determining the loads as Varying Axial Load at the interface of the structure during structural qualification level test and validation of the FE idealization with test data.

Keywords : *Varying Axial Load; Launch Vehicle*

Introduction

Launch vehicle design has become presently more challenging with the requirements for faster realisation with higher reliability, repeatability, lower cost and better payload capability. To achieve these objectives the cycles of design, fabrication, and qualification of launch vehicle structures are crucial in terms of time, quality and

cost. Launch vehicles are built as an assemblage of several stages which may be solid, liquid, cryo /semi cryo, etc. depending on the propulsion systems employed. In multi-stage launch vehicle, the inert stages, which have performed their function, are jettisoned sequentially as flight progresses. This is enabled by staging/separation systems which are essentially pyro / explosive

based systems. Launch vehicle structures play following vital roles:

- Provide necessary external shape as directed by the aerodynamic considerations
- Provide housing for the payload, propulsion, guidance and control systems, etc.
- Withstand the load and environmental conditions.
- Shall be of lightweight and cost effective in construction, ensuring structural integrity while being reliable.

The inter-stage structure (ISS) (**Figure 1**) dealt with in this paper, is part of the core vehicle of a 3T class launch vehicle. In addition to being a primary load bearing structure, the ISS also houses a few propulsion system modules. The structure experiences both tensile and compressive loads during different flight regimes. Traditionally, design is carried out for circumferentially uniform tension or compression such that all parts of the structure experience the same stress. The main loads experienced by a primary structure in a launch vehicle include Axial force (AF) and



Figure 1 : The Inter-stage Structure (ISS)

Bending moment (BM). These two are combined to form an Equivalent Axial Load (EAL) which generates the same stress level as the AF and BM together.

Concept of Equivalent Axial Load

$$EAL = P_a + P_b$$

From bending equation, $\sigma = M y / I$

$$P_b = \sigma * A = 2M/R$$

$$EAL = P_a + 2M/R$$

where

EAL = Equivalent axial load

P_a = Axial load

M = Bending moment, and

R = Radius

P_b = Equivalent axial load due to bending moment

I = Moment of Inertia

y = Distance from the neutral axis

Actual structures have one or more cut outs - rectangular or circular openings for vehicle integration related purposes; the portions near and around the cut out are suitably modified to compensate for weakening caused by the opening. The EAL concept, since it applies an artificially greater load at many areas of the structure, may cause unnecessary reinforcement around the cut out area leading to increase in mass. EAL concept is suitable for structures subjected to inertia and aerodynamic loads, as aerodynamic bending moment can act in any plane. But for

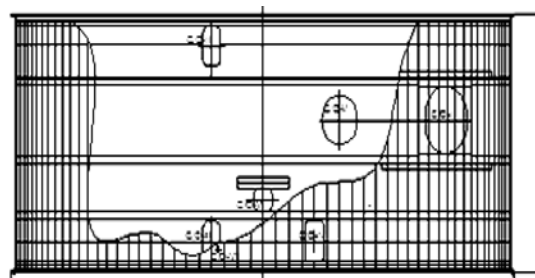


Figure 2 : Configuration of ISS Structure

structures experiencing concentrated load, EAL is not suitable. A more accurate representation of the load, if available, has been used to design and qualify an optimum aerospace structure for flight. For this interstage, the strapons are attached to the fore end of the core stage; the axial thrust load is being transferred at a thrust transfer point located just 4m from the FE of ISS. So it was essential to deviate from the EAL concept during the design and qualification phase simulating a more realistic load distribution at the interfaces.

This paper highlights the two phases followed for the qualification process of ISS, namely

estimation of non-uniform loads for testing purpose

validation of FE analysis results [strain and displacements] with test data.

Brief Description of Geometry

The ISS is designed as a closely stiffened shell structure with externally placed axial stiffeners of hat section [placed close to each other] and three rings in between two interfacing rings at fore end and aft end. The diameter and height of the structure is 4000mm and 1650mm respectively. The D/t ratio is approximately 3200mm. (Figure 2). Closely spaced hat stiffeners (placed in the axial direction) are used to enhance the buckling strength of the structure. These are separate components fastened to the shell outer surface, and running parallel to the vehicle axis. Ring stiffeners attached to the inner side of the stiffened skin serve as local hard points for mounting of propulsion system modules including 9 nos. of He gas bottles. There are 9 cutouts in this hardware, the maximum sized one being 500 mm x 500 mm.

Load Cases for Design

Loads acting on the structure vary with respect to flight sequence. The following load cases were considered for design of ISS.

Load Case 1: Tension- non uniform (LC_1)

Load Case 2: Tension- uniform (LC_2)

Load Case 3: Compression. (LC_3)

Load cases 2 & 3 were used for the conceptual design phase and the final design checks and qualification were carried out for load case 1 & 3.

Summary of Design Process.

The preliminary design of freezing the sizes / shapes of components was carried out using empirical design equations. Later on a detailed FE model of the structure with all cutouts (9 nos) extending over a part of the vehicle was prepared for detailed design, and the design was updated based on the FE analysis.

Description of the FE Model: Design Phase

Two different FE models were used:

Flight model, of the ISS structure as a part of the core stage [Figures 3(a) and 3(b)].

Structural qualification Test setup configuration model [Figure 4(a), Figure 4(b)].

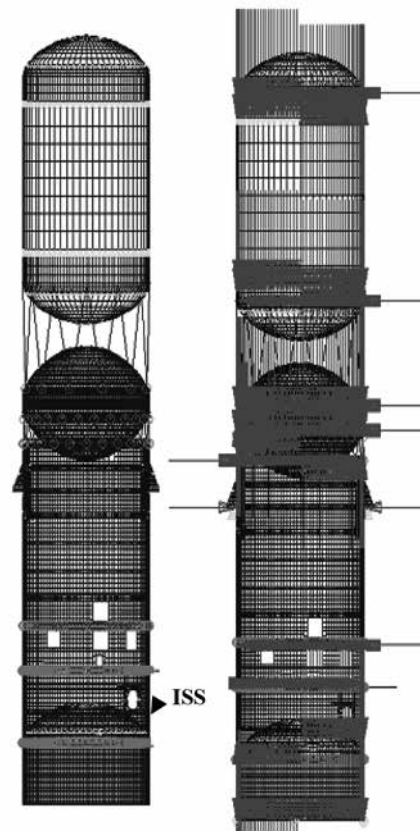


Figure 3(a) : Integrated FE model

Figure 3(b) : FE model showing loads applied as in flight

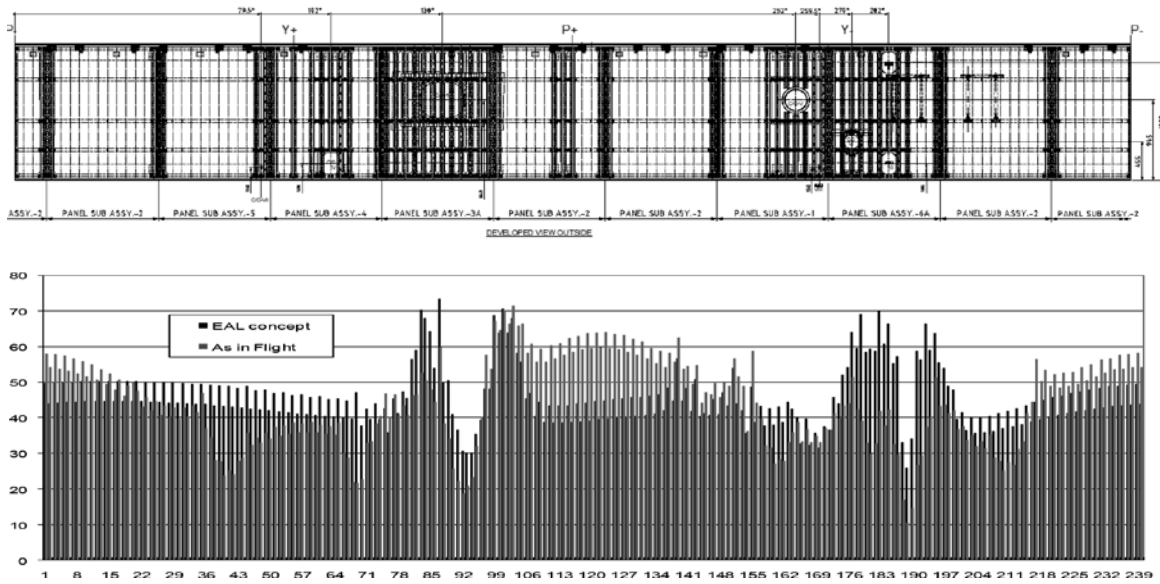


Figure 3(a) Distribution of loads at the Fore end Interface from FE Analysis, for Uniform Loading (EAL) and as in Flight Loading

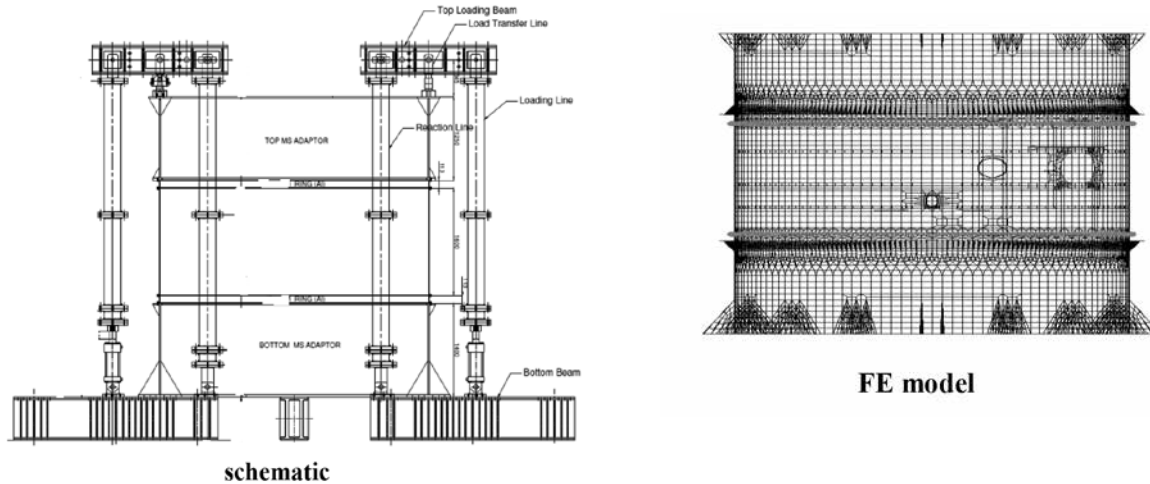


Figure 4(b) Configuration of the test setup

The structure was idealised in PATRAN with shell elements (CQUAD4) and beam elements (PBAR). The shell part of the structure, ring stiffeners, the end rings etc were idealised with shell elements. The stiffeners were idealised using beam elements which share nodes with the idealised skin.

The following features of the beam element of NASTRAN FE were used:

CG offset: Since the centroid of the stiffeners are non-coincident with the skin.

Beam orientation vector: Since the beam cross section orientation with respect to the local skin is to be effected.

Stress recovery points: Since extraction of stresses and strains are required at the most stressed locations of the stiffener, this option was also employed.

At the interfaces between structures, Multi-Point Constraint of NASTRAN FE package (MPC) with all the three translational DOF were made

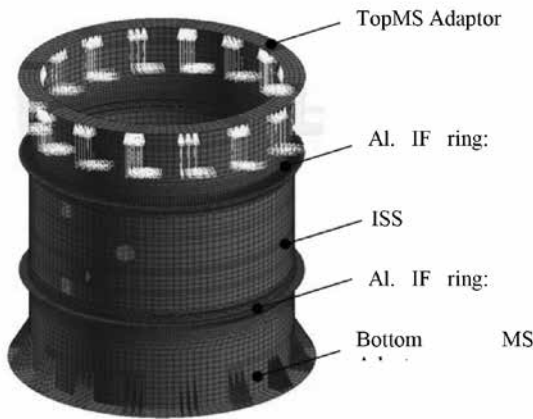


Figure 4(c) Configuration of the test setup: FE model(EAL) and as in Flight Loading



Figure 4(d) Configuration of the test setup

use of to represent the interface fasteners.

Total number of element in the model:

Integrated model: 65000

Test setup model: 30000

Total MPCs used : 792 in Integrated model & 480 in Test set up model.

Being part of a launch vehicle, ISS experiences loads from the structures above and below it. Since the ISS is located near to the aft of the vehicle, loads on all the other structures above the ISS were considered. To estimate the loads on ISS,

a FE model of large portion of the entire vehicle was used. (ref. **Figure 2(a)**). The ‘integrated’ model consisted of eight idealised structures in all with a half portion of tank below it. Loads were applied at defined locations as axial force, BM and SF (ref. **Figure 2(b)**); estimated on the fore side and aft side interface as distributed axial force along circumference. **Figure 2(b)**.

The load distribution on the interface of ISS was obtained from NASTRAN with the feature of ‘MPC force transmitted through the MPCs which were used to interconnect the inter stage structures above and below it. The distribution of interface load to the aft and fore end of ISS was obtained. The interface loads (ref. **Figure 3**) is a non-uniform distribution which has peaks around the cutout corners, and at axis (P+/P-) locations where the axial thrust of the solid boosters get transferred in the core stage of the launch vehicle. The fig. also shows the distribution of interface loads when EAL is applied at the AE nodes of the idealized model, constraint being provided at the thrust transfer locations at P+ & P-.

The design was to be validated by a structural qualification test before the impending flight. If the structure is tested with EAL, the panels at P+ & P- axis regions will be under tested., and application of higher EAL is not the solution since that would exceed the capacity of bolts provided at the interface and call for undue tension stress to the designed hardware.

This gave rise to the problem: How to simulate this loading on the flight structure while conducting the structural qualification test at ground.

The distribution (LC1 in sec. 3) is essentially a 240 point distribution, in that the load value at the 240 fasteners at

the top interface of the inter stage is to be recreated to simulate flight loads in the test setup. Thus an altogether

different approach to the qualification loading scheme had to be evolved to qualify the hardware for flight.

Proposed Structural Qualification Test Set-up

The test setup consists of a different stack of structures [sub assembly] than the idealized flight configuration.

The test article consists of prototype ISS, two nos. of Mild steel (MS) adaptors interfaced with two nos. of aluminium adaptor rings, one each at top and bottom. This test set-up is mounted on a test bed and loaded using a loading scheme consisting of 16 loading jacks, the loading of each jack had to be controlled independently. **(Figure 5)**. The primary difficulty faced was the finalization of the pattern of differential loading across the 16 jacks to accurately recreate the 240 point desired distribution at the fore end and aft end sides as experienced by the hardware during flight. As a first step towards solving the problem, an idealization of the test set-up to simulate the qualification of ISS as close to the actual was essential., and then the quantification of the loads at the 16 locations.

VAL Concept: evolution

Two possible procedures were thought of to estimate the 16 point loading:

Procedure 1: An analytical solution whereby the 240 point distribution created by each of the

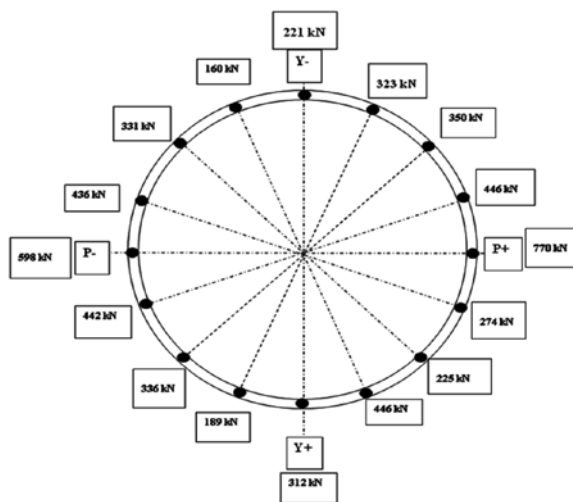


Figure 5 Finalised layout of loads at the 16 jack locations

16 jacks separately (only 1 jack loaded at a time) is first calculated with FE (16 such distributions now available) and then a logic is to be found out to apply 16 weight factors to those distribution to recreate the desired 240 point distribution. However these 16 weight factors could not be calculated easily, the 2nd procedure was followed.

Procedure 2: In this method, a reverse procedure is followed. In place of applying 16 point loading to create a [target] 240 point distribution, the target 240 point distribution is applied as a 240 point loading on the desired part of the inter stage and the non-uniform reactions caused by this loading on the 16 jacks is estimated.

Single point constraints (SPC) constraints of NASTRAN FE package are applied to the location of loading jacks to obtain these reactions. From the previous analysis procedure a distribution consisting of 16 reactions were obtained, at the jack locations. In the next step, these reactions were applied as loading on the structural test set-up and the resulting 240 point distribution at the fore end interface of the inter stage was extracted from MPC forces of the post processor of NASTRAN FE package. This was then compared with the actual distribution from the flight integrated model.

Iterations in the loading distribution were carried out in the 16 point loading scheme of structural qualification level test to get a better match with the target distribution of interface loads of the ISS as in flight. **Figure 6** shows the distribution finally obtained for the test set-up vis-à-vis as in the flight case.

The next phase was the planning of instrumentation scheme.

Instrumentation Scheme for Test

The structure was required to be qualified for the design load cases and the capacity of the structure to withstand these load cases is to be physically demonstrated on ground before being qualified for flight use. Hence, meticulous effort was made to plan the instrumentation scheme such that the qualification test captures the deformation

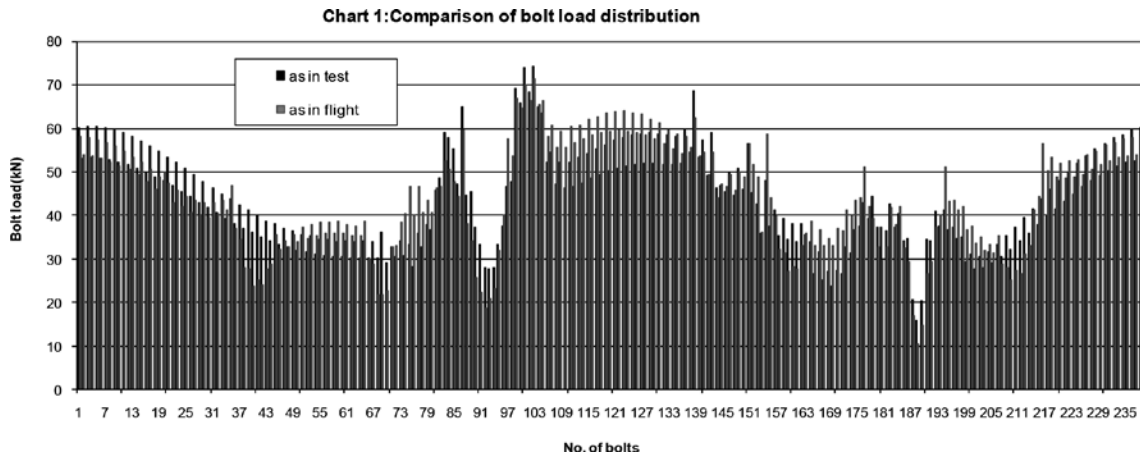


Figure 6 : Distribution of loads obtained from FE analysis at the interface at FE, for as in flight loading and the proposed design qualification level test

behaviour (strains and displacements) of the structure adequately. The following are the important aspects addressed at this stage. The locations for instrumentation were fixed to measure locations of high /localized stress gradients and stress distribution in addition to displacements.

Displacement measurements using DTs (Displacement Transducer) helped later to estimate the ring stiffener rotations and cutout opening at the maximum sized cutout (500 mm x 500 mm Approx).

Location and Number of Strain Gauges

On skin outside and inside

- surfaces: axial and hoop directions: 100 nos.
- Stiffener crown: axial direction: 92 nos.
- Ring stiffeners: at web: hoop: 7 nos.
- End rings: radial/axial direction: 4 nos.

Location and Number of DTs

- End rings: axial dir: to measure axial shortening of the structure: 8 nos.
- Skin: radial: 4 nos.
- Cut out horizontal edges: 2 nos.
- Ring stiffeners: at web ID and OD: axial direction 2 nos.

Strain Gauges in Stress Concentration Zone near Cutout :

Cutouts are known locations of stress concentration; the extent of stress concentration depends on various factors like cut out size and shape, radius of cutout corners and the method of stiffening provided at the cut out location. The common cut out reinforcement schemes includes enhanced shell thickness and provision of reinforced stiffeners close to the cut out edges. The highest value of stress is observed close to the cut out corners where high stress gradient is also present. This high gradient poses problem in strain prediction. This depends on accuracy of the FE model idealizing the actual local geometry at cutout corner zones and the actual location of the strain gauge mounted on the hardware vis-a-vis the location on the FE model where prediction is made; otherwise large mismatch can occur.

Hence additional whole field measurement methods- the Digital Image Correlation [DIC] technique and the method of photo elastic coatings were also employed, at six critical locations in the structure. These locations were concentrated at two out of the nine cutouts existing in ISS.

Prediction for strains at the strain gauge locations on the skin was obtained directly from NASTRAN FE package. For stiffeners which were idealised using beam elements, strain was estimated from values of stress - axial and bending, at stress



recovery points. Displacement values at all the instrument locations were taken from the contour of axial/radial displacements. The predictions for the strains and displacements thus extracted from the NASTARN FE package were provided to the testing agency much ahead of the scheduled date of test.

Qualification Test Results

Test were carried out for three load cases as mentioned in Load cases for Design Section.

Comparison of predicted and measured strain for the VAL

The predicted and measured strains in the skin, stiffener, ring stiffeners are compared and the percentage variation is given from **Table 1 and 2**: representative values are only given. Distribution of strain along the length and circumference of the stiffener and skin of ISS are shown in **Figure**

7 to Figure 9. The following are the observations from the comparison of predicted and measured strains.

- The strains are linear and within the elastic limit as expected from the FE results.
- Fairly good match was observed between the predicted and measured strain in most of the instrumented locations.
- Maximum strain recorded in skin is 4239 $\mu\epsilon$ as against the predicted strain of 4150 $\mu\epsilon$, just 2.09% higher than that of prediction.
- Maximum strain recorded in the stiffener is 3780 $\mu\epsilon$ as against the predicted value of 3736 $\mu\epsilon$, just 1.16% higher than that of prediction.
- Fairly good match was observed between the predicted and measured strain at the maximum size cutout. The strains are within the limit

Table 1: Comparison of predicted and measured strains ($\mu\epsilon$) in skin (top bay along the circumference)

SG No:	Measured	Prediction	% Deviation	SG No:	Measured	Prediction	% Deviation
149	3828	3840	0	180	3521	3530	0
150	2496	2810	-13	181	3444	3690	-7
151	2277	2790	-23	182	3313	3720	-12
152	2462	2530	-3	183	3440	3710	-8
157	2193	2280	-4	184	2128	1850	13
158	1271	1550	-22	185	3806	3715	2
159	1279	1520	-19	186	3510	3520	0
160	2077	1784	14	187	3598	3860	-7
161	2463	2640	-7	188	3412	3910	-15

Table 2: Comparison of Predicted and measured strains($\mu\epsilon$) in stiffener(bottom bay along Circumference)

SG No:	Measured	Prediction	% Deviation	SG No:	Measured	Prediction	% Deviation
1	2761	2326	16	25	1004	1248	-24
2	2764	3230	-17	26	2987	2666	11
3	3035	2770	9	27	3217	2851	11
4	3174	2801	12	28	3430	3249	5
5	2287	2156	6	29	3492	3265	7
6	2371	2196	7	30	2952	2771	6
7	2401	2245	7	33	2230	2512	-13
8	2465	1599	35	34	2307	2546	-10
9	2519	2353	7	35	2188	2014	8

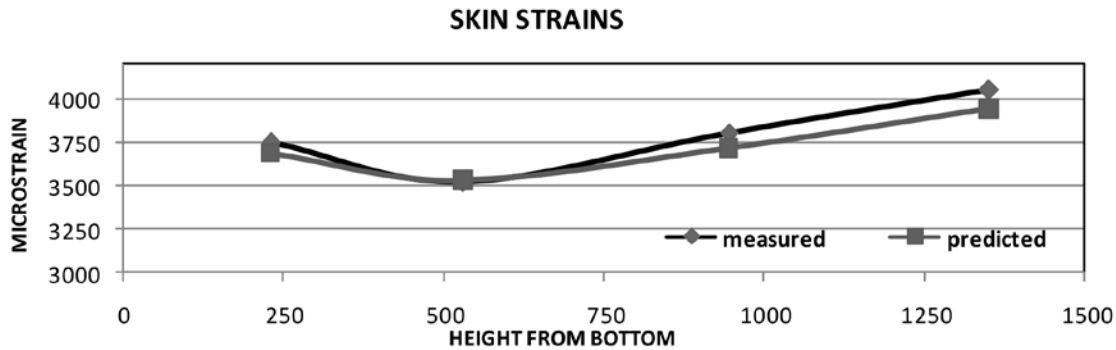


Figure 7 : Strain variation along the height of the SKIN

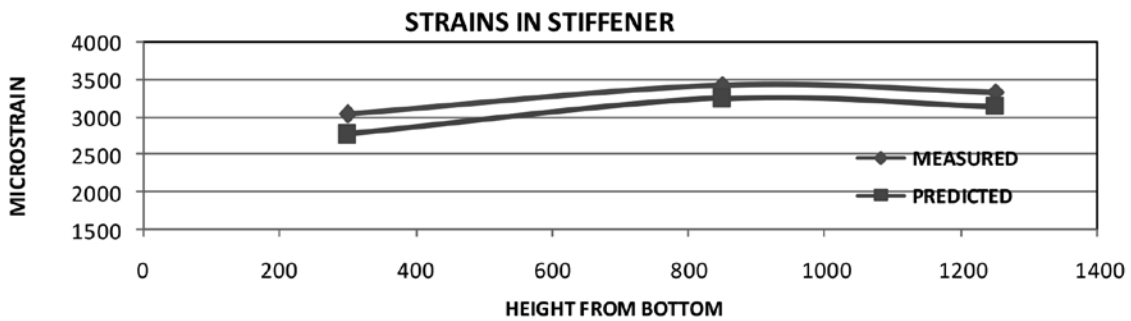


Figure 8 : Strain variation along the length of the Stiffener

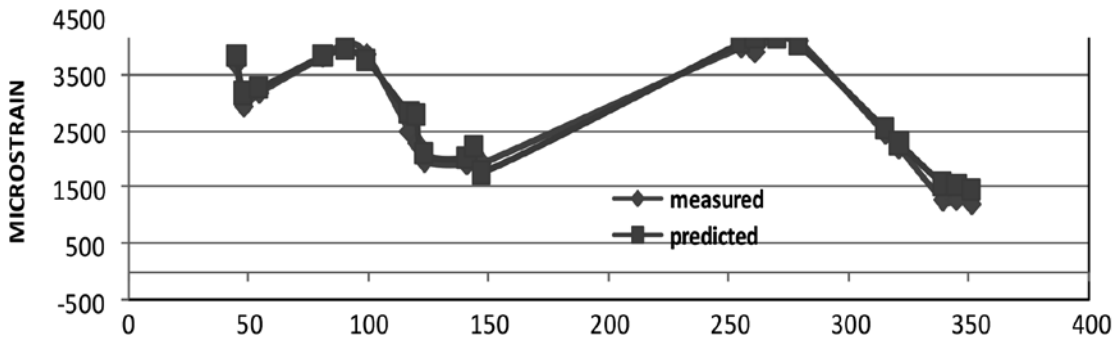


Figure 9 : Skin axial Strain Distribution along Circumference, on top bay

- Difference was observed in measured strain and predicted at the gauges located at top and bottom end rings and ring stiffener locations. The strains at the regions were however very small of the range around $200\mu\epsilon$.

Strain at Cutout Locations

Figure 10 and Figure 11 show the strain values around the maximum sized cutout (size is 500 x 500 mm approx). The predicted strain at cutout locations is compared with that measured using DIC and photoelastic coating. The maximum

predicted strain is $5970 \mu\epsilon$ in FE whereas the maximum value obtained from DIC is $5300 \mu\epsilon$.

Comparison of Predicted and Measured Displacement

Good match was observed between the predicted and measured axial elongation. Fairly good match was seen on displacement at other locations. The measured cutout opening is 2.77 mm as compared to the predicted value of 2.68mm [maximum sized cutout].

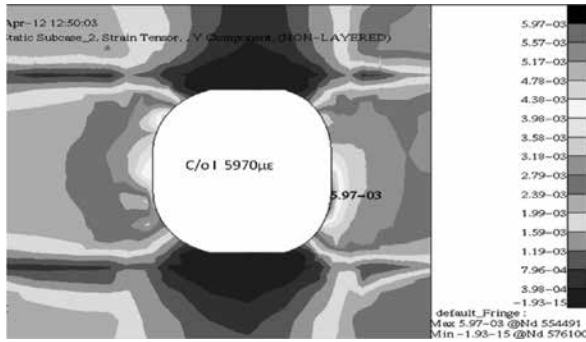


Figure 10 : Strain values predicted near Maximum Sized cutout

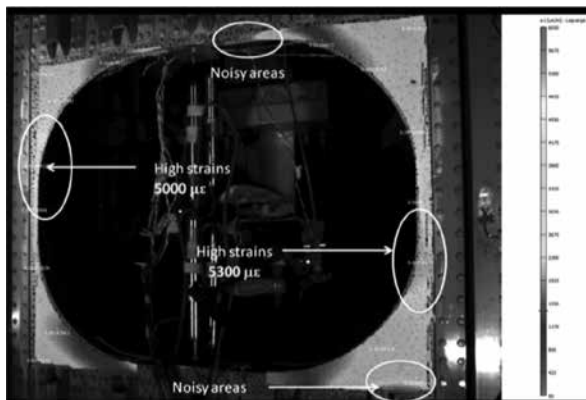


Figure 11 : Strain values measured by DIC near Maximum Sized cutout

Conclusion

Structural qualification testing is an important step in the design and qualification process of any new structure. Two major aspects of this process are (i) simulation of flight condition loading and (ii) validation of the FE analysis model for the prediction of strain and displacement. Details on how these aspects are addressed both in the design and structural qualification processes are explained in this paper, wherein the effect of thrust

transfer from strapon stage to the core is more pronounced than the uniformly loaded condition. A new concept of VAL was evolved during the process of achieving one to one comparison between the response of ISS for flight as well as for structural qualification. The predictions made from NASTRAN FE package closely match with the measured values at all the areas of interest indicating that good simulation of loading had been done during structural qualification.

Acknowledgement

The authors wish to acknowledge Dr. S. Unnikrishnan Nair, Deputy Director, STR Entity, Sri. S. Sirajudeen, Group Director, SDEG and Sri. B. S. Raju, Head, SDED, for the encouragements and technical advice, Sri. Isac Daniel, Group Director, STG (Structural Testing Group), Sri. Jeby Philip, Head EXMD (Experimental Mechanics Division, along with their team members for active participation and support for the qualification of the structure and smooth conduct of the test, Sri. S. V. Sharma, Advisor, Aeronautics and structures-ISRO, Sri. S. Sivakumar, Dy. Project Director, LVM3 for the critical review comments and suggestions during the entire design, analysis and qualification stages and Sri. V. J. Saji, DPD, PSLV Structures for the technical comments for improvements during the review of the paper.

References

1. Aerospace Structures-Present Practices and Future aspirations in launch vehicles SKD Rachel et al; Journal of Institution of Engineers (India), 20th National Convention of Aerospace Engineers 2006.

Design and Fabrication of Slipstream Deflection Mechanism for a Remotely Controlled Airship

**Kapse Subhash Prachi¹, Dhanashree Ahire¹, Gauri Borhade¹,
Milind Murugkar¹, Rajkumar S Pant²**

¹*Department of Mechanical Engineering, K. K. Wagh Institute of
Engineering Education & Research, Nashik 422003*

²*Department of Aerospace Engineering, IIT Bombay, Mumbai 400046*

✉ prachi28194@gmail.com

Abstract

Airship is a lighter-than-air aerial vehicle which is powered and controllable. Remotely Controlled (RC) airships are being used worldwide for a variety of applications such as aerial surveillance. Thrust Vectoring (TV) is introduced in airships to enhance their manoeuvrability and improve the handling characteristics. This paper describes an experimental investigation of the efficacy of a light weight and simple TV system using slipstream deflection mechanism. The proposed slipstream deflection method results in least disturbance to the propulsive unit, which is a highly desirable feature of a TV system. Structural analysis was carried out to determine the appropriate dimensions of various components of the TV system, viz., Duct, Louvers and the Linkages. A test rig for thrust measurement was designed and fabricated, and the thrust force generated at 0, 45 and 90 degree deflection angle of the Louvers was measured. Visualization of the flow behind the duct at these angles was also carried out. It was concluded that this system would enable the airship to maneuver in upward and forward directions, with a single mounted motor.

Keywords: *LTA systems; Airships; Thrust Vectoring system; Slipstream deflection mechanism; Thrust test rig.*

Introduction

Airships are the forgotten systems of Aviation, and are coming back in the reckoning due to the immense advantages that they offer over aircraft, as a low-cost environment friendly transportation system. Indoor RC airships are very useful in demonstrating the working principles of airships, and also as an aerial platform for product promotion, aerial surveillance and many more applications. The manoeuvrability of airships can be greatly enhanced by vectoring the thrust of its propellers, which also leads to reduction in total propulsion system weight. This report describes a light-weight and simple thrust vectoring system

using a duct, louvers and a servomotor that was designed, fabricated and tested. This system is later aimed to be used as a propulsive device of for an indoor remotely controlled airship.

Thrust vectoring is a maneuver effector which can be used to augment aerodynamic control moments throughout and beyond the conventional flight envelope. Thrust vectoring, also thrust vector control is the ability of an aircraft, rocket or other vehicle to manipulate the direction of the thrust from its engines or motor in order to control the altitude or angular velocity of the vehicle. It is a technology that deflects the mean flow of an engine jet from the center line in order to transfer

some force to the aimed axis. By that imbalance, momentum is created and used to control the change of altitude of the airship.

Thrust Vector Control (TV) is currently achieved by complex arrays of mechanical actuators capable of modifying the geometry of the nozzle and thus deflects the flow. There are three ways of providing TV in an airship powered with a brushless D.C. motor driven propeller, viz.

- a) Vector the entire propulsion system [1]
- b) Vector only the propeller [2]
- c) Deflect only the slipstream behind the propeller.

The slipstream deflection method leads to the least disturbance to the propulsive unit, which is highly desirable. Although tilt rotor thrust vectoring system is effective, it can be heavy, complex, difficult to integrate and aerodynamically inefficient. This variable geometry used in other methods mentioned above greatly increases weight and maintenance to the engine, and therefore limits the benefits from vectoring the thrust. Slipstream Thrust Vector Control is a technology aiming at the above listed benefits by the use of duct and louvers, implying less complexity and faster dynamic responses and can be potentially implemented with mechanical actuators consuming less power. Different concepts have been developed in the last decade to redirect the thrust of an airship.

This report describes the design and testing of a simple light weight slipstream deflection mechanism and a test rig for measurement of thrust. Result of flow visualization study is also presented.

Design Methodology

A duct made from Polyvinyl chloride material is fabricated having 280 mm diameter and 450 mm length. This duct is cut in a slanted manner at an angle of 45 degrees at one of its end. Fabricated of Polyvinyl chloride material, 15 number of louvers are fixed to the end with the slant cut. These louvers have integral rod like projections at their ends which go inside holes along the periphery of the slanted cut end. Plastic sleeves are used to take

care of the play between the projections and the holes. The louvers are linked to each other using a rigid link which in turn is connected to a couple of links. The last link is appended on the shaft of a servo motor of 4.10 kg torque. This linkage is so designed as to give the louvers a collective rotation of about 90 degrees. A brushless DC motor is fixed on the other end of the duct with a propeller on its shaft. A 30 amp Electronic Speed Controller (ESC) is used to control the motor speed. The system is powered by a 12V, 3 cell Lithium Polymer (Li-Po) battery. The system is controlled using a nine channel radio control transmitter- receiver set.

The propeller pushes air inside the duct, with the duct turning it into a channelized flow. The direction of this flow and so the thrust, then can be manipulated by changing the collective deflection of the louvers with the help of a servo motor, thus, a thrust can be obtained in directions ranging from zero to 90 degree

The test rig (**Figure 1**) designed and fabricated is a right angle lever comprising vertical arm of teak wood and horizontal arm of mild steel. The lever is pivoted at, and swivelled about its vertex on a roller bearing to reduce friction and obtain smooth operation. A play less steel rod is passed through the bearing which is fixed at its both ends inside two wooden blocks on either ends. A swivel able wooden plate is mounted at the top of the vertical arm which has an aluminium clamp to hold the TV assembly. An angle plate to measure the angle is provided with the swivel able plate. All this is mounted on a heavy base plate to provide support and stability by adding weight to the system. The



Figure 1 : Setup of slipstream deflection mechanism

reaction on the motor which is mounted on the vertical arm is then transferred to the horizontal arm, which is pressed against the electronic weighing machine and the force in kilograms is obtained.

Components Design

Structural analysis was carried out to determine the appropriate dimensions for various components of the TV mechanism such as the duct, louvers, linkage, servo motor rig arms. The selection criteria for the basic components used in the Slipstream deflection mechanism was based on the design and availability of materials. Standard procedure was being used for the duct design.

As per the requirements the Round duct was selected due to its advantages over the other ducts. The duct diameter selected was of 280 mm for the given motor propeller assembly with a propeller span of 9 inch and the length of the duct was optimized to be 450 mm. An elliptical cut section is provided at the exhaust section of the duct. In order to know the effect of temperature and humidity of the TV mechanism, the Mach number was computed to determine the compressibility effects. The flow to the inlet of was found to be subsonic as Mach number, $Ma = 0.02865$ [3]. The pressure loss and head loss across the inlet and exhaust section of the duct are calculated by using Darcy-Weisbach equation,[4].

$$\Delta p_f = k_f \left(\frac{L}{D} \right) \left(\frac{\rho v^2}{2g} \right)$$

Where, f = friction factor

L = length of duct or pipe, m

D = diameter of duct or pipe, m

v = mean air velocity in duct, m / s

ρ = density of air, kg / m³

k = constant = 5.35×10^{-5}

The graphical representation of the effect of change in Velocity of air on the Static Pressure drop across the duct is known as Characteristic Curves represented by **Figure 2**.

Array of flat plates provided at the exhaust of duct known as louvers were used at exhaust section of

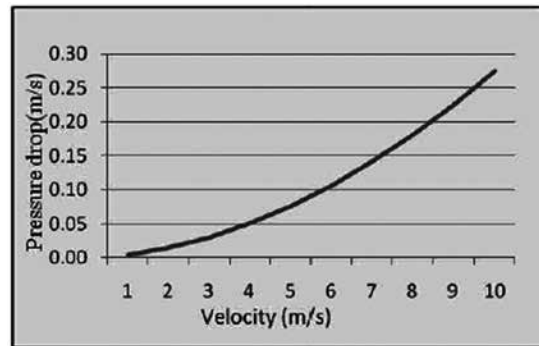


Figure 2 : Graph of pressure drop across duct against velocity

the duct for thrust vectoring. The distribution of louvers at elliptical cross section of the duct was determined by considering the condition that the cross-sectional “free area” of the louver must be equal to or larger than the cross-sectional area of the discharge unit openings to allow for optimum velocity and reasonable pressure drop across the louvers. The distribution was obtained by using AUTOCAD™ software, by which 15 louvers of 22 mm width, 3 mm thickness and of varying length were selected. As the louvers are subjected to the thrust, force analysis is carried out by using Newton’s second law of motion considering louvers as flat plate [5] along with the maximum holding force required which is about 6N [6]. The maximum Bending moment is about 357.075 N-mm with 2.07 as the Factor of safety (FOS). **Table 1** represents the impact forces exerted due to airflow on louvers at 12m/s velocity and at various angles.

The linkage is so designed as to give the louvers a collective rotation of about 90 degrees. The graphical procedure used for synthesizing the dimensions of the links of four bar mechanism was

Table 1 : Forces exerted on the louvers at various angles

Angle, θ , degree	Impact Force, F_n , N
0	0
30	5.64
45	7.98
60	9.78
90	11.29

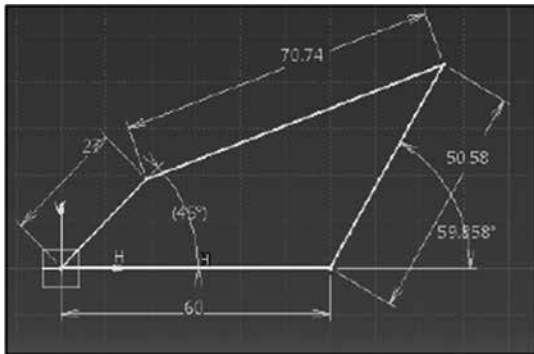


Figure 3 : Snapshot of animation of mechanism carried out in CATIA software

determined by using Three Position Synthesis by Inversion Method. The animation (**Figure 3**) was carried out in CATIA™ software to determine the motion of the mechanism. In order to rotate the array of louvers through a specific angle against the load acting on it, a servo of required specifications was selected from manufactures catalogue. The servo was so selected as to have rated torque greater than the load torque which is about 3.395 kg-cm.

Table 2 represents the specifications of the servo motor selected which was Futaba S3003 Standard with rated torque greater than the load torque.

Figures 4, 5 and 6 represent the CATIA™ model of duct with louvers at 0°, 45° and 90°.

Test Rig Design

This project focuses on designing an experimental setup of a propeller test rig for calculating the thrust of a propeller with and without the thrust vectoring control mechanism [7]. A provision is also made to accommodate the TV mechanism, it also measures vectored thrust. Along with that, frictional losses have also been considered for

Table 2 : Specifications of servo motor

Parameter	Values
Torque	6.0V: 4.10 kg-cm
Speed	6.0V: 0.19 sec/60°
Weight	37 gm
Dimension	39.9mm×20.1×36.1
Rotational Range	60°
Gear Type	Plastic

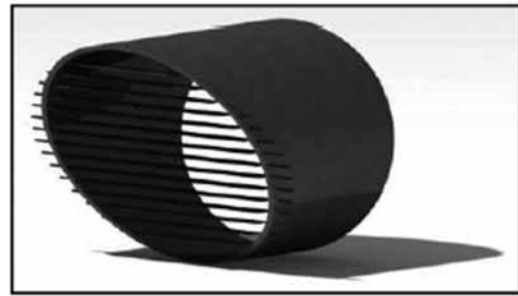


Figure 4 : CATIA model of duct with louvers at 0°

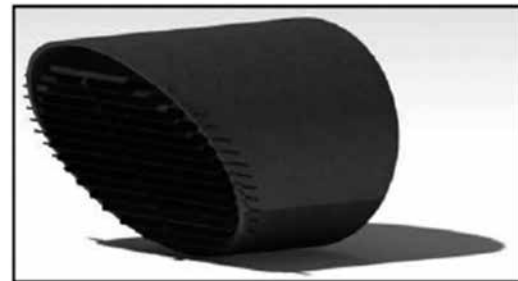


Figure 5 : CATIA model of duct with louvers at 45°

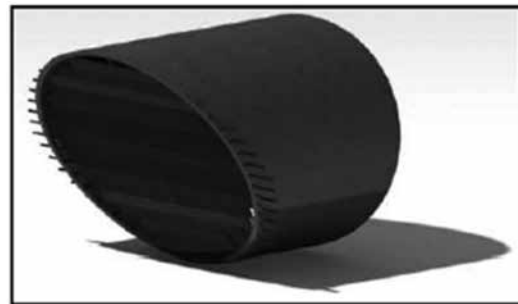


Figure 6 : CATIA model of duct with louvers at 90°

up gradation of the propeller test rig. Standard procedure was followed to determine the dimensions of the test rig arms [8]. The test rig designed and fabricated is a right angle lever with the specifications given in **Table 3**.

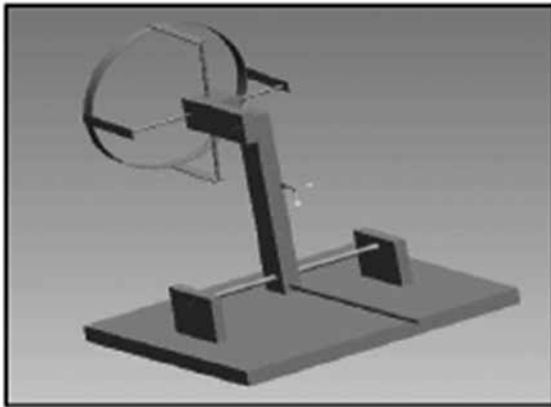
Figure 7 shows the 3D model of Right Angle Lever Mechanism of the test rig which was made in Pro-e Wildfire™ Version 4.0 software.

Testing, Observation and Results

A systematic series of static tests were carried out in order to determine the characteristics of the Thrust vector control mechanism in its vectored state and without thrust vectoring. The velocity and thrust readings were taken for various configurations. The flow visualization was carried

Table 3 : Specifications of test rig

Parameter	Values
Ultimate tensile strength of Teak wood	118 MPa
Yield strength of MS	250 MPa
Length of vertical arm, L	300 mm
Length of horizontal arm, L	300 mm
Factor of safety, F.O.S.	2
Vertical arm thickness	30 mm
Vertical arm width	45 mm
Horizontal arm width	10 mm
Diameter of clamp	280 mm


Figure 7 : Assembly in Pro-e Wildfire 4.0

out to get a physical feel of the TV system in vectored condition.

Experimental Procedure

A series of experimental tests were carried out in order to determine the thrust and velocity readings. These tests were conducted at increasing values of deflection angle of louvers with respect to the horizontal axis.

Testing was carried out in two stages. First velocity was calculated with the help of anemometer by holding it perpendicular to the direction of flow. A clamp was designed to hold the anemometer in the perpendicular direction of the flow. Velocity readings were taken when propeller is operating without duct, propeller with only duct, propeller with duct and louvers at 0° , 45° , and 90° . Similarly thrust readings obtained on the electronic weighing machine were taken with

the help of thrust measurement rig for the same conditions as taken during velocity measurement.

Experimental Observation and Results

During the initial phase of testing of the TV mechanism, the air velocity coming out of the propeller without the duct was determined. Later the air velocity at the outlet of duct without the louvers was determined. During the later phase of testing, the air velocity was determined at the exhaust section of the duct with louvers at 0° , 45° and 90° . **Table 4** shows the velocity readings corresponding to different conditions.

The thrust readings were obtained for the same configuration of the setup. **Table 5** shows the variation in thrust component corresponding to different conditions.

Flow Visualization using Threads

Flow Visualization using threads was carried out as free air is injected into the intake of the propulsion unit. The resulting plume was highlighted using woolen threads. Images were captured using a digital video camera to get the physical feel of the TV system in vectored condition. **Figure 8**, **Figure 9** and **Figure 10** are represented by the flow visualization carried out on the TV system.

Table 4 : Velocity readings for different conditions

Condition	Velocity, m/s
Only propeller	13.2
Only duct without louvers	12.5
0°	9.5
45°	7.9
90°	6.1

Table 5 : Thrust readings for different conditions

Condition	Thrust, g	
	Horizontal Component	Resultant Thrust
Only propeller	452	456
Only duct without louvers	427	432
0°	391	399
45°	377	385
90°	288	298

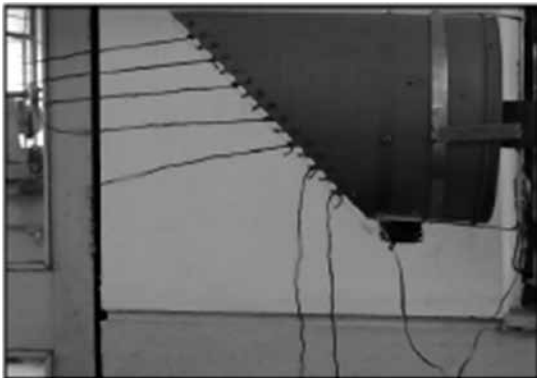


Figure 8 : Flow visualization for louvers at 0°

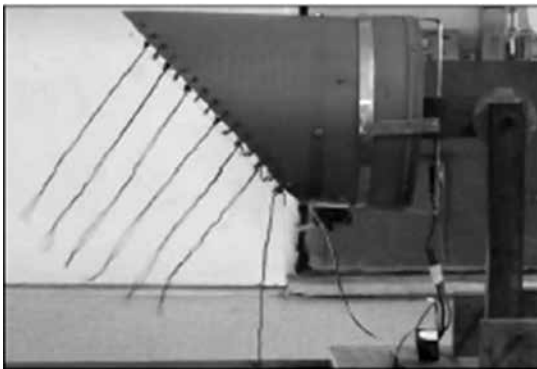


Figure 9 : Flow visualization for louvers at 45°

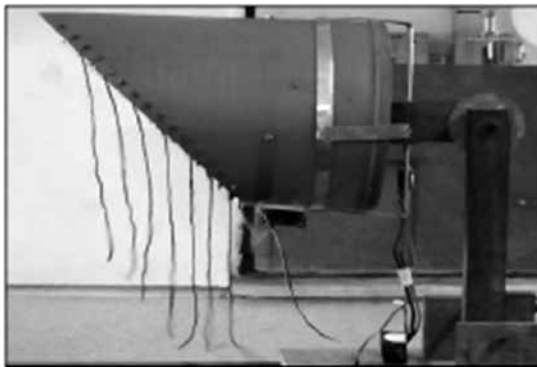


Figure 10 : Flow visualization for louvers at 90°

Conclusions

The testing results show that thrust and velocity reading goes on decreasing with increase in the deflection angle of louvers. The flow visualization shows that the flow at the exhaust section of the duct becomes transient at a distance of about

150 mm. This study is in progress and can be improvised in future. The work included in this report covers the design of a generalized system. More specific work can be carried out to design TV mechanism for specialized missions.

Acknowledgements

The authors would like to thank Mr. P. K. More, Mr. K. Maind, Mr. S. B. Kumbharde and Mr. Lokesh Shewade for help in fabrication and testing of the TV mechanism and thrust measurement rig used in this study. We would also like to thank Mr. Chetan Dusane, project Engineer, IIT Bombay for constant help and encouragement throughout the course of this study.

REFERENCES

1. R. Belapurkar, K. Deshpande and R. Sangole, "Design, Fabrication and Testing of a Remotely Controlled Airship with Thrust Vectoring," Proceedings of International Seminar on challenges in Aviation Technology, Integration and Operations(CATIO-05), Mumbai, Dec. 3, 2005.
2. S. Mohan and R. S. Pant, "Design and Fabrication of a Thrust Vectoring System for an Indoor Airship," LTA Systems Laboratory, Aerospace Engineering Dept., Indian Institute of Technology Bombay, Mumbai, India, Jan. 2014.
3. A. H. Shapiro, "The Dynamics Of Compressible Fluid Flow," Vol. 1, Ronald Press Company, 1953.
4. S. K. Wang, "Handbook of Air Conditioning and Refrigeration-ASHRAE," Second Edition, McGraw-Hill, 2000, November 7.
5. S. K. Agrawal, "Fluid Mechanics and Machinery", Eleventh Edition, Tata McGraw-Hill Education, 2006.
6. B. L. Singhal, "Turbo Machines", 2013 Edition, Tech-Max Publications, 2013.
7. A. Khalid, "Thrust measurement by using Mechanical System: Freshmen Research Project: Design, Development, and Testing of Variable Pitch Propeller Thrust Measurement Apparatus - A Case Study", Southern Polytechnic State University, 2012.
8. R. S. Khurmi, J.K. Gupta, "Machine Design", Third edition, S. Chand Publisher, 2005.

Design and Fabrication of a Portable Semi-Rigid Airship

Loharkar Shubham Anil.¹, Alap Kshirsagar², Rajkumar S. Pant³

^{1,3}Department of Aerospace Engineering, IIT Bombay, Mumbai 400076

²Department of Mechanical Engineering, IIT Madras, Chennai 600036

✉shubhamloharkar5474@gmail.com

Abstract

This paper describes how a semi-rigid airship is designed and fabricated within specified dimensional limits. The design of Semi-rigid airship is crucial as it is dependent on numerous parameters such as structural weight, material, envelope shape, overall size, payload requirements, etc. Along with the functional parameters various other parameters are also considered, such as the portability of the structure, Envelope attachment to the structure, payload mounting, etc. are also considered. Along with that different tests, such as Helium Leak detection and making structural samples for checking strength, are performed so as to ensure that there is minimum variation in conceptual and actual design. The paper describes entire design and fabrication process followed to design a Semi-Rigid Airship as small as 4m in length which is capable of carrying a considerable amount of payload. The paper shows the process used for selecting a proper envelope shape and size according to design requirements. Rigid structure able to be dismantle is used as the structure of the airship. The weight of the structure is a critical parameter and hence various types of materials are considered. The paper not only gives an approach for design and fabrication, but also shows how the fabrication is carried out.

Keywords: *Lighter-Than-Air systems; Semi-rigid airships*

Introduction

An airship (or dirigible) is a powered, controllable, lighter-than-air aircraft. A predominant portion of lift in airships is obtained by the buoyancy of a lifting gas whose density is lower than that of ambient air. The highest lifting capacity per unit volume is for Hydrogen, which is also easily availability in large quantities, but is highly inflammable. Compared to Hydrogen, Helium has around 7% lower lifting capacity per volume [1], and is non flammable, but its availability is limited, and it much more expensive. The outer envelope of an airship may be formed from a single gas bag, or may be a separate supported skin. Besides the main envelope, an airship also has engines and crew and payload accommodation, typically in a gondola hung beneath the envelope.

Based on the structural configuration of the envelope, one can classify an airship as rigid, non-rigid, or semi-rigid. Rigid airships have a rigid structure mounted on an internal framework; hence they tend to be heavy. Non-rigid airships do not have any internal framework, and entire load is carried by the pressurized envelope itself. The semi-rigid configuration has a supporting structure (keel) that runs along the length of the airship, on which an envelope of flexible material is mounted, with or without any internal framework. There is still the need for a slight overpressure to maintain the envelope shape attached to the keel. The keel allows for a place to mount engines and fans such that the overall load is distributed along the entire airship. More or less integrally attached to the hull framework and/or the keel are the gondola, engines



and sometimes the empennage. The framework has the task of distributing the suspension loads of these attachments and the lifting gas loads evenly throughout the entire hull's surface, which partially relieves the stresses on the hull during maneuvers. In early airships which relied on nets, fabric bands, or complicated systems of rope rigging to unite the lifting envelope with the other parts of the ship, semi-rigid construction was able to achieve improvements in weight, aerodynamics, and structural performance [2]. A semi-rigid Airship is generally smaller in size as compared to rigid airship for the same payload carrying capacity, but it may be larger than an equivalent non-rigid airship.

Most remotely controlled airships are of non-rigid type, due to ease in fabrication and transportability, and lower weight. However, in this configuration, the engines and payload can be installed only on a gondola that is generally mounted below the envelope. Further, the envelope design can be quite a problem, because it has to meet the dual requirement of gas retention, as well as handling all the loads acting on it.

A semi-rigid airship, on the other hand, provides more flexibility in location of payload and engines, since there is a rigid framework on which these can be directly mounted; this can result in higher maneuverability and better wind-disturbance handling capability. One might be able to use a thinner (hence lighter) envelope material, since it is only supposed to meet the requirement of gas retention.

The presence of a rigid framework and keel in a semi-rigid airship can result in a heavier structure, and hence lower payload capacity, compared to a non-rigid airship of the same size. By careful selection of suitable material for envelope and structural framework, it might be possible for offsetting some of this disadvantage. Further, if the structure can be designed to be quickly and easily dismantled, then the transportability of a semi-rigid airship can be greatly enhanced.

This paper describes a sizing methodology for a semi-rigid airship with a structural framework

that can be quickly dismantled. The semi-rigid airship is designed and fabricated for the purpose of indoor demonstrations, which poses severe dimensional restrictions. As indoor demonstrations are planned to be carried out in a foyer or in an open hall, the typical dimensions of entry doors are considered as constraints on maximum width and height of the airship. The sizing of a semi-rigid airship is a function of numerous parameters such as envelope shape, weight of the structural framework, specific weight of envelope material, and payload requirements.

Various other parameters and issues, have to also be considered, e.g., the portability of the structure, envelope attachment to the structure, and payload mounting, to name a few.

In this paper, we describe the process followed for selecting a suitable envelope shape and sizing it according to the specified design requirements. A rigid framework which can be easily and quickly dismantled is used. The weight of the structure is a critical parameter, and hence various types of materials are considered. A three-dimensional CAD model of the structure is created, to check the dimensional interaction between the structure and the envelope. The model has also been used to estimate weight of various structural elements and fasteners, which helps in accurate determination of the payload carrying capacity of the airship. Apart from outlining the systematic approach followed for the design and sizing of a quick-dismantleable semi-rigid airship, the paper also describes the procedure followed for its fabrication.

Design Requirements

Based on the past experience of design, development and flight demonstrations of an indoor non-rigid airship [3], the following broad design requirements were finalized for this indoor airship:

- It should be possible to assemble/dis-assemble the structure of the airship within one man-hour.
- The nose of the airship should be attachable to the existing mast for indoor airships [4].

- Total length of Airship ≤ 4 m.
- Maximum width of the envelope ≤ 1.35 m

The constraints on the length and envelope width were arrived based on a survey of the dimensions of entry doors and demonstration space of several indoor auditorium and large classrooms.

Envelope

The envelope itself is the outer surface, usually surrounding one or more gas-bags and or ballonets within it. It is a gas containment member which encloses the lifting gas and provides protection from the environment.

For a semi-rigid airship, the envelope is one of the major structural elements, hence it deserves special attention. Materials, design and workmanship must be of the highest standard possible. Additionally, material performance and overall cost need consideration. Since these requirements are in some aspects contradictory, the challenge is to find the best compromise. The following standard envelope profiles were studied in order to decide the design specifications of the envelope:

- GNVR [5-6]
- Modified GNVR [7]
- Zhiyuan-1 [8]
- Custom shape (Sphere + Cylinder + Parabola)

CAD of Envelope

A scaled CAD model of the envelope was prepared in Auto Desk Inventor software, as shown in **Figure 1**. This model was further used for making the 3D assembly. The CAD model helps in understanding the relationship between the structural assembly and the envelope attachment.



Figure 1 : CAD model: envelope

Envelope Material selection and Sizing

Using the relation between various dimensional parameters and net lift, the most suitable shape and dimensions are chosen, and the GNVR shape was selected, as it resulted in the lowest surface area per unit volume.

The material of envelope is also an important factor to be decided as its characteristics greatly affects the overall performance of the Airship [9]. The following features are considered while selecting the envelope material:

- High Strength
- High Strength to weight ratio
- Low Permeability to LTA gas
- Low Creep
- Low Weight
- High Tear strength
- Good adhesiveness
- Resistance to environment degradation
- Good flexural and abrasion resistance
- Sealing ability

After a detailed market search and several experiments with various materials, a commercially available Low Density Plastic (LDP) was selected as the envelope material, to ensure low self-weight with adequate strength. LDP can be easily heat sealed and hence the envelope can be sealed in-house on Heat sealing machine, which reduces the fabrication cost and time. The values of key design parameters of the envelope are listed in **Table 1**, assuming pure Hydrogen as the lifting gas, and ISA Sea level conditions.

Frame

Semi-rigid airships have some characteristics of rigid airships and non-rigid airships. A rigid keel with an aerodynamic shape runs from nose to tail along the bottom surface of the air vehicle. In these airships, the keel supports the primary loads. This keel is used to eliminate the main function

Table 1: Key design parameters of the envelope

Parameter	Value
Profile	GNVR
Material	LDP of 70 gsm
Diameter	1.3 m
Volume	3.25 m ³
Surface Area	12.6 m ²
Envelope Weight	0.882 kg
Gross Lift	3.983 kg
Weight of LTA Gas	0.285 kg
Net Lift	2.816 kg

of the catenary curtain and evenly distributes the gondola weight along the airship's entire length. The interaction of keel and envelope may be partially favourable and partially unfavourable. The mutual support between the structure and envelope is good for resisting and distributing the bending moments between them while the poor fit of keel to envelope causes them to act against each other and generate additional stress. Thus, an accurate characterization of the interaction of envelope and keel and their mutual effects is a crucial consideration for semi-rigid airship design. It can be anticipated that semi-rigid airships have weights between those of non-rigid airships and rigid airships, since the keel on the bottom acts like a structural load bearing member.

Conceptual Design

Design is conceptualised based on the design requirement and it is decided to have a structure able to be dismantled, instead of a foldable structure, as it is more portable and suits the design requirements. It was decided to place the envelope inside the structural framework; to allow quick dismantling, and permit mounting of different equipment directly on the framework. Keeping the envelope outside the framework would also lead to complications and result in leakages at places where equipment and gondola is mounted. Also, having the structural framework visible from outside is also advantageous from demonstration point of view.

The structure consists of two circular and two

semi-circular frames, on which several longerons and the nose hook are mounted.

Structural Joints

The joint of the structure, able to be dismantled was the most important part to be decided, as it has a significant impact on the portability of the structure. The joint was desired to be strong and light weight. Different types of joints were studied and accordingly, sandwich type joint was selected which is shown in **Figure 2**.

The joints on different parts of the structure is shown in **Figure 3**, where

Type a : Longerons to full ring

Type b : Longerons to half ring

Type c : Longerons to half ring

Typed : Longerons to Longerons (rear)



Figure 2 : CAD model: Sandwich joint

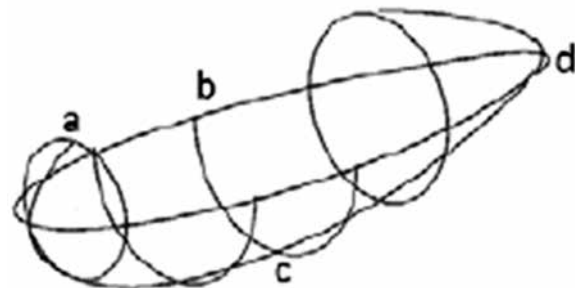


Figure 3 : Joints in semi-rigid airship

It was decided to use nuts and bolts for fastening purpose, as they are easily available, and are also easy to handle. Mild steel nuts and bolts do provide high strength, but are quite heavy. Hence, nylon nut bolts of 6 mm diameter were used, which are light weight and provide sufficient joint strength.

Material Selection for Structural Framework

Material selection for the semi-rigid structure was the most critical step to be taken, to ensure adequate strength and other structural properties, without too much increase in weight. The semi-rigid structure is expected to serve as a framework for rigidly attaching the envelope to it. Apart from the envelope, it must be capable of carrying power plant, batteries, radio receiver and nose hook for attaching it to the mooring mast. Various materials were short listed and tested, as described in the sub-sections that follow.

Jute Reinforced Plastic (JRP) Rods

JRP is a composite with a combination of Jute and a plastic polymer (**Figure 4**). Jute is easily available and is economical which makes these rods affordable, as compared to carbon fiber rods. JRP rods can be easily bent, but they lack the capability of retaining the bent profile. JRP has a high spring back and thus is unable to maintain the given profile. The density of Jute fiber reinforced plastic is found to be around 540 kg/m^3 .

Jute Reinforced Plastic (JRP) Plate

This material is similar to JRP rods, but it is in a plate form. A flat plate can be machined to get required profile using laser cutting or milling. Such a precise machining process guarantees to get desired profile. The density of the plate was found to be 790 kg/m^3 .

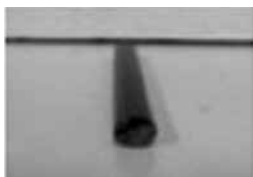


Figure 4 : Jute reinforced plastic rod

Balsa

It is a well-known light weight material used for aeromodelling (**Figure 5**). A desired profile was obtained by laser cutting the balsa sheets and strength testing was carried out. It was found that even though balsa has excellent in-plane strength, it has very poor out-of-plane strength. Thus it was decided to avoid using Balsa for Longerons. Apart from this, the unavailability of large Balsa sheets also posed additional restrictions.

Carbon Fiber Reinforced Balsa (CFRB)

Carbon Fiber is well known for its high tensile strength and low weight (**Figure 6**). CFRB has a similar weight, but has significantly lower cost. A sample was made using resin (LY 556) and hardener (HY 951). Parameters such as weight, density, manufacturability and strength were tested. It was found that it had a density of 472 kg/m^3 and had adequate strength.

Carbon Fiber Reinforced Polyurethane (CFRPU) Foam

PU foam is Polyurethane foam which has properties similar to that of thermocol (**Figure 7**). But it has lower strength than required and hence CFRPU is considered which gives an added advantage of increase in strength. The density of this composite is found to be around 290 kg/m^3 .

Carbon Fiber Reinforced Depron (CFRD)

Depron™ is extruded polystyrene foam which has

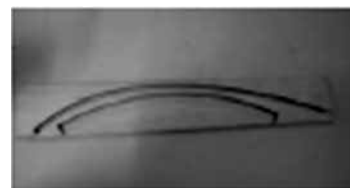


Figure 5 : Balsa



Figure 6 : Carbon fiber reinforced Balsa

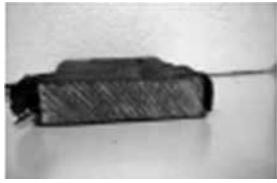


Figure 7 : Carbon fiber reinforced PU foam



Figure 8 : Carbon fiber reinforced Depron

low density, but it has low out of plane strength (**Figure 8**). If it is reinforced with a composite carbon fiber, this shortcoming is removed. CFRD has a better strength as compared to Depron™ and has lower cost as compared to CFRs. The density is found to be 300 kg/m³.

Material Selection

From all the above alternatives, CFRPU foam was shortlisted as the material for the structural framework, due to following reasons:

- PU Foam, of desired shape and size, is easily available. Balsa is available only in small sizes which make it impossible to be used.
- It is available at low cost (Rs. 95 per sheet) as compared to that of JRP or Balsa.
- The Resin and Hardener required for bonding of composite is easily available.
- CFRPU foam can be machined to get desired profile which is not the case with carbon fiber alone, as it is quite difficult to machine carbon fibre.
- It has higher strength compared to Depron™, PU foam or Balsa.

Nose and Tail Attachment

A nose batten is provided in airships, to facilitate its attachment to the mooring mast. A nose hook is provided for this airship with a view to facilitate ease in assembly and disassembly of the structure.

Four extended hollow portions are provided which accommodate the four Longerons. Holes are provided so that the Longerons can be bolted to the nose hook. The nose hook has a cylindrical projection at the front, which is used for attachment with the mooring mast. Tail hook is designed on the similar lines, so as to accommodate the Longerons. Holes are provided on both Nose and Tail so as to bolt the Longerons. Both nose- and tail hooks are expected to have adequate strength and should be capable of performing their function along with least possible weight. It was decided to go for 3D printing of these parts in ABS plastic. **Figures 9a and 9b** shows the CAD models for the nose- and tail hook, respectively.

Detailed CAD Model

After finalising the geometry of the structure and material selection, a detailed CAD model was made in AUTODESK Inventor™, as shown in **Figure 10**.

The CAD model provided a base to estimate the quantity of material required for the structure, and



Figure 9 : CAD for nose and tail hook

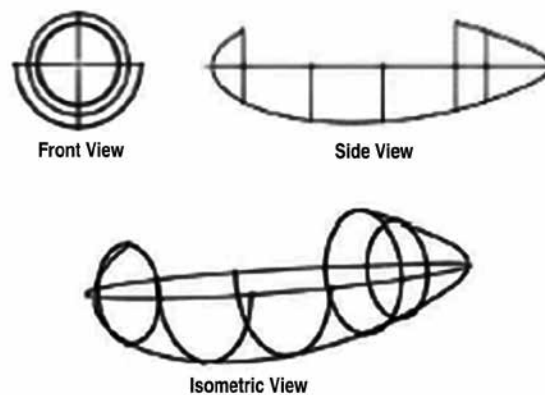


Figure 10 : 3D structural assembly

also gave a rough estimate of the weight of the semi-rigid structure.

Joint and Fasteners

The design of structural joints was a crucial part of this study. It was essential to select a joint keeping in mind the need of a quick dismantlable structure of the airship. It was decided to go with a sandwich type of joint, and use plastic Nuts and Bolts of 6 mm diameter as fasteners, for ease in assembly and disassembly, and low weight. A total of 32 fasteners were needed due to the long length of the airship. The plastic nut bolts provided adequate joint strength along with significant weight reduction.

Fabrication And Assembly

Composite Material Fabrication

First the composite material was made using Carbon Fibre mat, PU foam sheet and Resin and hardener mixture. The Resin and hardener was mixed in the ratio of 10:1. The mixture was applied on PU sheet and then it was wrapped with the carbon fibre mat. The composite was then soaked for 24 hours, after which it was ready for further machining. One needs to take proper care while using Araldite as adhesive. The resin hardener mixture starts to have an exothermic reaction and the adhesive loses its flow-ability. In such a case, it becomes difficult to apply the adhesive on PU sheets. To avoid this, the adhesive was applied as soon as the resin and hardener are mixed together. The composite sheets were adequately cured before machining.

Profile Cutting

A carbon fibre with mixture of resin and hardener forms a very strong bond and ultimately a strong composite. Laser cutting had virtually no effect on the composite and hence profile cutting using water jet machining was considered. The water jet machining gives a fine profile cutting. Few samples were machined for initial testing of strength. **Figure 11** shows photographs of some results of profile cutting.

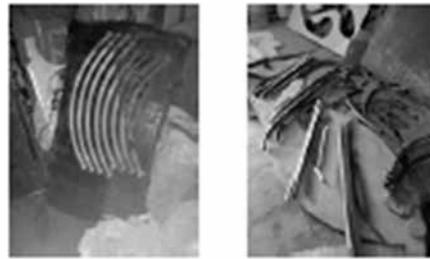


Figure 11 : Profiles cutting for longeron

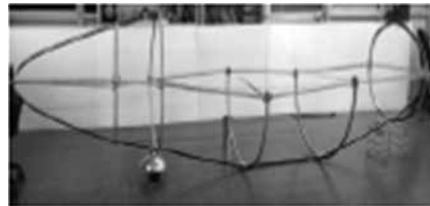


Figure 12 : Structural assembly

Structural Assembly

The Profiles were then prepared for assembly. Sandwich type of joint was used for assembly. For this, a transverse extruded joint was glued at the ends of the profile, using Araldite. The assembly was started from the nose end and was finished at tail end. The 3D printed Nose hook was used as a start point for assembling the structure, which eliminated the need for aligning the front longerons relative to each other. After the front longerons, first full ring was attached using Nylon nuts and bolts. The full ring was then used as a support for assembling the further longerons and other rings and semi rings. The structure alone without envelope is not capable of standing by itself. Hence it is supported on its sides by using various supports, as shown in **Figure 12**. Also a ribbon is used to tie two semi rings and to tie the front part with the rear part to avoid sagging.

Envelope Sealing

Envelope sealing is a very important and a crucial part of the semi rigid airship. Heat sealing machine was used for envelope sealing. Proper care was taken while deciding the temperature and holding time of the sealing machine. The envelope was made of eight identical petals, which were created using the methodology explained in [3]. The petals are sealed together properly, and special

care was taken at the ends of the envelope. The envelope ends have a high tendency of leakage. All the petals are sealed properly and was then inflated using an air Compressor. The air inflation was important as it gives an overall idea of volume and leakages present in the sealed Envelope. All the visible leakages are sealed and then, leak detection test was performed. A fabricated airship envelope is shown in **Figure 13**.

Helium Leak Detection Test

The envelope generally has some leakages associated with it, due to imperfections while heat sealing the edges. Helium leak detection test is performed so as to determine the locations of these leakages in the envelope. A small volume of Helium is filled in the envelope, and then the remaining volume is filled with air. A Sniffer probe, connected to the leak detector, is moved along the envelope surface, so as to detect all the possible leakages. The detected leakages were sealed using sealing tape and again a leak detection test was performed.

Structure and Envelope Assembly

The structure was assembled starting from the nose hook to the tail hook, and was kept supported before attaching the envelope to it. The Longerons are first inserted into the nose hook and their other ends were attached to the circular frame. Similarly, all other set of Longerons were assembled and



Figure 13 : Fabricated airship envelope



Figure 14 : Assembly of semi-rigid airship

the last set was attached with the help of tail hook. The envelope was then inserted inside the structure and was attached at ten different points on the structure. The Envelope was then inflated with lifting gas and the assembly was ready for further testing and trials. The assembly of semi-rigid airship is shown in **Figure 14**.

Conclusions

This paper described the design methodology and fabrication procedure of a dismantlable semi rigid airship. The design phase involved review of various shapes and configurations. The most suitable design was chosen through systematic comparisons of possible alternatives. A large variety of materials were considered for the airship structure. Different composite materials were prepared in-house and their samples were tested. The keel-frame was designed to be dismantlable and light-weight. Finally, the entire envelope and frame were fabricated and assembled for flight-testing.

Acknowledgments

The authors wish to thankfully acknowledge the financial support provided by the Research Internship Scheme 2014 of Industrial Research and Consultancy Cell of IIT Bombay. The authors are also like to thank Mr. Amit Wani and Mr. Chetan Dusane, Interns, Aerospace Department, IIT Bombay for their help and support in envelop fabrication and leak testing.

References

1. E. Moforth, "Basic Principles" In Airship Technology, Khoury G. A., ed., pp.8-15, Vol. 2, Cambridge University Press, 2012.
2. L. Liao and I. Pasternak, "A review of airship structural research and development," Progress in Aerospace Sciences, vol. 45, pp. 83-96, May-July 2009.
3. G. Bansal, U. Bhardwaj, N. Jain, S. Mulay, S. Sawardekar and R. S. Pant, "Design Fabrication and Flight testing of a Non-rigid Indoor Airship", AIAA-2013-1297, Proceedings of 20th AIAA LTA Systems Technology Conference, 25-27 March 2013, Daytona Beach, FL, USA.



4. K. Syed, U. Bhardwaj, and R. S. Pant, "Design, Fabrication and Testing of Mooring Masts for remotely Controlled Indoor and Outdoor airships", *Journal of the Institution of Engineers (India): Series C, Mechanical, Production, Aerospace and Marine Engineering*, Springer, ISSN: 2250-0545, 2014.
5. S. Sundaram, "Wind Tunnel Tests on 1:7 and 1:28 scale Aerostat models," Technical Report, Experimental Aerodynamics Division, NAL, Bangalore, India, 2000.
6. C. Narayana and K. Srilatha, "Analysis of aerostat configurations by panel methods," BLISS project Document CF 0010, NAL, Bangalore, India, 2000.
7. R. Joshi, A. Raina and R. Pant, "Conceptual Design of an Airship using Knowledge Based Engineering," AIAA-2009-2861, Proceedings of 18th AIAA Lighter-Than-Air Systems Technology Conference, Seattle, Washington, USA, 4-7 May 2009
8. X. Wang, G. Fu, D. Duan and X. Shan, "Experimental Investigations on Aerodynamic Characteristics of the ZHIYUAN-1 Airship," *Journal of Aircraft*, vol. 47, pp. 1463-1468, 2010.
9. T. Miller and M. Mandel, "Airship Envelopes: Requirements, Materials and Test Methods"



Design Feasibility Study of an Agriculture Remote Sensing UAV

R S Anand, M Dineshkumar

GDD/CGDG/CGSE, Vikram Sarabhai Space Centre

Indian Space Research Organisation, Thiruvananthapuram 695022

✉ dinesh286@gmail.com

Introduction

Unmanned Aerial Vehicles (UAVs) have become a hot research topic in the last decade worldwide. UAV is currently having wide application ranging from military and special operation to civil application. Electric propulsion systems are widely used in UAVs because of its simplicity in operation and handling. Electric UAVs use BLDC motor and Lithium polymer batteries for propulsion. The design of electric UAV is a multilevel complex process which includes aerodynamic, structural, electric propulsion and performance analyses. The three important phases UAV design and development is the Conceptual, Preliminary and Detail design. The general design principles of manned aircraft are used for UAV design in the initial phase [1]. Traditional aircraft design methodology is expensive method and requires expert designers from several disciplines [2]. There is no systematic procedure for the designing of UAV. A simple methodology is developed to estimate the feasibility of the given electric UAV for the given mission. The methodology can be extended for design of optimum UAV for the given mission. The methodology is developed as software in MATLAB. A case study of an UAV used for agriculture remote sensing is given in this paper.

Literature Survey

Large amount of literature and experience exists in design of manned aircrafts. Specific literature for UAVs of small size is less common, however there has been increasing activity in this area

during the past years. The size of UAV varies according to the applications. In many cases the design and constructions of UAVs faces new challenges.

A conceptual design methodology for sizing of UAVs for specific mission requirements is developed by Turnbull [3]. The design methodology uses simple calculations to estimate mass, aerodynamic coefficients, performance parameters for each mission segments. The selection of the power plant is based on the mission power and mass. The genetic algorithm is coupled with an design to arrive at an optimum design. Since the methodology considers only jet engine for propulsion, electric UAV cannot be designed.

An UAV design based on data mining is developed by Daniel [4]. In this method, a large database is created with existing UAVs which contains geometric, airfoil, power plant, aerodynamic, performance data. Data mining is used to categorize existing UAV designs, assisting configuration decisions using database driven methodology. For the mission requirement the package will selects aircraft designs from the database using data mining and decision tress. Performance evaluations are carried out for each design and the optimum aircraft design is selected by the genetic algorithm. This method cannot adopted to check the feasibility of an aircraft configuration for a given mission requirement.

Details of Design Methodology

The typical UAV assumed in this study is given

in the **Figure 1**. Commercially this type is called as First Person View (FPV) models. Advantages of FPV UAVs are, cameras and payloads shall be placed without the interference of the motor and propeller, has larger payload bay. The UAV model is assumed as pusher type with rectangular wing planform. Fuselage and wing are made of 4 layers of carbon fibre composite. The vehicle body consist of two section, fuselage and boom rod. Wing is placed above the fuselage and the fuselage and tail are connected through a tail boom. Motor is placed at the trailing edge of the fuselage and payload is placed inside the fuselage near the leading edge. The tail volume ratios considered for horizontal and vertical tail are 0.5 and 0.04 respectively. The optimum CG location of the UAV is assumed in between 25% to 35% of the wing mean aerodynamic chord.



Figure 1 : Baseline model

The design algorithm consists of five modules. The modules are - Input, Mass & centre of Gravity (CG), Aerodynamic, Mission, Powerplant module. **Figure 2** illustrates the design architecture. Each module is discussed in the coming sessions. When there is an infeasible design or constraints are violated, penalty functions is incremented and the process is terminated.

Input Module

Input for the design are two types design variables and design constants. Design variables are the user defined inputs. Design constants are the constants for the particular type of UAV. Though the inputs are defined as variables and constants, both can be interchangeable depending upon the requirements. Typical design variables and design constants are as given in **Table 1**.

Mass & CG Module

In this module two operations are done in parallel,

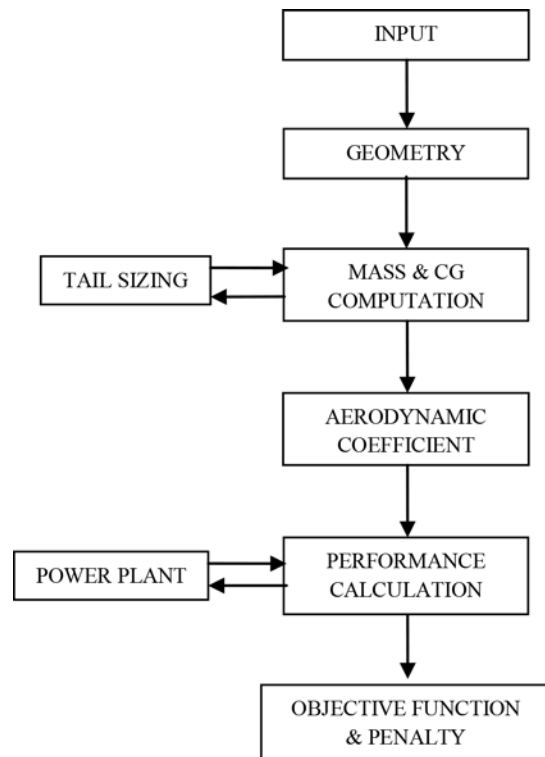


Figure 2 : Design architecture

Table 1 : Design variables and design constants

Design Variables	
Wing span	
Wing area	
Aspect ratio	
Motor	
Propeller	
Battery	
Airfoil	
Vehicle length	
Design mass	
Design Constants	
Fuselage diameter	
Fuselage length	
Area density of carbon composite	
Taper ratio	
Payload mass & CG	
Mission requirements	

they are centre of gravity estimation and tail sizing. The payload, motor, battery masses are



given as input. Mass of fuselage and wing are estimated from their surface area. Tail dimensions and mass are estimated from the tail volume ratio and fuselage length. Computation of mass & CG of individual components and knowing its locations, total mass & CG are estimated. The estimated CG location is checked for the permissible range. Wing location is adjusted to get the optimum location during the process, tail size is fine tuned in parallel. Since CG calculation and tail sizing are interdependent, they are carried out in an iterative manner. Iteration ends once the CG is in the optimum location, else the penalty is incremented and the total process is terminated

Aerodynamic Module

Aerodynamic module estimates the aerodynamic coefficient to analysis the performance from the given geometry. Tornado [5] is used for estimation of the aerodynamic coefficients. Tornado is open-source aerodynamic analysis software, which uses Vortex lattices method for aerodynamic coefficient estimation. The coefficients estimated are max lift coefficient (CL_{max}), Oswald's efficiency factor (k) for the wing and zero-lift drag (C_{D0}).

Power Plant Module

Powerplant module and mission module work in parallel. Power plant module consists of motor, propeller and battery data. Motor, battery and Propeller data are collected and archived as a database. The available database consists of 57 propellers, 71 motors and 103 batteries. Each data is accessed using the serial number. The serial number is mentioned in the Input module. This module takes input from the mission module and estimates propeller rpm, motor current & voltage. Propeller efficiency and rpm for each mission is estimated from the propeller performance data. Motor power required is estimated from power and propeller efficiency. The motor voltage, current and efficiency to deliver the required power[6] is estimated from equations(1) (2) (3). The battery capacity and motor power are compared with the mission power and energy to check the feasibility of the power plant combination.

$$P = \left[\left(V - \frac{rpm}{Kv} \right) \frac{1}{R} - I_o \right] \frac{rpm}{Kv} \quad (1)$$

$$I = \left(V - \frac{rpm}{Kv} \right) \frac{1}{R} \quad (2)$$

$$\eta = \left[1 - \frac{I_o \cdot R}{V - \frac{rpm}{Kv}} \right] \frac{rpm}{V \cdot Kv} \quad (3)$$

when,

I : Current

V : Voltage

R : Internal resistance

Kv : Motor speed constant

I_o : No load current

η : Efficiency and

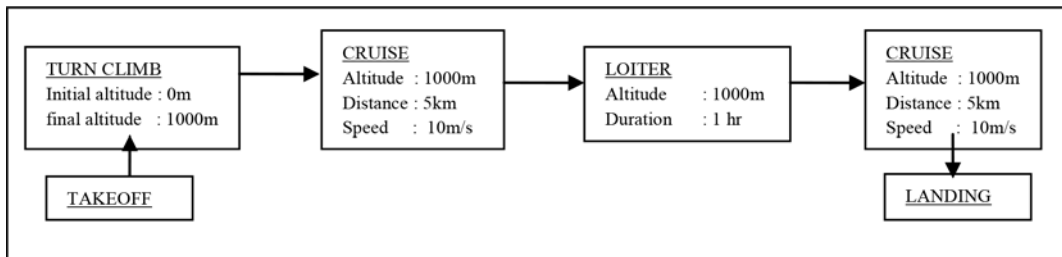
rpm : Rotations per minute

Mission Module

As mentioned earlier mission module and power module works in parallel. Mission module estimates the power and energy required for the mission requirements. The typical mission requirements are climb, turn climb, loiter, and glide. Power required for the each mission segment is computed using the mass details from Mass & CG module, aerodynamic coefficient from Aerodynamic module. The Power required is compared with the available motor, propeller and battery. If the required power is not delivered penalty function is incremented and the process is terminated.

Example of A Feasibility Study

The example considered is a typical hand launched agricultural UAV for aerial remote sensing. The mission requirement is shown in the **Figure 3**. The UAV is launched and allowed to climb up to 1000m, cruise upto 5km at 10 m/s, loiter is carried out for 1 hr, and then cruise back to the initial position.


Figure 3 : Mission requirements

Loiter considered is for 1 hr which is sufficient for an remote sensing UAV, within the stipulated period wide area shall be covered. The UAV payload mass considered is 500 g, which is sufficient for a typical remote sensing UAV for agricultural purpose.

Table 2 : Design Constants

Design Constants	
Fuselage diameter	0.175 m
Fuselage length	0.4 m
Density of carbon composite	0.2 kg/m ²
Wing Taper ratio	0.75
Payload mass	500g

Table 3 : Design Variables

Design Variables	
Wing span	1.2 m
Wing area	0.225 m ²
Aspect ratio	6.4
Airfoil	SPICA
Vehicle length	0.7 m

Table 4 : Technical specifications for brushless dc motor

Motor Name	Speed constant (rpm/V)	No load current (Amp)	Resistance (ohm)	Voltage (V)	Current (amp)	Weight (gm)	Diameter (mm)	Length (mm)
AvionicN3548 KV900	900	2.9	0.035	22.2	37.8	170	35	48

Table 5 : Specification of Lithium Polymer Battery

Battery Name	Capacity (mah)	Voltage (V)	Discharge rate	Length (mm)	Width (mm)	Height (mm)	Weight (gm)
Wolf pack White	4200	7.4	35	135	42	18	231

The design constants and design variables are given in the **Table 2** and **Table 3** respectively. The details of battery, propeller and motor are also given below. APC 10X6.5 propeller is chosen based on the power requirement of the UAV.

Propeller

APC propeller of diameter 10" and pitch 6.5" is selected.

Motor

Brushless dc motor is selected for the power plant. The details are given in **Table 4**.

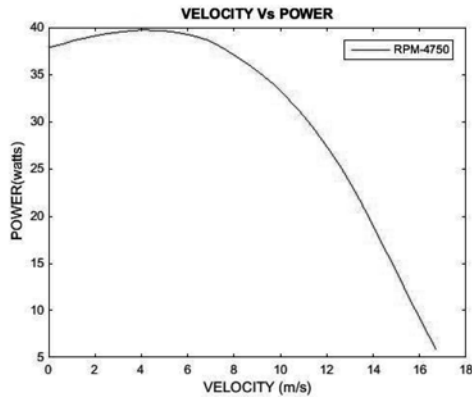
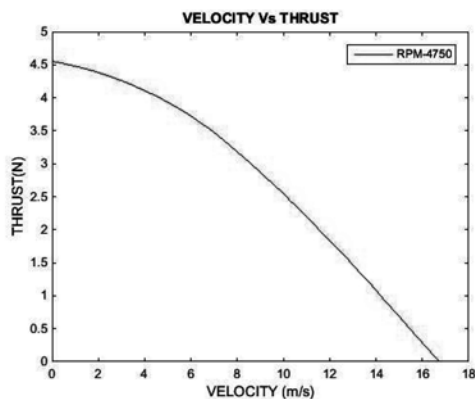
Battery

The details of Lithium polymer battery is shown in **Table 5**.

The aerodynamic coefficients and mass computed for the UAV are given in the **Table 6**. Performance curves of motor and propeller are shown in the **Figure 4** and **Figure 5** respectively. For this configuration, the penalty function achieved in zero. From this analysis, it shows that the given UAV configuration is feasible for the given mission. But the optimality of the configuration cannot be established with this configuration.

Table 6 : Aerodynamic coefficient and Design mass

Aerodynamic coefficients	
K	0.022519
CDo	0.028601
CLmax	1.1207
Design Mass	
Mass	1.3319 kg

**Figure 4 : Velocity vs power available****Figure 5 : Velocity vs propeller thrust**

Conclusion

The methodology is developed for establishing feasibility of the given configuration of UAV for

the given mission. Penalty is introduced for cases violating constraints. The method is validated for a remote sensing UAV for agricultural application. Feasibility of the UAV is established for the given mission. The methodology shall be extended for achieving optimal configuration.

Acknowledgement

The authors are thankful to Head, GDD, Group Director, CGDG, Deputy Director, CGSE in VSSC for given an opportunity for working in UAV

Reference

1. M. Sadraey, "A Systems Engineering Approach to Unmanned Aerial Vehicle Design" 10th AIAA Aviation Technology, Integration, and Operations (ATIO) Conference, September 13-15, 2010, Fort Worth, Texas.
2. Perez, R., Chung, J. and Behidinan, K., "Aircraft Conceptual Design Using Genetic Algorithms" Proceedings of the 8th AIAA/USAF/NASA/ISSMO Symposium on Multidisciplinary Analysis and Optimization.
3. Turnbull A., "Preliminary Sizing Method for Unmanned Aircraft using Multi-Variate Optimization" Craneld University, 1987.
4. Daniel J. Neufeld and Joon Chung, "Unmanned Aerial Vehicle Conceptual Design using a Genetic Algorithm and Data Mining", Infotech@Aerospace, September 26-29, 2005, Arlington, Virginia AIAA 2005-7051.
5. User's Guide TORNADO 1.0 Release 2.3 2001-01-31.
6. Ohad Gur, Aviv Rosen, "Optimizing Electric Propulsion Systems for Unmanned Aerial Vehicles", Technion—Israel Institute of Technology, Haifa 32000, Israel, July–August 2009.

Drones for Precision Agriculture

K V Srinivasan

National Design of Research Forum

The Institution of Engineers (India), Bangalore 560001

✉ vskowlgi@gmail.com

Introduction

By the year 2050, it's expected that the world's population will reach 9.2 billion, 34 percent higher than today. Much of this growth will happen in developing countries like Brazil, India and China which covers largest area in the world with arable land for agriculture. To keep up with rising populations and income growth, global food production must increase by 70 percent in order to be able to feed the world. The answer to that daunting challenge lies in real time data gathering and analysis. Scientists are researching how "precision agriculture" techniques and technologies can maximize food production, minimize environmental impact and reduce cost. We have the opportunity to make a difference using relatively cheap drones with advanced sensors and imaging capabilities which are giving farmers new ways to increase yields and reduce crop damage.

Precision Agriculture

Traditional agriculture is practiced by performing a particular task, such as planting or harvesting, against a predetermined schedule. But by collecting real-time data on weather, soil and air quality, crop maturity, equipment, labour costs and availability, predictive analytics can be used to make smarter decisions which is known as precision agriculture. With precision agriculture, control centres collect and process real time data to help farmers make the best decisions with regard to planting, fertilizing and harvesting crops. Sensors placed throughout the fields are used to measure temperature and humidity of the soil and surrounding air. In addition, pictures of fields are taken using satellite imagery and robotic drones. The images over time show crop maturity and

when coupled with predictive weather modelling showing pinpoint conditions 48 hours in advance.

Precision agriculture is one of the well known many modern farming practices that make production more efficient. With precision agriculture, farmers and soils work better, not harder. It is a well known fact that farmers are the first land stewards. They use research about weather patterns, soil temperature and humidity, growth, and other factors. They rotate crops to improve diversity, and monitor irrigation rates to prevent salts accumulation. They also use precision agriculture practices to apply nutrients, water, seed, and other agricultural inputs to grow more crops in a wide range of soil environments. Precision agriculture can help farmers know how much and when to apply these inputs.

Yield of Dreams

Precision agriculture has already turned one of the oldest sectors into one of the most high-tech, but the best is yet to come. The next step likely involves "big data". Farmers and agribusinesses are increasingly considering how best to take advantage of their treasure troves of data to boost profits and make agriculture more sustainable. In the year 2013, for example, the agriculture giant Monsanto acquired the Climate Corporation, a start-up founded by two Google alumni to use weather and soil data to create insurance plans for farmers and generate recommendations for which crop varieties are best suited to a particular plot of land. Another low-hanging fruit for big data is research on how to use equipment. For example, it's not clear how fast a tractor should be driven when planting corn: too slow makes for an inefficient process, but too fast results in uneven planting, which hurts yields. After



collecting data on the tractor's speed, the eventual yield of the crop, and other factors, however, one could determine the optimal speed for planting. In order to harness big data's power, companies will probably have to pool information across farms. So far, it is the agricultural-input suppliers and agricultural cooperatives that have been able to



Figure 1: Drones collecting data

collect data and some of that big data may come from drones.

With the United States largely out of Afghanistan and Iraq, some suppliers of military hardware have turned their attention to the agricultural market. The move might be smart: small, unmanned aircraft can capture regular images of crops to guide irrigation, pesticide application, and harvesting. And unlike satellites, drones are largely unaffected by cloud cover. Given the operating expense and expertise required, drones will most likely be used commercially at first only for high-value crops, such as wine grapes. Using drones for crop surveillance can drastically increase farm crop yields while minimizing the cost of walking the fields or airplane fly-over filming. A typical application of drone in precision farming activities is shown in **Figure 1**.

The Benefits of Drones Applications in Farming

Number of benefits derived through application of drones in agriculture and farming are as follows.

- Increase Yields
 - Find potentially yield limiting problems in a timely fashion.
- Save Time
 - While all farmers know the value of scouting their crops, few actually have time to cover the acres on foot.
- Return on Investment
 - At an average of \$2 per acre for a walking visual inspection or an aerial survey to take an image of crop fields, the ROI on the purchase of an aerial helicopter drone can be met quickly. In most operations, the ROI for the drones can be achieved in a crop season or less, leaving you owning a drone that reduces your operating costs and improves your crop yield by giving you the timely information you need for quick management intervention.
- Ease of use
 - UAV products can be very complex to set-up and operate, but with proper training, new operators can handle the UAV with ease and confidence.
- Integrated GIS mapping
 - Draw field borders for flight pattern
- Crop Health Imaging
 - Seeing the true health of field in a colour contrast allows one to see how much sunlight is being absorbed by the crop canopy.
- Failsafe - The Drone Flies Home
 - sensilize, a company in ISRAEL, uses a micro-UAS platform to map fields with an integrated application-driven sensor called Robin-Eye, whose eight-band calibrated sensor provides ultra-high-resolution multispectral images of

vegetation in almost all light conditions. Sensilize's cloud-based Robin-Mind software automatically analyzes these images and then – within 24 hours — provides the farmer with a true colour image of the area as well as interpreted maps to enable optimal decisions to enhance efficiency, maximize yield and minimize resources.

Results of the Case Study

Today, basic insights about the crop of the case study can be achieved. In future, it is possible to identify and quantify specific issues, allowing the farm manager to take measured action only when financially appropriate. A difference line can be drawn in between today and tomorrows' vision as follows.

Today	Tomorrow
Spotlight areas of interest for ground investigation	Spot certain insects, diseases, weeds and pests
Determine crop height and growth	Determine economic intervention threshold levels
Calculate crop health with NDVI	Count livestock and determine grazing land health
	Time series and predictive analytics

Drones for Crop Scouting

Drones in the form of crop scouts perform a key service to farmers to ensure crop success. Typically, they are engaged to identify crop issues, (i.e., pests, soil condition, disease, plant health, weeds, etc.) and to make recommendations for treatments/interventions. Currently, they periodically sample small areas and generalize their findings to the whole field. In the near future, crop scouts will use drones to analyze the complete planting area, quickly identify issues, and provide recommendations for highly localized treatments. **Figure 2** shows the application of drone for crop scouting as well as comparison of NDVI values taken with drones and other conventional methods.

The need for Precision Farming in India

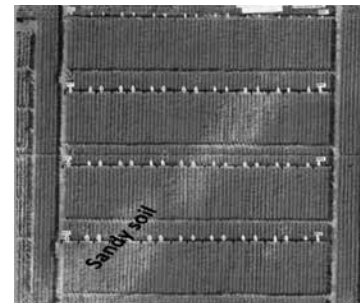
The 'Green revolution' of 1960's has made India self-sufficient in food production. In 1947, India produced a little over six million tonnes of wheat, in 1999 Indian farmers harvested over 72 million tonnes, taking the country to the second position in wheat production in the world. The production of food grains in five decades, has increased more than threefold, the yield during this period has increased more than two folds. All this has been possible due to high input application, like increase in fertilization, irrigation, pesticides, higher use of High Yield Varieties, increase in cropping intensity and increase in mechanization of agriculture. **Figure 3** shows a typical concept of application of autonomous agricultural vehicles.



Collecting color infrared imagery using Hexcopter and Canon T4i NDVI camera



Collecting NDVI data using the Trimble® GreenSeeker® crop sensing system



Yellow Arrows: GreenSeeker Row
Green Stars: N Reference Strips

Figure 2: Comparing UAS with modified NDVI cameras values to greensseeker NDVI values



Figure 3: Concepts of autonomous agricultural vehicles

Fatigue of Green Revolution

Green revolution of course contributed a lot. However, even with the spectacular growth in the agriculture, the productivity levels of many major crops are far below than expectation. Even the lowest level of potential productivity of Indian high yielding varieties have not yet achieved, whereas the world’s highest productive country have crop yield levels significantly higher than the upper limit of the potential of Indian High Yield Varieties (HYV’s). Even the crop yields of India’s agriculturally rich state like Punjab is far below than the average yield of many high productive countries. **Figure 4** illustrates the trends that will shape Crop farming strategy through the year 2030.



Figure 4: Trends that will shape crop farming through 2030

Through recent advancements in drone technology, the cost of collecting vast amounts of information on large areas of land has decreased to pennies per acre. New, sophisticated sensors let us gather data at the plant (leaf) level at a moment’s notice, which supports speedy decision-making and an opportunity for farmers to attain higher crop yields. By adding additional data sources, we expect to find hidden relationships and make further improvements in farm management. This combination of drones, sophisticated sensor hardware, and big data predictive and prescriptive analytics will revolutionize farm management in the near future.

Figure 5 shows the future trends in agriculture with increased mechanization and application of drones. In future, with increased automation and Drone assisted farming will lead to increased farm yield by 10 % and decreased inputs by 25 %.



Figure 5: The future is here

Conclusions

The interest in precision farming (PF) and its introduction has resulted in a gap between the technological capabilities and scientific understanding of the relationship between the input supplies and output products. Development of PF has been largely market-driven, but its future growth needs collaboration between private and public sectors. The potential of this technology has already been demonstrated, but in practice, meaningful delivery is difficult as it needs large scale commercial application to realize the benefits. The main objective of PF is to optimize yield with minimum input and reduced environmental pollution. The scenario, status and strategies for the adoption of PF in small farm in India have been discussed.. PA is facilitating the prospects and scope for switching over to modern agriculture leaving the traditional one by utilizing right resources in right time and management, which results an environment friendly sustainable agriculture.



Kalman Filter based INS-GPS Integration for Navigation Over Short Distances and at Low Speeds

C V Navyashree, Sachit S Rao, V Parameswaran

*International Institute for Aerospace Engineering and Management,
Jain University, Jain Global Campus, Karnataka 562112*

✉navya.neo@gmail.com

Abstract

The navigation of an Unmanned Aerial Vehicle (UAV) is usually performed using data from its on-board Inertial Navigation System (INS). This process leads to errors, which grow with time, as it involves numerical integration. A technique which is used to check the growth of these errors is by using Global Positioning System (GPS) data to correct and update the INS data. However, as the INS data is inherently noisy and GPS data may not be available at the same data rates as the INS, a data fusion algorithm is required to achieve accurate navigation. Both these issues can be addressed with the use of a Kalman filter which now provides a platform for INS-GPS integration. In this paper, this integration is experimentally demonstrated to perform navigation of a vehicle moving at low speeds and over short distances. The navigation is performed by estimating the heading angle of the vehicle moving in the horizontal plane.

Keywords: UAVs; Navigation; INS-GPS integration; Kalman Filter

Introduction

Unmanned Aerial Vehicles (UAVs) are increasingly being used for a wide range of civilian applications, such as surveying, urban mapping etc. The effective use of UAVs for these applications can be increased by lending autonomy to the UAV by ensuring that they fly safely, especially in urban environments. To do so, it is essential to know exactly where the UAV is located at all times. This process forms the heart of navigation, which ensures that the vehicle can be safely and efficiently maneuvered from one point to another.

Traditionally, navigation has been performed using the on-board Inertial Navigation System (INS) which uses sensors to determine accelerations and angular rates [1] in some reference frame. Using this system, given the information about the vehicle's initial position, velocity, and attitude and the instantaneous accelerations and angular

rates of the vehicle along the travelling path, the current position, velocity, and attitude can be obtained by suitable integration of the resolved values of accelerations and angular rates in the same reference frame, in Equation (1), the yaw rate R is integrated to obtain the yaw angle ψ . However, this data is contaminated by noise and the presence of unknown biases, which leads to errors in the estimation of position, velocity, and attitude. Moreover, the numerical integration process causes the errors to grow with time. Hence, there is a need to check the growth of these errors.

One possible solution to limit the growth of such errors is by using corresponding data from the Global Positioning System (GPS) to update the current INS values which can then be used to estimate the future values of these states [2], [3]. GPS is a satellite-based navigation system and a minimum of four satellites is required to compute

the positional information of the system on which the GPS sensor is mounted. In this work, it is assumed that the GPS position data is accurate. Even with this assumption, GPS data alone cannot be relied upon for positional estimation as the satellite signal could be poor due to constraints from satellite geometry or due to interference in urban or hilly terrains. In such cases, a common method that is used for estimation is to integrate both the GPS and INS data.

This process requires the use of a data fusion algorithm that will pick the most accurate estimate of position and the most commonly used fusion algorithm is the Kalman filter [2], [4]. This filter is an optimal estimator, which is used to estimate the states of a dynamic system subjected to process as well as measurement noise. Thus the term filtering, which is apt in such cases, is the process of reducing the effects of noise and simultaneously providing an optimal estimate for the states. Thus, for INS-GPS integration, the Kalman filter (KF) uses the outputs from both the INS and GPS and based on the dynamic model that is selected, provides an estimate of the desired states [5].

In this work, the KF-based INS-GPS integration is studied for a UAV that can be approximately modelled by the simple dynamics

$$\begin{aligned}\dot{X} &= V \cos \psi \\ \dot{Y} &= V \sin \psi \\ \dot{\psi} &= R\end{aligned}\quad (1)$$

where, X, Y are the coordinates of the location of the UAV in a known reference frame, V is the airspeed, ψ is the heading angle, and R is the turn or yaw rate. Equation (1) can be understood to denote the simplified lateral dynamics of a UAV, which holds true under the assumption that the longitudinal dynamics as well as that of the roll and side-slip angles are being controlled by an effective autopilot. The heading angle is directly measured using the INS, which is subjected to both process and measurement noise and has a certain update rate. In addition, the GPS is assumed to provide the coordinates at a much lower rate.

This simple model is selected for the study as emphasis is placed on estimating the heading

angle to calculate X, Y using INS-GPS integration and the KF. In addition, this work focuses on the cases of low airspeed and small flying times. This scenario and the model (1) become applicable in applications involving slowly moving ground vehicles, for instance, in precision agriculture¹.

The layout of this paper is as follows. In section II, the problem is formulated. In section III, the theoretical background of the concepts used in the work is highlighted. In section IV, experimental results are presented. Finally, in section V, the conclusions and future scope of work are listed.

Problem Formulation

Problem Statement

The problem tackled in this paper can be defined as follows: Estimate the heading angle by INS-GPS integration based on a single channel measurement using the KF for low speed and short duration test conditions in systems that can be defined by (1). The equations given in (1) are known as the kinematic equations of the Dubin's car [6]. This model has been used to develop planning algorithms for robots and other non-holonomic systems. These can also be used to describe the simplified navigation equations of a UAV, which are valid under the flat-earth assumption [7].

The block diagram of the solution adopted to solve this problem is as shown in **Figure 1**, the KF, which acts as the data fusion algorithm,

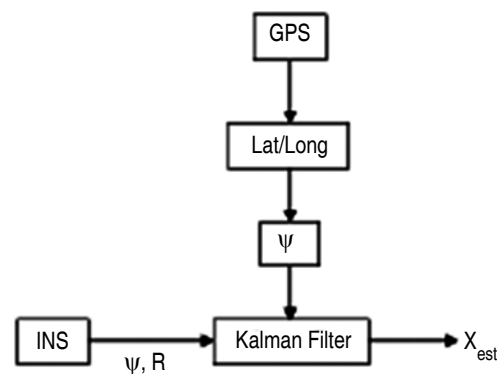


Figure 1 : Block diagram of the KF-based INS-GPS integration

uses both the INS and GPS-based heading angle measurements, as and when they are available, to estimate the position of the vehicle. In this case, the KF uses the heading angle dynamics defined in (1).

Sensor Features

To motivate further the use of the KF, the raw heading angle data as provided by the INS and its features, primarily its noise characteristics, are analyzed. The sensor used in the experiments is the ARN-NS0535 (Aeron Systems); this sensor provides heading angle data with an accuracy of less than 1. The raw INS heading angle data when the sensor is kept in a stationary condition is shown in **Figure 2**. As can be observed from this figure, both the heading angle and yaw rate measurements are noisy and in addition, in the stationary condition, the yaw rate has a non-zero value, indicating a bias. Thus, to yield estimates of the heading angle in the presence of noise, the KF is used.

The use of the KF assumes that the noise in the sensor output has a normal Gaussian distribution. Fortunately, for the sensor used in the experiments, this condition is true. This can be seen in **Figure 3**, where the noise in the measurement process can be modelled as a Gaussian distribution with a standard deviation $\sigma = 0.45^\circ$ and a mean $\mu = 0.88^\circ$.

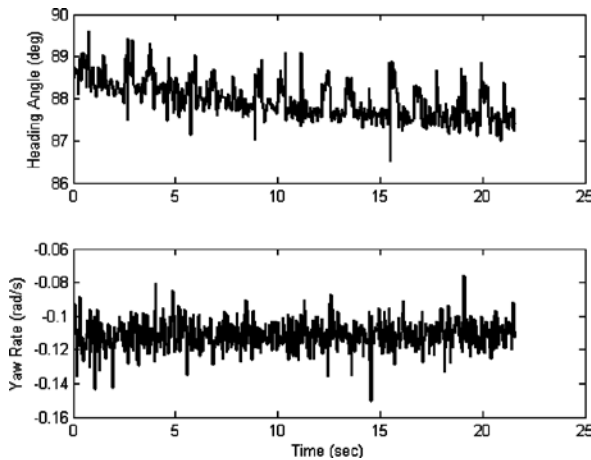


Figure 2 : Raw INS data when this sensor is stationary

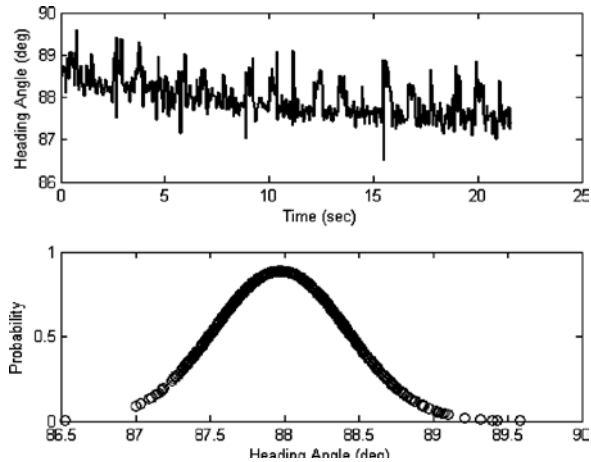


Figure 3 : Noise characteristics of the sensor used in the experiments

In the experimental set-up, as both the INS and the GPS receiver are integrated into a single package, the coordinates of the receiver are calculated by estimating the heading angle using both these sensors. Moreover, the INS-based heading angle values are counted only between $\pm 180^\circ$, which is corrected in the KF implementation, so that this angle is measured in the same reference frame as that from the GPS.

Theoretical Background

A few basic details on the usage of GPS data to calculate heading angle as well as that of the KF are provided in this section.

GPS to Calculate Heading Angle

As is well known, GPS is a one-way ranging technique used to provide highly accurate position and velocity based on range and range-rate measurements. The GPS receiver used in this work displays the position as latitude, longitude, and altitude and the formulae for this conversion can be found in [8]. Based on this data, the heading angle information is calculated as follows: from (1), this angle can be expressed as

$$\tan \psi = \frac{\dot{Y}}{\dot{X}} = \frac{\partial Y}{\partial X} \tag{2}$$

where, the displacements ∂Y , ∂X denote the displacements along the East and North directions, respectively. To calculate these displacements from the lat-long data, it is assumed that these

displacements are small and that the earth is a perfect sphere. These assumptions are valid for the low speed cases that form the focus of this work. Thus $\partial Y = R_E \partial \lambda$, $\partial X = R_E \partial \phi$, where $\partial \lambda$ and $\partial \phi$ are the changes in the longitude and latitude values, respectively, and R_E is the radius of the earth. The value of the heading angle calculated this way is used in the KF, which is briefly described next.

Kalman Filter

The KF, which is model-based, is implemented in discrete time with a step-size, denoted by Δt . Thus, the discrete-time heading angle dynamic model, given by (1), which is contaminated by process and measurement noise, now becomes

$$\begin{aligned} \psi(k) &= \psi(k-1) + \Delta t R(k-1) + q \\ \psi_M(k) &= \psi(k) + r \end{aligned} \quad (3)$$

where, $\psi_M(k)$ is the measured heading angle at time instant k and q and r are the standard deviations of process and measurement noise, respectively.

The KF implementation consists of two steps:

1. Predictor step: where the estimate of the state at instant k is calculated based only the past measurements of the output and is based on the assumed dynamic model. This estimate, denoted as the a priori estimate, is given by

$$\psi_{prior}(k) = \psi_{post}(k-1) + \Delta t R(k-1) + q$$

where, ψ_{post} is the so-called a posteriori estimate. Next, an a priori covariance is calculated using the formula

$$P_{prior}(k) = P_{post}(k-1) + q^2$$

where, P_{post} is the so-called a posteriori covariance. Note that during the initialization, ψ_{post} and P_{post} are guesses and these values quickly converge to their real counterparts.

2. Corrector step: where this estimate is refined using the so-called time-varying Kalman gain, which is calculated using

$$K(k) = \frac{P_{prior}(k)}{P_{prior}(k) + r^2}$$

Now, using this gain, the a posteriori estimate is updated from

$$\psi_{post}(k) = \psi_{prior}(k) + K(k) (\psi_M(k) - \psi_{prior}(k))$$

and the a posteriori covariance is updated from

$$P_{post}(k) = P_{prior}(k) (1 - K(k))$$

Using these iterative steps, the KF yields $\psi_{post}(k)$ as the estimate of the real heading angle. Note that $\psi_M(k)$ in these equations can either be the output of the INS or the GPS sensor, depending on which signal is available. The effectiveness of KF-based INS-GPS integration on experimental data is presented in the next section

Results and Discussions

In this work, a single sensor which provides both INS and GPS data was used. The INS data could be measured every 30 msec and the GPS data could be acquired every 1 sec. Two experiments were conducted and in both cases, the movements were restricted to almost be in a straight line not coinciding with either North or East; this was done to ensure that there are changes in both latitude and longitude.

The two cases were:

1. Movement on foot at a speed of about 0.3 m/s
2. Movement on a ground vehicle at a speed of about 10 m/s.

In the first case, the experiment involved moving in one direction, then performing a U-turn to return to the point of origin. The position coordinates calculated using the INS and GPS data are shown in **Figure 4**.

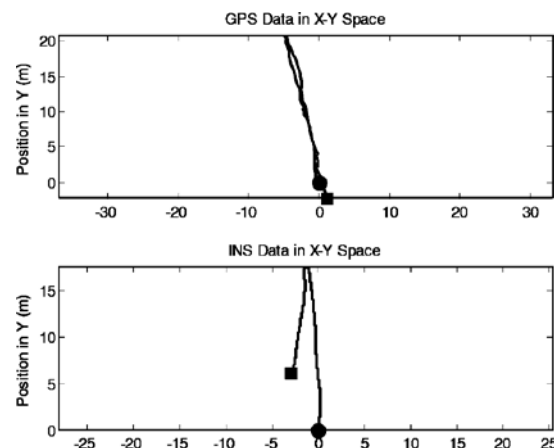


Figure 4 : Position of the user calculated from GPS and INS data

In this figure, the circular marker indicates the start position (shown as zero only for plotting purposes) and the square marker indicates the final position. As can be seen from this figure, there is a significant difference in the positions as calculated from both the sensors. If the GPS data is assumed to be accurate, then the deviation in the INS data can be explained due to integration errors.

Prior to implementing the heading angle calculated from the GPS data using (2), these values were analyzed. Note that as the GPS data gives only lat-long information, the heading angle is calculated as

$$\tan \psi = \frac{\partial \phi}{\partial \lambda} \quad (4)$$

where, the lat-long data provided by the GPS has units of degrees, minutes, and seconds. It was observed that there are abrupt changes in these values – a phenomenon that is physically impossible to attain in the given testing conditions.

These jumps can be attributed to noise in the GPS data at the arc second level, especially in the values of latitude. Thus, only those parts of the GPS data, which are physically close to the values given by the INS sensor are used for analysis.

Case 1 – Results

Although the position data provided by the GPS for this case is close to the actual path traced by the user, see **Figure 4**, this result may appear to hold promise in the estimation of heading angle. However, the heading angle data, calculated using Equation (4) and shown in **Figure 5** does not support this promise. In this figure, the raw heading angle data is presented for only one direction of movement.

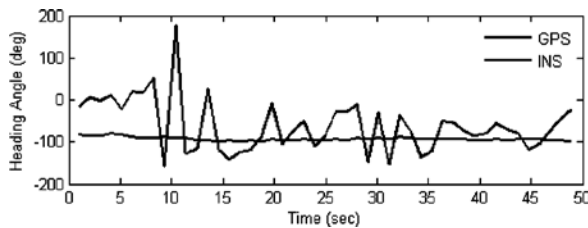


Figure 5 : Heading angle calculated using INS and GPS data for case 1

As can be seen in this figure, there are sudden jumps in the heading angle data as provided by the GPS sensor. In comparison, the INS data appears relatively smooth. Hence, only the INS data is used as inputs for position estimation using the KF. These results are shown in **Figure 6**.

This result indicates that the INS-GPS integration to yield heading angle information may not be suitable for such testing conditions. Hence, a high resolution INS sensor may be better suited in these cases.

Case 2 – Results

For this test case, as can be seen in **Figure 7**, there are sudden jumps (green line) in the GPS-based heading angle data – the reason for which was mentioned earlier in this section. To still study the

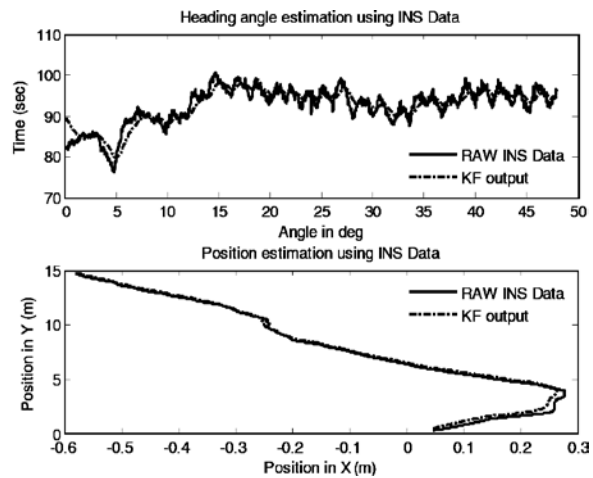


Figure 6 : Position estimation using the KF for case 1

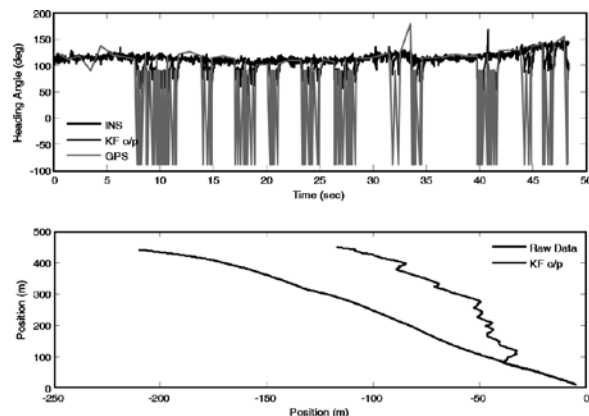


Figure 7 : Estimation in the presence of jumps in the GPS-based data for Case 2



applicability of the INS-GPS integration in this case, these jumps were removed in the data by calculating ψ only when both $\psi\lambda$ and $\psi\phi$ change. This simplification is valid as the approximate value of the heading angle is about 100 degrees and hence does not lie on the North or the East axes. The raw data with this modification is shown in **Figure 8**.

The KF was implemented on both sets of data and the results of position estimation are also shown in the lower subplots of **Figure 7** and **Figure 8**. In these figures, the blue line indicates the calculated position based on the raw INS heading angle data and the red line is the estimation with the KF-based integration.

As is evident, the integration when the GPS data with the sudden jumps is used, leads to greatly diverging estimates. On the other hand, when the data without these jumps is used, the estimation is close to that estimated using the raw data. The effect of applying the KF on only the INS data was also studied. These results are shown in **Figure 9**. As can be compared from these figures, the position estimation with and without INS-GPS integration are almost comparable. This again indicates that the integration would be suitable for much higher speeds or for longer test durations.

A final analysis was performed to estimate the position without the KF filter and using the heading angle values determined from the INS and GPS sensors at the same time instant. This analysis

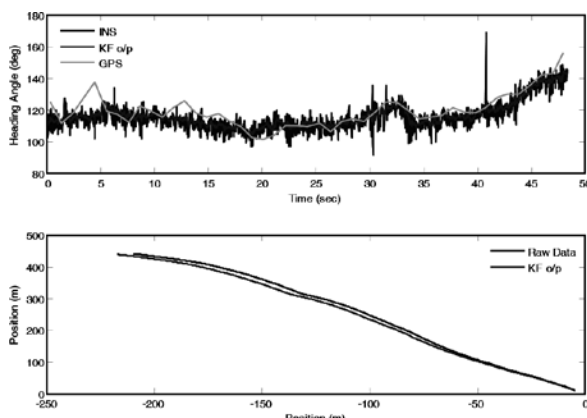


Figure 8 : Position estimation with modified GPS-based heading angle data for Case 2

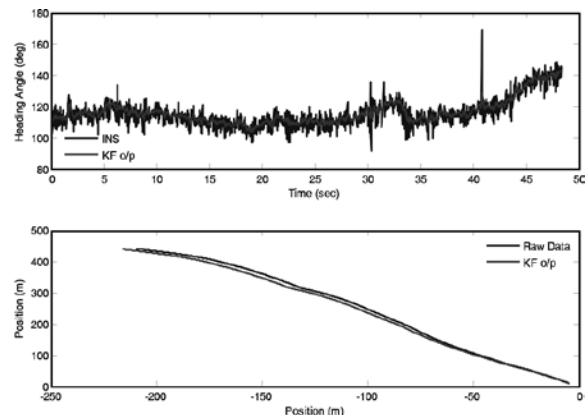


Figure 9 : Position estimation using only the KF data

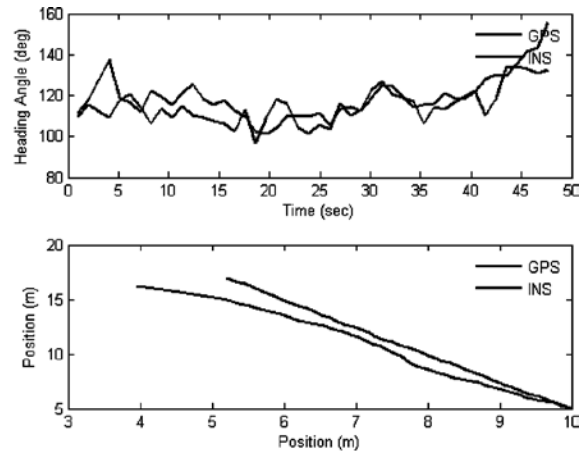


Figure 10 : Position estimation without the use of KF

was performed to study the effect of different data sampling rates. These results are shown in **Figure 10**. As can be seen from this result, there is considerable deviation in the position estimates, thus implying that faster sampling and usage of the INS data alone may be sufficient for these testing conditions.

Conclusions

The experimental results show that the KF-based INS-GPS integration over short distances and time durations do not increase the accuracy of position estimation. In some cases, due to noise in the GPS signal, estimation can also be erroneous. It should be highlighted that the distances covered in the experiment were in the same order of magnitude as the well known values of GPS accuracy, which



is about 3 m. This fact could also explain the errors in heading angle estimation using GPS data. The applicability of INS-GPS integration could have been justified better if the low speed experiment were to have been conducted over a longer distance.

Similarly, in the experiment of shorter duration but at a higher speed, the heading angle estimates obtained from the INS and GPS sensors are almost comparable. This again may raise doubts about the use of GPS integration in such cases. It should again be emphasized that a better quality GPS receiver could have yielded favourable results.

These results indicate that the INS sensor may be sufficient for position estimation for such testing conditions. Of course, accuracy in estimation can be increased with the use of a high resolution and better calibrated INS sensor. This fact is also supported by one of the results published in this work which showed a non-zero yaw rate even when the sensor was completely stationary.

While the KF has proved to be an effective data fusion algorithm, its efficiency is decided by the quality of inputs. As was shown in one of the results, the highly noisy GPS data would not have improved the working of the KF.

References

1. M. Tooley and D. Wyatt, Aircraft Communications and Navigation Systems: Principles,

Maintenance and Operation for Aircraft Engineers and Technicians: Routledge, 2007.

2. N. Magnusson and T. Odenman, "Improving absolute position estimates of an automotive vehicle using GPS in sensor fusion," Department of Signals and Systems, CHALMERS UNIVERSITY OF TECHNOLOGY. 2012. Master's Thesis.
3. M. S. Grewal, L. R. Weill, and A. P. Andrews, Global Positioning Systems, Inertial Navigation, and Integration: Wiley, 2004.
4. Padhi, R. Course on Advanced Control System Design for Aerospace Vehicles. [Online] IIT-Roorkee. <http://nptelonlinecourses.iitm.ac.in/courses/101108047/>.
5. A. Sharma, P. Kumar, S. M. Ratnaker, and S. E. Talole, "Accurate navigation of a UAV using Kalman Filter based GPS/INS integration," 5th Symposium on Applied Aerodynamics and Design of Aerospace Vehicles, Bangalore, 2011.
6. A. Balluchi, A. Bicchi, A. Balestrino, and G. Casalino, "Path tracking control for Dubin's cars," Proceedings of the 1996 IEEE International Conference on Robotics and Automation. Vol. 4, pp. 3123-3128, Minneapolis, 1996.
7. B. L. Stevens and F. L. Lewis, Aircraft Control and Simulation: Wiley-Interscience, 2003, 2nd edition.
8. Course on Global Positioning System (Web). [Online] IIT Roorkee. <http://nptel.ac.in/syllabus/105107062/>.



Real Time Obstacle Avoidance and Navigation of a Quad-Rotor MAV Using Optical Flow Algorithms

Prashanth K Ramaswamy, B Nagaraja, Govind R. Kadambi, S.R. Shankapal

M. S. Ramaiah University of Applied Sciences, Bangalore 560058

✉ prashanthkr.tce@msruas.ac.in

Abstract

Visual based autonomous navigation of Micro Air Vehicles (MAV) in unknown locations is an interesting but challenging problem. This paper analyzes a computer vision based Optical Flow [OF] technique to realize autonomous navigation and obstacle avoidance capability of MAV. The requirement of integration of the OF vector computation algorithm, the decision logic algorithm as well as their interface with an autopilot of Quad rotor MAV have been addressed in requisite technical details. The utility of Horn and Schunck algorithm and the feasibility of its implementation on OMAP 3530 processor placed on board a Quad rotor MAV for its navigation in Yaw and Pitch planes have also been demonstrated in this paper.

Keywords: *MAV; Optical Flow [OF]; OMAP 3530 and Computer Vision*

Introduction

Recent studies have shown considerable interest in the development of Micro Air Vehicles (MAVs) for surveillance and reconnaissance purposes. MAVs of various designs and sizes are under development depending on mission requirements, endurance and range. Their designs vary from fixed wing aircraft to rotorcraft (VTOL) and wing spans range from a few centimeters to nearly half a meter. Propulsion systems that power the MAV include miniature jet engines, IC engines and DC motor driven propellers. The onboard payload systems include electric power sources, navigation and data communication equipment and cameras.

Autonomous navigation of MAVs is best suited for surveillance and reconnaissance during disaster management or in hostile situations. It is a very challenging problem and various factors have to be considered. Other than the methodology to identify obstacles and avoid them, the hardware built on the MAV for such an application is considered to be of prime importance. The hardware on it forms the payload of the vehicle.

The hardware also includes a number of sensors like accelerometers, ultrasounds sensors, gyroscopes, GPS, magnetic needles, infrared sensors with associated electronics.

The many sensors onboard with the associated electronics not only increase the payload and disturb the stability of the MAV but also consume a lot of power. Some of these systems do not work in GPS denied conditions. In order to address these critical issues and overcome some of the drawbacks, a research project was undertaken by the team members at MSRSAS. The research proposed to develop an autonomous MAV which uses only an onboard camera as a sensor to autonomously navigate and avoid obstacles in its path overcoming the limitations of the general MAVs. OF algorithms were identified as one of the computer vision techniques which would be applied to the captured images to identify and locate obstacles. The concept has been proved on sub-class of mini air vehicles – The Pelican® Quadrotor.

Computer vision [1] is a discipline that builds on the theory for developing artificial systems

that obtain information from images. Computer vision studies and describes artificial vision systems that are implemented in software and/or hardware. There are many motivations to develop autonomous artificial systems like robots, MAVs and UGVs. Artificial systems can replace humans in various situations like heavy weight lifting, microscopic visual inspection, video recording in tense situations like wars and similar situations for scene reconstruction, event detection, tracking, object recognition, learning, indexing, motion estimation, and image restoration.

One of the techniques that can be used for computer vision is OF. OF [2] is the pattern of apparent motion of objects in a visual scene caused by the relative motion between an observer and the scene. OF algorithms provide mapping of 3D velocities on 2D image space. OF can give important information about the spatial arrangement of the objects viewed and the rate of change of this arrangement. Discontinuities in the OF can help in segmenting images into regions that correspond to different objects. The success of an OF algorithm is judged by three basic requirements of robotic vision such as the robustness, computational speed and the accuracy. Although there are various algorithms for OF, they do not satisfy all the above mentioned requirements. Even if there is a real time implementation of one such algorithm, it requires a high end computing device. As a result robotic researchers find it difficult to obtain reliable OF estimates in practical scenario. There are different methods to compute OF namely: Block matching based correlation algorithm, Gradient based Horn and Schunck and Lucas and Kanade algorithm as well as the Frequency based (phase and energy) algorithm.

Ted Camus [1] in his work on 'Real Time Optical Flow' suggests that correlation based method for computing OF though robust, is still computationally expensive and results are ambiguous as there is discontinuity in OF flow vectors and hence will not yield real time image velocity measurements rendering it unsuitable for wide range of robotic applications. Christopher

[3] states that correlation based methods are computationally time consuming and leads to ambiguous results. He also compares the gradient based algorithms Horn and Schunck with Lucas and Kanade. According to [3], Lucas and Kanade provide very accurate results but with a higher computation time. The higher computation timing plays an important role in real time navigation and hence an appropriate trade off between accuracy and longer computational task seems to inevitable. The results of [3] clearly suggest that Horn and Schunck algorithm can be used for OF computation in real time navigation. It is also supported by works of Bouden et al. [4] and Zuloaga et al. [5]. Based on previous implementation studies and experiments backed with requisite literature survey, it was inferred that Horn and Schunck algorithm is well suited for real time obstacle detection and avoidance for unmanned aerial vehicle navigation with both on and off board processing.

The subsequent sections describe the detail steps involved in development of an autonomous navigation system using OF Algorithms.

Processor Implementation

Initial experiments were carried out on a toy car that used the concept of Ground Control Station to navigate the UGV. A wireless camera mounted on the vehicle transmitted the video to a PC considered as a base station. Frames from the transmitted video were extracted and the OF algorithm was implemented on it to generate the flow vectors. The obtained OF vectors were used for navigation and obstacle avoidance with appropriate decision logic.

However, the experiments were extended with the replacement of a PC based ground station by an on board system comprising of a camera and OMAP 3530 processor mounted on a Quadrotor to navigate it efficiently at a desired altitude and environment. The OMAP 3530 DevKit8000 [7] was chosen the onboard processor as it has a dual core 600MHz ARM Cortex™-A8 core and 412MHz DSP core. Some other features like the LINUX supporting OS, network port, S-VIDEO

interface, Audio input and output interface, USB OTG, USB HOST, SD/MMC interface, series port, SPI interface, I2C interface, JTAG interface, CAMERA interface, TFT interface, interface for touch screen and keyboard, bus interface as well as HDMI interface make it (OMAP 3530 DevKit8000) very attractive for the chosen application.

The codes for the OF vector computation, navigation and obstacle avoidance were developed in C and compiled on LINUX-2.6.28 OS. For process compilation, the ARM cross compiler was installed on Linux system and the executable file created was loaded on to OMAP 3530 which was executing the obstacle avoidance algorithm.

Real Time Processing in Quadrotor

The choice of MAV to carry out experiments was finalized based on stability, endurance, range, and navigation capability, electronic interfaces with autopilot and payload capabilities. As a survey the rotary wing micro aerial vehicles like the L4-ME Quadcopter, ASC TEC PELICAN, md4-200, Draganflyer-X4 and Idea Forge Technologies were looked into. However comparisons were drawn and the AscTec Pelican quad rotor shown in **Figure 1** was chosen to be ideal for desired application. The AscTec Pelican quad rotor has specifications like the VTOL launch type, running with four DC motors having 920 rpm/V and drawing 4.5-5A. It has 10 inches propellers with all necessary sensors like Autopilot, GPS, and MEMS Gyro for stable navigation and some of the



Figure 1 : Asc Tec Pelican quad rotor

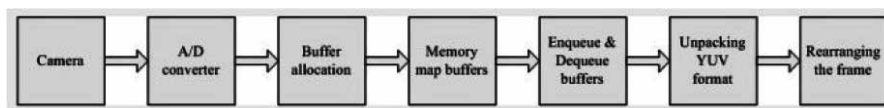


Figure 2 : Block diagram of Video Capturing Algorithm on OMAP 3530 Devkit 8000

other required design and technical specifications can be found in [8].

Figure 2 shows the Video capturing algorithm implemented on OMAP 3530 Devkit 8000 which was mounted on the Quadrotor. The algorithm involves the following steps

- Initialization of capturing device
- Buffer allocation and memory map the buffers
- Enqueue and Dequeue buffers
- Unpacking YUV format and rearranging the frame

From the captured video, image frames are extracted and the OF algorithm is applied to every consecutive frame. In addition to OF vectors, an obstacle avoidance algorithm or logic is a must to navigate the MAV efficiently.

For two consecutive images with no change in background, the OF vectors have no magnitude or direction. Consider an instance when a person is moving a chair in front of the MAV. At this instance, background remains unchanged and there is motion associated with the person and the chair. Using the frames extracted from the video, the OF vectors are computed using Horn and Schunck algorithm. The results showed that OF vectors are present along the direction of motion of chair and person and zero magnitude vectors elsewhere. Based on this inference, the logic of navigating the MAV along the direction of minimal magnitude was developed. The developed logic renders the MAV the autonomous ability to roll, pitch and yaw.

The developed logic gives a 5 directional movement – pitch up and down, yaw –right and left and move forward along a straight line.

Figure 3(a) depicts a scenario of the Yaw action. From the results of **Figure 3(b)**, it is observed that the magnitude of vectors is maximum on the



Figure 3 (a)

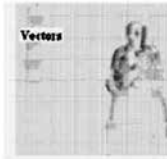


Figure 3 (b)

Figure 3 : Optical Flow Results for Motion in Yaw Plane

right half of the image because of the presence of an obstacle. The obstacle is thus detected and hence the vehicle avoids it by navigating along the direction of minimal magnitude.

For the development of decision logic whose output will determine which direction the MAV has to be navigated to avoid the impending obstacle ahead of it. The image is actually split into two equal halves in two different ways as shown in **Figures 4 (a) and (b)**. The two ways of splitting into two equal halves are:

[L (Left) and R (Right)]

[T (Top) and B(Bottom)]



Figure 4 (a)

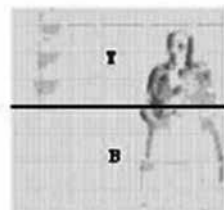


Figure 4 (b)

Figure 4 : Optical Flow based Decision Logic



Figure 5 : Packed YUV interlaced frame



Figure 6 : Complete frame

If the magnitude of OF vector is maximum in the Left (L) half, the MAV will navigate towards Right(R) half and vice versa. If the magnitude of OF vector is maximum on the Top (T) half, the MAV will navigate on Bottom (B) half which corresponds to pitch down and vice versa. As a whole, a comparison of the magnitude of OF vectors on all the four designated halves is carried out. The halve where the magnitude is minimal is chosen as direction for MAV navigation to avoid the detected obstacle. In case of zero magnitude of OF vectors in all the four designated halves, the MAV will continue to navigate along its current flight path.

A serial interface between OMAP processor and the autopilot board has been successfully established to control the Pitch and Yaw motions of the Quad rotor. Based on the OF vector magnitude and arrived decision logic, navigation commands are serially sent to the autopilot to control the required motion of MAV.

Results and Discussion

The developed algorithm was initially tested in MATLAB and then implemented in the processor. The algorithm is implemented on the video/image frames acquired by the OMAP 3530 board in packed YUV (YUV 4:2:2) interlaced format as shown in **Figure 5**. The acquired interlaced frame consists of two fields namely odd field (odd lines in a frame) and even field (Even lines in a frame). The odd and even fields are combined to get complete frame as shows **Figure 6**.

The algorithm was applied to one such instance where the captured frames (**Figure 7 (a)**) showed a person moving his hand downwards from what is assumed to be a reference position. The resultant OF vectors obtained indicated the motion in the



Figure 7 (a) Input frames

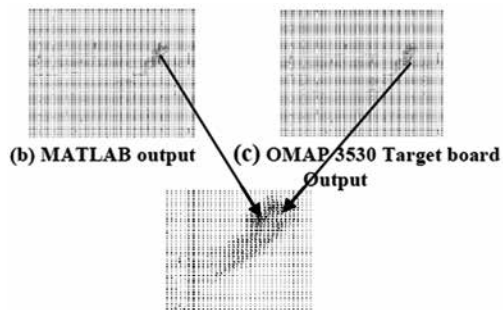


Figure 7 (d) Resultant vectors

Figure 7 : Comparison of Results of Optical Flow obtained from MATLAB and C code on OMAP 3530

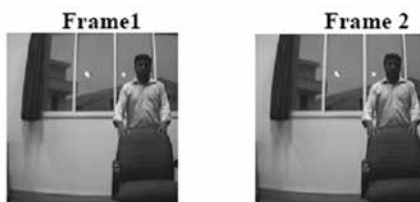
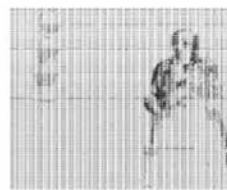


Figure 8 (a) Input frames



8 (b) OF vectors

Figure 8 : Optical Flow Results from Motion in Yaw Plane

downward direction as seen in **Figures 7(b), (c), and (d)**. As a validation, it was observed that the vectors obtained from both MATLAB code and the C code implemented on OMAP processor were the same. The time for processor to execute Obstacle avoidance system algorithm is 0.91 second for an image size of 144X180.

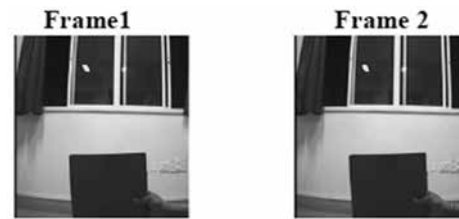


Figure 9 (a)



9 (b) OF vectors

Figure 9 : Optical Flow Results for Motion in Pitch Plane

As already mentioned in the previous section, the decision logic is applied to autonomously navigate the quad rotor MAV. Based on the output of the decision logic, MAV is guided to navigate in the region where OF vectors have minimal magnitudes. A few illustrations to demonstrate Yaw and Pitch actions were carried out and algorithms were tested with MATLAB and the C code implemented on OMAP processor. A scenario shown in **Figure 8 (a)** demonstrates Yaw action. In **Figure 8(b)** obstacles are visualized on right half of the Image frames and OF vectors are computed using the acquired images. Since the magnitude of OF vector is maximum at the right half, the decision logic in the autonomous navigation algorithm commands MAV to steer left. Again, the results of MATLAB and C code implemented on OMAP processor showed identical results of OF vectors and decision logic.

Figure 9 (a) demonstrated Pitch action, In **Figure 9 (b)** obstacles are visualized on Bottom (B) half of the image frame and the corresponding OF vectors are computed. Since the magnitude of OF vectors is maximum at the Bottom (B) half, the decision logic that controls navigation of MAV commands the steering to Top (T) half.

Conclusion

This paper attempts to provide a succinct



understanding and proof of concept OF algorithms which can be used for vision based autonomous navigation of UGV and MAVs. As an initial study, implementation of Horn and Schunck OF algorithm and obstacle avoidance algorithm has been successfully carried out on OMAP 3530 interfaced with an autopilot module of the quad rotor MAV. For a full execution of obstacle avoidance and navigation control algorithm, the OMAP processor onboard MAV logs 3.64 seconds for an input image size of 576 X 720. For an input image size of 288X360, the corresponding execution time of the processor is 1.82 seconds. For a further reduced image size of 144X180, the execution time is found to be 0.91 seconds. To extend the reported study of this paper to MAV with relatively high velocity (> 10 m/s), further optimization of the algorithms and or more advanced DSP processors must be examined. From the studies carried out, it is clear that flight stability, speed of the Quad rotor MAV and computation time for the execution of the algorithms are very critical for accurate obstacle detection and avoidance. In addition, there should be appropriate synchronization between all of them.

References

1. T Camus, "Real Time Optical Flow Computation", Ph.D Thesis, Brown University, 1994,
2. S. S. Beauchemin and J. L Barron, "The Computation of Optical Flow", ACM Computing Surveys, Vol. 27, No. 3, pp. 433-467, 1995.
3. M C Christopher, "MS Thesis on Performance of Optical Flow Techniques for Mobile Robot Navigation", Department of Computer Science and Software Engineering, The University of Melbourne, Australia, 2005.
4. T Bouden, N Doghmane and A Lachouri, "Optical Flow Computation on Image Sequences, Journal of Engineering and Applied Sciences", Vol. 2 (3) pp. 472-480, 2007.
5. A Zuloaga, L José and M J Ezquerro, "Hardware Architecture for Optical Flow Estimation in Real Time", International conference on Image processing, Vol. 3, pp. 972-976, 1998.
6. B K P Horn and B G Schunck, "Determining Optical Flow", Artificial Intelligence, Vol. 17, pp. 185-203, 1981.
7. OMAP 3530 DevKit8000 User Manual, Version 5.1; Release: 2010-05-13.
8. AscTec – Autopilot- manual-v10, Ascending Technologies, Germany.



Swarming Nano Airborne Drones (SNAD) Artificial Intelligence in Drones for Defence Indoor Surveillance on hijacked Buildings

B. Madhan Kumar

*Department of Aerospace Engineering
Madras Institute of Technology, Chennai 600044
✉madanadan92@gmail.com*

Abstract

Unmanned Flying Systems (UFS) is an emerging sector in the aerospace industry with greater opportunity and market demand that can be leveraged to high profitability in near future. This paper discusses a distinct and unique unmanned technology, Swarming Nano Airborne Drones (SNAD), that have taken the entire aerospace field in to next generation. SNAD systems are nano scaled flying system capable to fly individually, as well as in teams and group of teams to perform a specific task. This paper mainly discusses the surveillance capability of SNAD systems inside hijacked buildings. SNAD consist series of 2 distinct Nano Aerial Vehicles (NAVs), one is a quadrotor of 10 gram, 3x3 cm with a live streaming onboard HD camera and the other one is a 90 milligram, 0.3 cm diameter, vertical takeoff and Landing (VTOL) copter with nylon fibre legs and a pusher propeller. The 90 milligram VTOL copter has the shape of spider and invisible while flying. The swarming of NAVs are enhanced by a new kind of programing concept called Infant Programming Module (IPM). These NAVs are useful to monitor the hijacked buildings to estimate the exact situation before planning for commando operations.

Keywords: *UFS; SNAD; NAV; IPM; Swarm; Indoor Surveillance*

Introduction

The SNAD NAV (**Figure 1**) program seeks to push the technology threshold for UAVs beyond the gains demonstrated with ordinary drones. The SNAD program is focussed on design and development of an air vehicle in nano scale capable of autonomous operations to facilitate intelligence and surveillance operations in a restricted interior environment. The NAV program seeks to stimulate research in the field to overcome many technological challenges (including aerodynamics propulsion and energy storage systems for a nano scaled device) facing the development of an air vehicle this size capable of useful military missions in near future and to demonstrate this system in indoor environment. The diminutive size and weight of the nav requires

advancements in design for structure, light weight and efficient propulsion and energy storage systems, autonomous guidance, navigation, sensors and communication subsystems and advanced manufacturing techniques to achieve.

NAV

The NAV “as airborne vehicles no larger than 7.5 cm in length, width, or height, capable of performing a useful military mission at an affordable cost and gross takeoff weight (GTOW) of less than or equal to 10 grams.” The NAV dimensions place it in the smallest class of UAVs. The SNAD program is the first step to explore the NAV category to determine the efficacy of current and future technology to design and build such a small platform and to explore the characteristics and potential missions of NAVs.

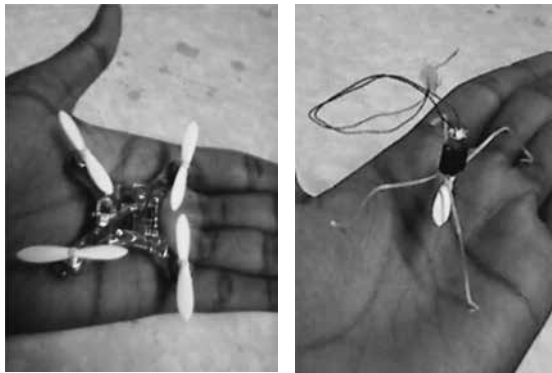


Figure 1 : SNAD NAVs

Swarm

Swarm behaviour, or swarming, is a collective behaviour exhibited by entities, particularly animals, of similar size which aggregate together, perhaps milling about the same spot or perhaps moving or migrating in some direction. It is highly interdisciplinary topic. From a more abstract point of view, swarm behaviour is the collective motion of a large number of self propelled entities. It is an emergent behaviour arising from simple rules that are followed by individuals and does not involve any central coordination.

Swarm Robotics

The application of swarm principles to robots is called swarm robotics, while ‘swarm intelligence’ refers to the more general set of algorithms. ‘Swarm prediction’ has been used in forecasting real time problems and formations of NAVs to rectify the prescribed problem.

Swarm Intelligence

Swarm Intelligence (SI) is the collective behaviour of decentralized, self organized systems, natural or artificial. The concept is employed in work on artificial intelligence. SI systems consist typically of a population of simple agents interacting locally with one another and with their environment. The inspiration often comes from nature, especially biological systems. The agents follow very simple rules, and although there is no centralized control structure dictating how individual agents should behave, local, and to a certain degree random, interactions between such agents lead to



Figure 2 : Nano Quadrotor Prototype

the emergence of “intelligent” global behaviour, unknown to the individual agents.

Agility

Agility or nimbleness is the ability to change the body’s position efficiently, and requires the integration of isolated movement skills using a combination of balance, coordination, speed, reflexes, strength, and endurance. Agility is the ability to change the direction of the body in an efficient and effective manner. There are two commonly accepted approaches to study scaling in aerial vehicles. Mach scaling is used for compressible flows and essentially assumes that the tip velocities are constant leading to a condition angular velocity is inversely proportional to rotor radius. Froude scaling is used for incompressible flows and assumes that for similar aircraft configurations, the Froude number is constant, where g is the acceleration due to gravity. However, neither Froude nor Mach number similitudes take motor characteristics nor battery properties into account. While motor torque increases with length, the operating speed for the rotors is determined by matching the torque-speed characteristics of the motor to the drag versus speed characteristics of the propellers. Further, the motor torque depends on the ability of the battery to source the required current. All these variables are tightly coupled for smaller designs since there are fewer choices available at smaller length scales. Finally, the assumption that propeller blades are rigid may be wrong and the performance of the blades can be very different at smaller scales, the quadratic scaling of the lift

with speed may not be accurate. Nevertheless these two cases are meaningful since they provide some insight into the physics underlying which the craft is manoeuvrable. Froude scaling suggests that the acceleration is independent of length while the angular acceleration is inversely proportional to length. On the other hand, Mach scaling leads to the conclusion that linear acceleration is proportional to length, while angular acceleration is inversely proportional to square of length or area. Since quadrotors must rotate (exhibit angular accelerations) in order to translate, smaller quadrotors are much more agile.

The Nano Quadrotor

Configuration

The quadcopter prototype is shown in **Figure 2**. Its total structure is made of square PCB board on which the motors are fixed in the drilled holes on four corners. The PCB board is bevelled and aerodynamically trimmed to enhance the flight performance. PCB board has two layers, the bottom layer consist a custom motor controller circuit and top layer consists the main controller board. To produce lift, the NAV uses four fixed pitch propellers with propeller diameter three cm, the vehicle propeller tip to propeller tip distance is 8.5 cm and its weight without lithium polymer fuel cell is five grams. The hover time is approximately 11 minutes with a two cell 80 mAh LI-PO fuel cell that weighs five grams.

Electronics

Despite its small size this vehicle contains a full suite of onboard sensors. An FQ 31 processor, running at 72 MHz, serves as the main processor. The vehicle contains a 3-axis magnetometer, a 3-axis accelerometer, a 6-axis 2000 deg/sec rate gyro for the roll and pitch axes, and a single axis 500 deg/sec rate gyro for the yaw axis. For communication the NAV uses transceivers of 2.4 GHz.

Controls

Each quadrotor has a radio transceiver, operating at 900 MHz and 2.4 GHz. The base station sends, via custom radio modules, the desired commands, containing orientation, thrust, angular rates and attitude controller gains to the

individual quadrotors. The onboard rate gyros and accelerometer are used to estimate the orientation and angular velocity of the craft. The main microprocessor runs the attitude controller and sends the desired propeller speeds to each of the four motor controllers at full rate (600Hz).

The Nano Spiffly

Configuration

The nano spiffly is a single unit of a swarming, basic flying drones shown in **Figure 3**. Its structure is basically a propelling unit above which a capacitor is included. The propelling unit consists a 10 milligram motor and a 10 milligram pusher propeller. The propeller diameter is 3cm the propeller tip to tip distance is also three cm. four legs are made from nylon composite weighs 10 milligrams and 80 mAh, 3.5 volts capacitor is used as the power unit. The capacitor weighs 20 milligrams. The total weight of this NAV is 50 milligrams and can able to produce a lift force of 17 grams. Moreover the weight of this NAV is equally distributed to the four legs hence the weight carried by each leg is around 12.5 milligrams. Hence this NAV can able to land and stand firmly on a spider's web. Total structure of this NAV is made of white and shiny materials, which totally reflects all light hence totally invisible in flight, which is a cost effective camouflage technology very well suited for indoor surveillance.

Electronics and Control

The NAV Spiffly is still under observation, so there is no inbuilt electronic system is embedded. The free flight characteristics are analysed by placing

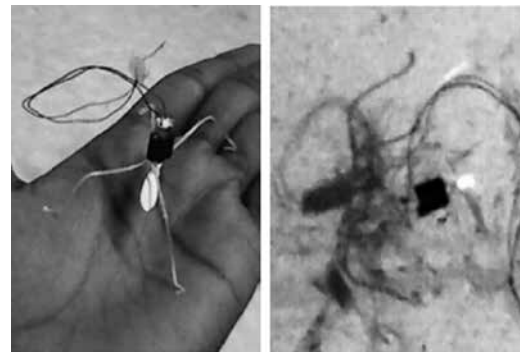


Figure 3 : Nano spiffly prototype and it is landed on spider web

a charged capacitor in the spiffly, controlled flying characteristics are analysed by connecting it with an external control system. The swarm behavior of nano spiffly is analysed by designing a wired loop functions as a artificial bee colony optimization and tested with a wireless IR controller. The altitude control is done manually by increasing or decreasing the propeller speed. The torque balancing is done with changing position of drone legs. The directional control is achieved by a new kind of system called mass piloting system, by changing the orientation of the motor weight the lateral and longitudinal moments as well as rolling moments are enhanced.

Dynamic Modelling

The nano quadrotor shown in **Figure 2** is used for dynamic modelling. The dynamic model and control of the quadrotor is determined by considering a inertial frame of reference and relating it with fixed body frame of reference. Let us consider fixed body frame of reference 'B' with unit vectors o, p, q , and a inertial frame 'A' with unit vectors l, m, n . 'B' is described in 'A' by a position vector 'r' with the centre of mass 'C' and a rotation matrix 'R' (**Figure 4**). The singularities are avoided by using the full rotation matrix to describe the quadrotor orientations. The angular velocity in body frame B is ω , where,

$$\dot{\omega} = RTR$$

$\dot{\omega}$ represents the skew matrix form of vector. The four rotors of the quadrotor are numbered 1-4, with odd number rotors having a pitch that is opposite to the even numbered rotors.

Angular velocity of the rotor is represented by ω_i , where ($i=1, 2, 3, 4$). Lift force 'F' and Moment 'M' are proportional to square of angular velocity (ω^2),

$$F \sim \omega^2, \quad M \sim \omega^2$$

$$F = c \omega^2$$

$$M = d \omega^2$$

c and d are constants that are empirically determined. The quadrotor motor dynamics have very less time constant, which is very fast when compared to the time scale of rigid body dynamics

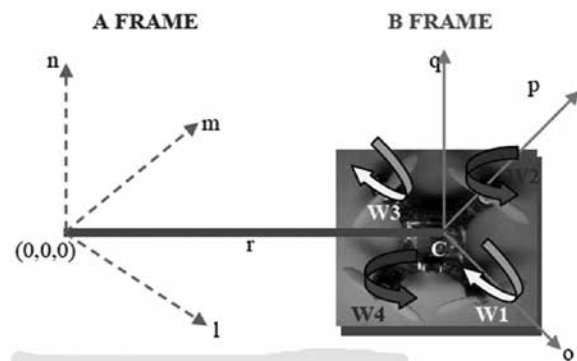


Figure 4 : Reference plane and propeller numbering convention

and aerodynamics. It means the force and moments of the quadrotor changed instantaneously since motor dynamics has its value in milliseconds.

The control input to the system is denoted by 'u', consists net thrust in direction of 'q'.

$$u_i = \sum_{i=1}^4 F_i$$

$$u = \begin{pmatrix} c & c & c & c \\ 0 & cL & 0 & -cL \\ -cL & 0 & cL & 0 \\ d & d & d & d \end{pmatrix} \begin{pmatrix} \omega_1^2 \\ \omega_2^2 \\ \omega_3^2 \\ \omega_4^2 \end{pmatrix}$$

Newton-Euler equations of motions are,

$$mr = -mga_3 + u_1 o$$

$$\dot{\omega} = I^{-1} \left(-\omega * I \omega + \begin{pmatrix} u_2 \\ u_3 \\ u_4 \end{pmatrix} \right)$$

By inverting the equation of system input 'u', the desired rotor speeds are determined to achieve desired 'u'.

Flight Characteristics

The quadcopter is nano scaled, so the flight characteristics are calculated by empirical relations and approximated with logical real time assumptions and datas thus obtained are nominal values when compared to the results of analysis on a large scaled model of the same quadcopter.

In order to analyse the flight characteristics of nano quadrotor it is useful to generate a equivalent simple physics model and analyse its characteristics. Consider the characteristic length, L , the rotor radius, R , scales linearly with L , the mass of quadrotor scales as L^3 and the moment of inertia scales as L^5 . On the other hand the lift or thrust, F , and drag, D , from rotors scales with cross sectional area and the square of blade-tip velocity. Since blade diameter is 3 cm, the velocity changes from hub to tip of propeller blade is negligible, so the propeller velocity is taken as blade tip velocity, v , and the angular velocity, ω is approximately equal to rotor RPS.

By propeller theory, lift F and drag D is assumed as

$$\begin{aligned} F &\sim \omega^2 L^4 \\ D &\sim \omega^2 L^4 \\ a &\sim (\omega^2 L^4) / L^3 \\ a &= \omega^2 L \end{aligned}$$

Where, 'a' is the linear acceleration. Thrust from the rotor produce moment with moment arm, L . Thus the angular acceleration is,

$$\begin{aligned} \alpha &\sim (\omega^2 L^5) / L^5 \\ \alpha &= \omega^2 \end{aligned}$$

The rotor speed ω also scales with length, since smaller motors produce less torque. The flight datas of quadrotor are shown in **Table 1**. The Cl vs Cd plot, shown in **Figure 5**, clearly shows that the lift force is far higher than the drag force, this is because of the motor power or propulsive power, that is 20 milligram motor with propeller used in nano quadrotor can able to produce 17 grams thrust.

Formation Flight

Basic Swarming

The Swarm Intelligence (SI) is induced in the nano quadrotors by flying them in a team or group of teams, capable of doing some specific tasks say indoor surveillance. Initially the formation flight or swarming is achieved by setting same frequencies for two or more transceivers and controlling them by a single radio controller. The basic formations are achieved by placing them in ground similar

Table 1 : Quadrotor Flight Characteristics

S.No	Nano quadrotor flight datas		
	Parameters	Values	Units
1.	Blade tip velocity (v)	3.33	ms^{-1}
2.	Angular velocity (ω)	3.33	deg s^{-1}
3.	Lift (F)	17	gram
4.	Drag (D)	20	milligram
5.	Linear acceleration (a)	0.44	ms^{-2}
6.	Angular acceleration(α)	11.08	deg s^{-2}

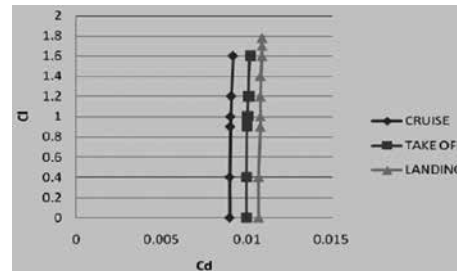


Figure 5 : Lift coefficients against drag coefficients

to the formation grid and make them fly. In order to enable the group of quadrotors to survey the hiacked building interiors, some optimization techniques are needed.

Optimization Techniques

On observing the swarm behaviour of insects and bird flocking mechanisms, the Bee colony optimization suits well for a nano scaled flying device especially implemented in real time indoor surveillance. Artificial bee colony algorithm (ABC) is a metaheuristic algorithm introduced by Karaboga in 2005, and simulates the foraging behaviour of honey bees. The ABC algorithm has three phases: employed bee, onlooker bee and scout bee. In the employed bee and the onlooker bee phases, bees exploit the sources by local searches in the neighbourhood of the solutions selected based on deterministic selection in the employed bee phase and the probabilistic selection in the onlooker bee phase. In the scout bee phase which is an analogy of abandoning exhausted food sources in the foraging process, solutions that are not beneficial anymore for search progress are abandoned, and new solutions are inserted instead of them to explore new regions in the search space. The algorithm has a well balanced for exploration and exploitation ability.

Infant Programming Module (IPM)

Infant Programming Module (IPM), is a new MATLAB based Artificial Intelligence (AI) program, specially designed for NAVs. This program includes an intentional memory space for each quadrotor to store the possible errors occurred during flight tests as executable programs and using it in the same kind of scenario or in real time. It enhances the training based situation reaction for mechanical systems which is to be used for defence purposes. Artificial situation reaction is really a giant leap in AI defence bots, fault tolerance and redundancy of formations are high in this program module, the formation is adjusted accordingly with respect to the error programs even some drones are defected during real time missions. Fault tolerance of this programming module is high due to decentralization of drone teams. The IPM is still in its developmental stages and the above stated are the initial program pseudo code, in this module the orientation of each drone in formation is also recorded with respect to change in time, t .

Conclusion

This paper describes the design, manufacture, modelling and control of SNAD NAVs, nano quadrotor, that has a 10 gram mass and is 8.5 cm in diameter, and the architecture and process for coordinating a team of nano quadrotors with experimental results. While the quadrotors doesn't rely on an external localization system for position estimation and therefore they are truly decentralized at this stage, these results represent the first step toward the development of a swarm of Nano quadrotors. The small size is shown to facilitate agility and the ability to fly in close proximity with less than one body length separation. Mixed IPM programming techniques are used to coordinate twenty micro quadrotors in known three-dimensional environments with obstacles.

References

1. Castillo, P., Dzul, A., Lozano, R., 'Modelling and Control of Mini-Flying Machines', Berlin: Springer, 2005.
2. Wikipedia. Org, <http://en.wikipedia.org/wiki/Quadrotor>. Date Accessed: September 12, 2008.
3. R C Helicopter Fun, <http://www.rchelicopterfun.com/rc-helicopter-material.html>. Date Accessed: September 24, 2008.
4. X-UFO SHOP, <http://www.xufo-shop.de>. Date Accessed: September 23, 2008.
5. Bramwell's Helicopter Dynamics, Second Edition. Done, George. David Balmford. Library of Flight Series. © 2001.
6. Boyd, Stephen. 'The Kalman Filter'. www.Stanford.edu/class/ee363/kf.pdf. Date Accessed: October 8, 2008.
7. Hussein, Islam. 'Observers and the Kalman Filter'. October 2008.
8. Bouabdallah, S., Noth, A., Siegwart, R., 'PID vs LQ Control Techniques Applied to an Indoor Micro Quadrotor: Autonomous Systems Laboratory'. Date Accessed: December 3, 2008.
9. 'Modern Inertial Technology: Navigation, Guidance and Control', Second Edition.
10. S. Bouabdallah, 'Design and Control of Quadrotors with Applications to Autonomous Flying'. PhD thesis, Ecole Polytechnique Federale de Lausanne, Lausanne, Switzerland, February 2007.
11. F. Bullo, J. Cort'es and S. Mart'inez, 'Distributed Control of Robotic Networks: A Mathematical Approach to Motion Coordination Algorithms. Applied Mathematics Series'. Princeton University Press, 2009.
12. J. P. Desai, J. P. Ostrowski and V. Kumar, 'Modeling and Control of Formations of Nonholonomic Mobile Robots', IEEE Trans. Robot., 17(6):905–908, December 2001.
13. M. Egerstedt and X. Hu, 'Formation Constrained Multiagent Control', IEEE Trans. Robot. Autom., 17(6):947–951, December 2001.
14. Dario Floreano, Jean-Christophe Zufferey, Adam Klaptocz, Jrg Markus Germann and Mirko Kovac, 'Aerial Locomotion in Cluttered Environments,. In Proceedings of the 15th International Symposium on Robotics Research, 2011.
15. V. Kumar and N. Michael, 'Opportunities and Challenges with Autonomous Micro Aerial Vehicles', In International Symposium on Robotics Research, 2011.
16. S. Lupashin, A. Schollig, M. Sherback and R. D'Andrea', 'A Simple Learning Strategy for High-speed Quadrocopter Multi-flips', In Proc. of the IEEE Intl. Conf. on Robot. and Autom., pages 1642–1648, Anchorage, AK, May 2010.



Tethered Aerostat Systems for Agricultural Applications in India

Rajkumar S. Pant

*Department of Aerospace Engineering
Indian Institute of Technology Bombay, Mumbai 400076
✉rpant@iitb.ac.in*

Abstract

This paper outlines two major problems faced by the farming community in India, viz., lack of an ICT infrastructure, and damage to agricultural produce due to bird and animal menace. The severity of these problems is highlighted and a review of existing interventions to handle it are touched upon. A self-contained and easily re-locatable Tethered Aerostat System for Agricultural Applications (TASAA) is proposed as a cost effective means for handling these problems. The features of TASAA are described, and the benefits of using it over other methods are brought about. The remaining part of the paper deals with issues like other application of TASAA, scope of scaling up and innovation, affordability, risks and their mitigation. Since the technology readiness level of Lighter-Than-Air systems in India is quite high, there is very little risk involved in design, fabrication and deployment of such systems for the benefit of the farming community.

Keywords: *Tethered Aerostat Systems; Agricultural Applications*

Background and Introduction

According to the latest General Census of India (2011), there are about 118.6 million cultivators in India, which constitutes ~ 24.6 % of our total workforce. Apart from this, there are several others who are indirectly associated with cultivation; the total workforce which earns its livelihood from agriculture and related activities is ~ 54.6 %. A major portion of these cultivators (~ 85%) are marginal and small farmers (possessing land below 2 hectares). Vast expanses of fertile land, a large pool of agricultural scientists, and hard-working farmers make India the second largest agricultural producer in the world. Yet, India's farm productivity remains low, and the farmers remain poor. Most farmers have small holdings; they lack information on the supply-and-demand conditions that affect local prices; have limited access to crop management know-how, and weather forecasts that impact agricultural operations. Access to such information could help transform their low-yielding plots to highly productive farms. To make matters worse,

Indian farmers are at the receiving end of an expensive, highly fragmented supply chain with underdeveloped infrastructure. These supply chains are largely controlled by unscrupulous middlemen, who plough back only a small share of the consumer price to the farmer. Due to these problems, the farmers have low income, and are perennially locked in the vicious cycle of low income, low investments, low productivity, resulting in low income.

Severity of the Problem

At 157.35 million hectares, India holds the second largest agricultural land globally. India has more arable land than China. This, despite the fact its total area is only a little over 34 percent that of China. However, China produces more rice and wheat than India does. India has a yield rate of 2.4 tons per hectare for rice, placing India at 27th place out of 47 countries. China has a yield rate of 4.7 tons per hectare. Even Brazil has 3.6 tons per hectare yield rate. India's yield rate of 3.15 tons per hectare places it 19th out of 41 countries

in case of wheat production. Whereas China leads us here as well by being at 4.9 tons per hectare. Even South Africa has a yield rate of 3.4 tons per hectare. There are multiple reasons for this low productivity; one of them being very limited access to ICT that is currently available to the Indian farming community.

Benefits of ICT Infrastructure for Farmers

The power of ICT (Information and Communication Technology) can be leveraged by providing this section of our workforce a timely and low-cost access to relevant data and information. This has been established by the outcome of two successful case studies carried out in India recently; viz., e-Chaupal and e-Sagu. e-Chaupal was initiated by the Agri-Business segment of India Tobacco Company (ITC) in early 2000 [1, 2]. Today, there are ~ 6500 e-Chaupal kiosks in 10 Indian states, serving more than 40,000 villages and 4 million farmers; a proof that a sustained business model for e-Community Center can have value creation for the stakeholders, on one hand, and can also yield substantial societal return, on the other. e-Sagu [1, 3] a joint initiative of Media Lab Asia and IIIT Hyderabad, which was started in 2004. Sagu in Telugu means cultivation, and e-Sagu created a system which provides Agriculture experts (Scientist's) advice to remote farmers through internet. It was initially launched as a pilot effort for 1051 cotton farms in Andhra Pradesh in 2004-05, and was eventually scaled up to 5000 farms and six types of crops across six districts in the state. This system has improved the productivity of the region and farmers are taking its benefit.

Damage to Agricultural Produce Due to Bird Menace

There is a lot of damage to standing crops in fields and fruits in orchards due to bird menace, which is mitigated by various active and passive means. Field experiments carried out in 1983 by Shiota et.al [5] in Japan concluded that balloons with large eyespots on them have a scaring effect

on birds, and the scaring effect remained for many weeks after the balloons were removed. This study was carried out using spherical balloons of 2.6 m diameter, with five eyespots of 0.6 m diameter painted on them. The balloons deployed for around two weeks were successful in completely mitigating the damage due to grey starlings (*Sturnus Cineraceus*) in peach farms and grape vineyards. It was also observed that once the birds were scared, they usually did not return to the same place again. Loss in agricultural productivity due to bird menace are estimated to range from 5% to 100%, depending on various factors.

Damage to Agricultural Produce Due to Animal Menace

Agricultural crop damage and associated yield reduction by animals like Macaques and Wild boar in India are substantial. The potential solutions to prevent crop losses by traditional methods have met with mixed success. Some of the control methods are costly and laborious. Most recommended practices for managing wild boar include growing thorny and repellent crops on the border, barbed fences, regular vigilance, cooperative guarding, olfactory masking by growing odorous crops, sulphur-coated twines, apart from sprinkling human hair on the border, and pig dung slurry spray, to prevent damages by wild boar. Apart from this, the Macaques are driven out using crackers, shouting, using Hanuman Langurs but none have proven successful. Many of the methods discussed above are already in vogue and the damage by Wild Boar and Macaques continue unabated.

Across the world, researchers have been successful in dispersing animals from agricultural lands, airports and urban areas using bio-acoustics. Bio-acoustics is natural sounds used by animals to communicate alarm and distress amongst themselves. They also respond to predator sounds. It is possible to drive the targeted animals from the agricultural fields using a set of calls from an electronic broadcasting platform.

Review of Existing Interventions/ Technological Solutions

Communication infrastructure in the last mile is either absent or woefully inadequate in remote farming areas. For providing communication networks, fixed towers (limited to a height of around 50 m) are used, but they occupy real estate, become perching locations for birds, and are not re-locatable. Active means for bird hazard mitigation e.g., acoustic repellents and loud alarms are very expensive, since they need continuous power supply and/or battery support. Passive means like making Scarecrows are very popular, since they involve low cost and are easy to make and install, but their efficacy is limited due to their fixed location and small size.

Proposed Solution

A Tethered Aerostat System for Agricultural Applications (TASAA) to address the problems highlighted above, viz., provision of ICT facility to farmers in remote locations, and mitigation of damage to agricultural produce due to birds and animals by scaring them away. An aerostat is an aerodynamically shaped balloon filled with a Lighter-than-Air gas (LTA) e.g., Hydrogen or Helium, and is tethered to the ground. They generate buoyant lift, due to which they can overcome the force of gravity; the magnitude of this buoyant lift depends on the volume of the envelope and difference between the density of ambient air and the LTA gas. Large scale aerostats commercially available in the market can be used to deploy payloads of several tons to altitudes as high as 4500 m (~15,000 ft), but such systems will be too expensive and unaffordable for agricultural applications. As far as the farmer is concerned, an aerostat can be considered to be an aerial platform for deploying any equipment or sensor to a desired altitude. A conceptual sketch of the proposed TASAA system is shown in **Figure 1**.

The envelope will be tethered using a conducting tether to a winching and mooring system, so that it can be raised and lowered as and when it is to be deployed to address a particular operational requirement. The manpower requirement for

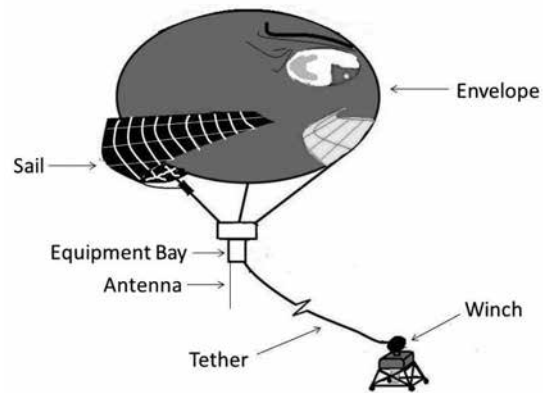


Figure 1: Conceptual sketch of TASAA

operating TASAA would be limited to one telecom operator, supported by few persons trained in setting-up and handling the system. TASAA can be sized using an existing design methodology [6-7], which takes care of the effect of certain user-specified parameters as well as the operating conditions. The aerostat envelope can be fabricated by joining the petals of a special-purpose multi-element coated or laminated material.

Benefits of using TASAA Over Existing Systems

An aerostat can act as an elevated aerial platform to install the necessary information relaying equipment and allied devices. In case of provision of wired internet in both e-Chaupal, and e-Sagutype systems using telephone lines or VSAT system, a Wi-Fi router can be installed on the aerostat making the systems less complicated. In this case, even cellular phones can be used to get the information, thus making the information itself mobile. Aerostats can remain afloat for days at a stretch making it a platform having more endurance. These aerostats can be made to be re-locatable, unlike fixed structures like the tower based systems. In this case, they don't take up permanent space and also their area of effectiveness can be changed altogether to facilitate the flow of information wherever required. Using the winch, the height of the balloon can be lowered or raised, thus providing optimum altitude of deployment meeting the specific needs. It may appear that

a tethered aerostat would be prone to getting damaged by birds or miscreants, but in reality they are quite resilient. The differential pressure between the LTA gas inside the envelope and the ambient air is minimal, so the leak rate is low, and on-board equipment allows the operators to monitor the pressure in the aerostat and the tension of the tether. If there is any leakage of the envelope, it is possible to bring the aerostat down safely. One can easily identify the locations of these leaks, patch them up, replenish LTA gas, and re-launch the system. Bioacoustics technology has not been tested using an aerostat platform in India. This model provides new lines of opportunity in dispersing problematic birds/ animals from agricultural fields with variable/ adjustable heights. The platform is highly suitable for dispersing animals from tall trees like Areca nut, coconut or other fruiting trees. In the present scenario, the acoustics played on the ground level in tall tree crops where Macaques are problematic; the sound signals do not reach the canopy adequately. This prevents Macaques from avoiding the area. If the sound signals are made to reach the treetops, for example, using an aerostat, the signals can be effectively conveyed to target animals. This alone can prevent Crores of rupees of loss the plantation farmers are incurring annually. The variable height of the aerostat platform also gives a leverage to control the height of dissemination of sound signals thus preventing acclimatization of target species. Sounds coming from different heights instill fear in the target species on a continual mode, and thus the crop would be saved in the process.

However, existing acoustic systems need to be customized for the aerostat payload. The design of the acoustic equipment, weight of the equipment, PCB design, modeling of the speaker chamber, etc., needs to be carried out in close association with companies

and agencies that develop and supply such systems. If the platform is using generator (captive energy) power, then ambient noise needs to be considered for determining the effective range of the acoustic equipment. Equipment currently

available can cover about 4-5 acres in an ambient sound level of 42dB. Onboard solar panel for energy requirement for running the equipment, duration required to be played, consideration on diurnal (daytime: Macaques) or nocturnal (night time: Wild boars) behaviour of the animal needs to be taken into consideration before the payload is designed.

Scope for Innovation

The most cost-effective and efficient (as far as lifting capacity per unit volume is concerned) LTA gas is Hydrogen, which is not very expensive and easily available, but suffers from the drawback of being highly inflammable. The next best option is Helium, which is also non-combustible, but it is very expensive and not easily available. One innovative approach would be to try out a mixture of Hydrogen and Helium up to a limit till which the mixture remains non-combustible. It is also possible to create a double chambered envelope, in which the core envelope is filled with Hydrogen, which is surrounded by a small annular chamber filled with Helium. This scheme has been suggested for airship envelopes by Gupta and Priyadarshi [8], but it has not been implemented in aerostats as yet. A basic concern that exists whenever an aerostat is to be deployed for long duration of time is, how to recover the onboard sensors and equipment in case the tether breaks due to some reason, resulting in a free flying breakaway envelope. To tackle this situation in an automatic manner, a payload recovery device has been developed by the investigators during previous studies [9, 10]. Such a device will be installed on the aerostat; it will automatically detect persistent loss of tension in the tether due to an accidental breakage, and deflate the envelope so that the payload can be recovered. In addition a remotely triggered Rapid Deflation Device [11] will also be installed to handle any emergencies.

Affordability

It is estimated that the initial cost of a TASAA envisaged to lift a payload of around 10 kg to an altitude of around 80 m (~ 260 ft) above ground would be around Rs. 3.50 Lakhs, if developed



indigenously. The variable cost of deploying this system would be around Rs. 0.50 Lakh per year, to take care of costs towards LTA gas top-up, general maintenance and replacement of batteries and tether. The initial and operating cost of TASAA depends on a variety of factors such as amount of payload to be carried, maximum expected duration of its deployment, and the ambient weather conditions expected to be encountered at the site of deployment. Its affordability can be justified by a comparison of the costs of other alternative solutions to provide the same or similar level of functionality and features. To further reduce the affordability of the system, the possibility of using superheated steam, or hot air to create the required buoyant lift will be investigated. This concept was investigated in a previous study by the investigators for a low cost transriver aerial ferry in 2008 [12]. In addition to the application described above, the TASAA can also be used as a system for several other possible applications to increase its affordability. Some such applications are listed below:

- Updating of land records by carrying out aerial surveys.
- Providing last-mile communications to remotely located communities.
- Aerial surveillance during management of natural disasters, e.g., Earthquakes.
- Providing telemedicine solutions in remote locations.
- Enabling E-Learning and E-Governance.
- Providing high intensity illumination for time-critical night farming needs.
- Creation of networked weather monitoring stations.

A comparative study of an aerostat based wireless communications system versus conventional Fixed Towers for providing last-mile connectivity to deprived communities was carried out by Bilaye et al. [13] in 2008. This study concluded that for cost of this Aerostat based system was nearly half of that for the tower based system,

over a life cycle of three years. Another study by Sharma et al. [14] in 2014 indicated that the life cycle costs over three years for an aerostat based aerial surveillance system was found to be 30 % lower compared to that with a fixed tower based system.

Potential for Scale Up

The prototype system can be easily scaled up to carry larger payloads, since the LTA systems enjoy the benefit of the square-cube law. The envelope is the heaviest and costliest component of the system; as its linear dimension is increased, its area (and hence its weight and cost) increases by a factor of square, but its volume (and hence the buoyant lift and payload carrying capacity) increases by a factor of cube. Beyond certain dimensions, however, the large size of the envelope can lead to excessively higher forces acting on the tether and hence the winching and mooring system.

Key Limitations and Risk Factors

TASAA can be deployed only in fair weather conditions, and when the ambient wind changes rapidly in magnitude and/or direction, it may be prudent to lower the system and moor it. In extreme weather conditions, it may be prudent to deflate the envelope and store it in a safe location. Non-availability of LTA gas (Hydrogen / Helium) at the deployment site can be a major risk, which can be mitigated by procuring and transporting gas in cylinders from nearby cities. Another issue could be intentional damage/rupture of the envelope or tether caused by miscreants in deployed condition, such as by small arms fire from the ground. The damage to the payload during such situations can be minimized using the PRD and ERDD system, as explained earlier.

Technology Readiness Levels in India

Aerial Delivery R&D Establishment (ADRDE), which is a laboratory under DRDO located in Agra Cantt., has developed several tethered aerostat systems since many decades, ranging from envelope volume of 90 m³ to 2000 m³; larger sized systems are on the drawing board.

In the Lighter-Than-Air systems Laboratory of IIT Bombay, several Tethered Aerostat systems have also been designed, developed and field tested for various applications, such as provision of last-mile data and voice connectivity in remote areas [13, 15] and aerial surveillance [14]. A small portable winch was also designed and fabricated [16], and field trials of a prototype of solar powered aerostat system were also carried out [7]. Some theoretical studies have also been carried out in the area of shape optimization of aerostat envelopes [17-19], modelling and simulation of breakaway aerostats [20-21], use of aerostats for power generation [22], low-cost trans-river aerial ferry [12], monitoring of snow patterns and avalanches [23], and winged aerostat for better station keeping [24]. A recent study highlights design of a tethered aerostat system for providing wireless communications in a university campus [25]. A study regarding prediction of tensile and fatigue failure of an Aerostat tether was also carried out [26]. Thus, it can be concluded that the preparedness level of this technology is quite high, and it is ready to be harnessed.

Acknowledgements

The author would like to thank Mr. S. S. Mahesh, CEO, Grus Ecosciences, Bengaluru, for providing the write-up and insights on the related to damage to agricultural produce due to bird and animal menace. Thanks are also due to Mr. Chetan Dusane and Mr. Amit Wani of Tata Center of Technology Development, IIT Bombay for providing background data and information on problems faced by farmers in India.

References

1. S. Majumdar, "Open & Distance Learning for Rural Development in India", A Workshop to Explore Innovation and Best Practices in Asia and the Pacific, Bangkok, Thailand, June 28-30, 2005.
2. B. Bowonder, V. Gupta and A. Singh, "Developing a Rural Market e-hub: The case study of e-Choupal experience of ITC", Indian Planning Commission Report, 2002.
3. P. K. Reddy, G. S. Reddy and B. Reddy, "Overview of e-Sagu and Future Plan", Proceedings of IEEE Conference on Technologies for Humanitarian Challenges, IIIT/TR/2009/257, Bangalore, India, 28th August, 2009.
4. Agriculture Census: All India Report on Number and Area of Operational Holdings, Report IND_2010_AgV_v01_M, Department of Agriculture and Cooperation, Ministry of Agriculture, <http://agcensus.nic.in>
5. Y. Shiota, M. Sanada, S. Masaki, "Eye spotted Balloons as a Device to Scare Gray Starlings", Journal of Applied Entomology and Zoology, pp. 545-549, Vol. 18, No. 4, 1983.
6. A. Kapoor and R. S. Pant, "A Methodology for Conceptual Sizing of a Tethered Aerostat", AIAA-2013-1274, Proceedings of 20th AIAA LTA Systems Technology Conference, Daytona Beach, FL, USA, March 25-27, 2013.
7. K. Gajra and R. S. Pant, "SoPTAS: Solar Powered Tethered Aerostat System", 1st International Conference on Non-Conventional Energy (ICONCE 2014), Kalyani, West Bengal, India, January 16-17, 2014.
8. N. Gupta and P. Priyadarshi, "A Multi-Chamber, Multi-Gas Configuration for Robust and High Performance Non-Rigid Airship", Proceedings of the 8th International Airship Convention, Bedford, 2010.
9. Bhat, C. and Pant, R.S., "Design of a Payload Recovery Device in case of accidental breakage of tether of an aerostat", AIAA-2011-7022, Proceedings of 19th Lighter-Than-Air (LTA) Technology Conference, Virginia Beach, Norfolk, Virginia, US, September 20-22, 2011.
10. N. Sharma, A. Mukhopadhyay, V. Sharma, M. Milind and R. S. Pant, "Design and Field Trials of a Payload Recovery Device for Tethered Aerostats", In Bajpai, R. P; Chandrasekhar, U.; Arankalle, A. R. (eds.), Lecture Notes in Mechanical Engineering, pp. 79-84, ISBN 978-81-322-1871-5, Springer India, February 22-24, 2014, DOI: 10.1007/978-81-322-1871-5-12.
11. V. Sharma, V. Pradeepkumar and R. S. Pant, "An Emergency Deflation Device for Remotely Controlled Airships", The Journal of the Airship Association, no.185, pp.11-16, September 2014
12. S. Banerjee, A. A. Raina and R. S. Pant, "Low Cost Trans-river Aerial Ferry", AIAA-2008-8851,



- Proceedings of 26th Congress of ICAS and 8th AIAA ATIO, Anchorage, Alaska, September 14-19, 2008.
13. P. Bilaye, V. N. Gawande and U. B. Desai, A. A. Raina, R. S. Pant. "Low Cost Wireless Internet Access for Rural Areas using Tethered Aerostats", Proceedings of 2008 IEEE Region 10 Colloquium and the Third International Conference on Industrial and Information Systems, IIT Kharagpur, December 8-10, 2008.
 14. N. Sharma, R. Sehgal, R. Sehgal and R. S. Pant, "Design Fabrication and Deployment of a Tethered Aerostat System for Aerial Surveillance", National Level Conference on Advances in Aerial/Road Vehicle and its Application, MIT, Manipal, July 18-19, 2014.
 15. Raina, A. A., Bilaye, P., Gawande, V. N., Desai, U. B. and Pant, R. S., "Design and Fabrication of an Aerostat for Wireless Communication in Remote Areas", AIAA-2007-7832, Proceedings of AIAA 7th AIAA Aviation, Technology, Integration, and Operations (ATIO) Conference and 17th Lighter-Than-Air Systems Technology Conference, Belfast, Northern Ireland, UK, September 2007.
 16. K. Bhandari, N. Wanjari, S. Kadam, G. Sequeira and R. S. Pant, "Design, Fabrication and Field Testing of Winch for Aerostat", Proceedings of National Seminar on Strategic Applications of Lighter-Than-Air (LTA) vehicles at High Altitudes (SALTA-07), SASE, Manali, October 12-13, 2007.
 17. C. Vijayram and R. S. Pant, "Multi-disciplinary Shape Optimization of Aerostat Envelopes", AIAA Journal of Aircraft, Vol. 47, No. 3, pp. 1073-1076, May-June 2010.
 18. C. Vijayram and R. S. Pant, "Multidisciplinary Shape Optimization of Aerostat Envelopes", AIAA-2007-7830, Proceedings of AIAA's 17th Lighter-Than-Air Systems Technology Conference, Belfast, Northern Ireland, UK, September 2007
 19. C. Vijayram and R. S. Pant, "An MDO Approach to Shape Optimization of Aerostat Envelopes, AIAA-2006-1613, Proceedings of 47th AIAA/ASME/ASCE/AHS/ASC Structures, Structural Dynamics, and Materials Conference and 14th AIAA/ASME/AHS Adaptive Structures Conference, Newport, Rhode Island, May 1-4, 2006.
 20. T. K. Reddy, C. G. Sesha Narayanan and R. S. Pant, "Modeling and Simulation of a Payload Recovery Device for Aerostats in Case of Accidental Breakage of Tether", Proceedings of 1st National Conference on Innovations in Mechanical Engineering, SIT, Lonavala, 19-20 April, 2012.
 21. R. Krishna, K. Bodi and R. S. Pant, "Dynamic Simulation of Breakaway Tethered Aerostat including Thermal Effects, AIAA-2013-1341, Proceedings of 20th AIAA LTA Systems Technology Conference, 25-27 March 2013, Daytona Beach, FL, USA.
 22. G. Civalier, C. Fridley, Li, J., J. Seabe, A. Stanciu, M. Willey and R. S. Pant, "Comparative Analysis of Three Concepts for Aerostat Based Electrical Power Generation System", AIAA-2011-7023, Proceedings of AIAA's 19th Lighter-Than-Air (LTA) Technology Conference, Virginia Beach, Norfolk, Virginia, USA, 20th to 22nd Sep 2011.
 23. A. A. Raina, K. M. Bhandari and R. S. Pant, "Conceptual Design of A High Altitude Aerostat For Study of Snow Pattern", Proceedings of International Symposium on Snow & Avalanches (ISSA-09), SASE, Manali, India, 6-10 April 2009.
 24. A. Kanoria, K. Bhandari and R. S. Pant, "Comparison of Conventional and Winged Aerostats for Monitoring of Avalanche Parameters", AIAA-2011-7024, Proceedings of AIAA's 19th Lighter-Than-Air (LTA) Technology Conference, Virginia Beach, Norfolk, Virginia, USA, September 20-22, 2011.
 25. J. H. Jadhwar and V. Sharma and R. S. Pant, "Design of a Tethered Aerostat System for providing Wireless Communications in a University Campus, Proceedings of the 10th International Convention of Airship Association, April 17-19, 2015, Friedrichshafen, Germany.
 26. Y. More, A. Guha, S. Trivedi and R. S. Pant, "A Model for Predicting Tensile and Fatigue Failure of an Aerostat Tether", Proceedings of XVIII National Seminar on Aerospace Structures, Nagpur, 15-17 December 2014.

Aerospace Engineering Division Board (2015-2016)

Members for the Session 2015-2016



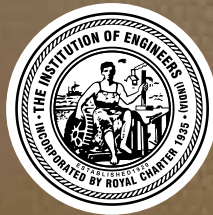
Mr S R Vijayamohanakumar, FIE
Chairman



Prof R M Vasagam, FIE
Member



Dr S C Sharma, FIE
Member



The Institution of Engineers (India)

8 Gokhale Road, Kolkata 700 020

Phone : +91 (033) 2223-8311/14/15/16, 2223-8333/34

Fax : +91 (033) 2223-8345

Website : <http://www.ieindia.org>

e-mail: technical@ieindia.org

iei.technical@gmail.com